2016

The Regulatory Role of Interleukin-1 Receptor Associated Kinase M in Toll-Like Receptor Signaling

Hao Zhou
Cleveland State University

THE REGULATORY ROLE OF INTERLEUKIN-1 RECEPTOR ASSOCIATED KINASE M IN TOLL-LIKE RECEPTOR SIGNALING

HAO ZHOU

Bachelor of Medicine

Tianjin Medical University

June 2007

Submitted in partial fulfillment of the requirements for the degree

DOCTOR OF PHILOSPHY IN REGULATORY BIOLOGY

at the

CLEVELAND STATE UNIVERSITY

March 2016

We hereby approve this dissertation for

Hao Zhou

Candidate for the Doctor of Philosophy in Regulatory Biology degree for the

Department of Biological, Geological and Environmental Sciences

and the CLEVELAND STATE UNIVERSITY'S

College of Graduate Studies

_____Date:_____

Dissertation Chairperson, Dr. Xiaoxia Li, BGES-CSU; LRI-CCF,

_____Date:_____

Dissertation Committee Member, Dr. George R. Stark, BGES-CSU; LRI-CCF,

_____Date:_____

Dissertation Committee Member, Dr. Crystal M. Weyman, BGES-CSU,

_____Date:_____

Dissertation Committee Member, Dr. Barsanjit Mazumder, BGES-CSU,

_____Date:_____

Internal Reader, Dr. Laura E. Nagy, BGES-CSU; LRI-CCF,

Student's Date of Defense: August 19, 2014

ACKNOWLEDGEMENTS

I want to express deep gratitude to my advisor, Dr. Xiaoxia Li, who has supported me throughout my research with her patience and knowledge whilst allowing me the room to work in my own way. During my time in Xiaoxia's laboratory, I have been extremely fortunate to be granted outstanding scientific resources and consistent guidance. I could not have imagined having a better advisor and mentor for my Ph.D. study.

Besides my advisor, I would like to thank the members of my advisory committee, Dr. George Stark, Dr. Crystal Weyman and Dr. Barsanjit Mazumder, for all their time and effort helping me to be a better graduate student. I am also grateful for all of the efforts of our collaborators. Their generosities are deeply appreciated. I also thank Dr. Laura Nagy and all the members of her laboratory for the tremendous help.

I thank all Li lab members including for helpful discussion and creating an excellent work environment. I especially thank to Dr. Youzhong Wan, Dr. Tae Whan Kim and Dr. Weiguo Yin for their initial contribution to my doctoral studies and teaching me all the techniques for working with mice and primary cell cultures. Dr. Jarod Zepp helped in the editing of this dissertation. His efforts are greatly appreciated.

Finally, I would like to dedicate this dissertation to my wife and my parents, for their constant love and enduring support for so many years.

THE REGULATORY ROLE OF INTERLUKIN-1 RECEPTOR ASSOCIATED KINASE M IN TOLL-LIKE RECEPTOR SIGNALING

HAO ZHOU

ABSTRACT

Toll-like receptors (TLRs) are one of the major groups of pattern recognition receptors. TLRs are able to recognize the pathogen-associated molecular patterns and transduce their signals through the adaptor molecule MyD88 and members of the IL-1R-associated kinase family (IRAK1, 2, M and 4).

IRAKM was previously known to function as a negative regulator that prevents the dissociation of IRAKs from MyD88, thereby inhibiting downstream signaling. However, we now found that IRAKM was also able to interact with MyD88-IRAK4 to form IRAKM Myddosome to mediate TLR7-induced MEKK3-dependent second wave NFκB activation. As a result, the IRAKM-dependent pathway only induced expression of genes that are not regulated at the posttranscriptional levels (including inhibitory molecules SOCS1, SHIP1, A20 and IκBα), exerting an overall inhibitory effect on inflammatory response. On the other hand, through interaction with IRAK2, IRAKM inhibited TLR7-mediated production of cytokines and chemokines at translational levels.

While the TLR-mediated inflammatory response is critical for innate immunity and host defense against infections, uncontrolled inflammation is detrimental to the host, leading to chronic inflammatory diseases. Alcohol-induced liver injury is induced by necrosis of hepatocytes and increased translocation of endotoxin from the intestinal tract

into hepatic portal system, which trigger chronic inflammation that is damaging to the liver together. We found that mice deficient of IRAKM, are protected from alcohol-induced liver injury. IRAKM mediates the up-regulation of Mincle, a receptor for danger signals release by damaged cells, in response to low level of LPS. Biochemical analysis revealed that low-dose LPS preferentially induces the formation of IRAKM Myddosome, leading to MEKK3-dependent NFκB activation. Mincle-deficient mice are also protected from alcohol-induced liver injury. We found IRAKM deficiency and Mincle deficiency drastically reduced alcohol feeding induced inflammasome activation in the mouse liver. *Ex vivo* studies showed that both IRAKM and Mincle are required for inflammasome activation by endogenous Mincle ligand, SAP130, which is a danger signal release by damaged hepatocytes. Taken together, we identifies an IRAKM-Mincle axis critical for the pathogenesis of alcohol induced liver disease through the activation of inflammasome.

TABLE OF CONTENTS

LIST OF FIGURES

CHAPTER I

INTRODUCTION

A. The Mammalian Immune System

The main purpose of the immune system is to detect and appropriately respond to foreign objects and pathogens [1]. The mammalian immune system is comprised of two parts: innate and adaptive immunity. The innate immune system, the first line of immune defense system, applies multiple layers to defend against invading pathogens[2]. One layer includes the physical barrier surface such as skin and epithelium[3]. Another layer is the immune cells which can active phagocytosis and inflammatory response. Macrophages and dendritic cells (DC), two important cell types of phagocytes, can recognize different groups of invading pathogens through conserved molecular patterns [4-6]. These recognition events lead to the subsequent production of inflammatory mediators by macrophages and DCs, such as pro-inflammatory cytokines, chemokines and interferons [7, 8]. These mediators can further promote inflammatory responses by modifying vascular endothelial cells to increase permeability to recruit leukocytes to infect tissues [9, 10]. They

can also enhance macrophage-mediated phagocytosis or even induce the apoptosis (programmed cell death) of infected cells [11].

While the activation of innate immune response depends on the recognition of pathogen associated patterns (PAMPs) as non-self ligands, the adaptive immune response is characterized by antigen specificity [4, 12]. Lymphocytes, including B cells and T cells, bear a large repertoire of antigen-specific receptors that are generated by gene rearrangement [13, 14]. Interaction between antigen-presenting cells and lymphocytes stimulates the expansion and activation of a sub-group of lymphocytes that bear receptors specific to the invading pathogens. Upon activation, B cells differentiate in plasma cells and secrete a large amount of antibodies, each of which recognize a specific antigen and mediate the neutralization of invading pathogens. Cytotoxic T cells can induce apoptosis of pathogen-infected cells and T helper cells are critical to regulate immune response.

B. Pattern Recognition Receptors

The innate immune system is the primary barrier to the invading pathogens and acts immediately. To eliminate the pathogens, the host immune system must be able to detect the difference between pathogens and host tissues, e.g. “non-self” and “self”. Recognition of microbial pathogens is essential for initiating the innate immune response. Germline-encoded pattern-recognition receptors (PRRs) that recognize pathogen-associated molecular patterns (PAMPs) play a central role in host cell recognition and immune response to invading pathogens [15]. Upon PAMPs recognition, PRRs initiate a series of signaling events which execute the first line of host defense[16]. The first PRR, the Toll

receptor, was identified in a mutant Drosophila line highly susceptible to fungal infection [17]. Subsequent screening studies identified the human and murine homologue of Toll receptor and lipopolysaccharide (LPS), a component of Gram-negative bacteria cell wall was confirmed as the ligand [18-20]. To date, four PRR families have been identified, including Toll-like receptors (TLRs), C-type lectin receptors (CLRs), retinoic acid-inducible gene (RIG)-I-like receptors (RLRs) and Nucleotide oligomerization domain (NOD)-like receptors (NLRs).

Toll-like receptors

Among all the PPRs, the members of TLR family have been studied most extensively[21]. So far, 13 mammalian members of the TLR family have been identified[22]. TLRs belongs to type I integral transmembrane glycoproteins characterized by an extracellular domain and a cytoplasmic signaling domain [8]. The cytoplasmic domain of TLRs is similar to that of the IL-1 receptor (IL-1R) family and appropriately named the Toll/IL-1 receptor (TIR) domain [23]. Therefore, the TLRs and IL-1Rs are grouped into a TLR/IL-1R superfamily. While the extracellular domains are markedly different: IL-1R family has an immunoglobulin (Ig) domain and TLRs contain a leucine-rich repeats (LRR) [24]. The LRR domain of TLR4 was shown to form a horseshoe structure with LPS binding to the concave surface [25]. The intracellular signaling of TLRs are primarily mediated by recruiting different TIR domain containing adaptor molecules such as MyD88, TRIF, TIRAP and TRAM [26-28]. All TLRs, except TLR3, recruit MyD88 and initiate MyD88-dependent pathway to activate multiple transcription factors, including NFκB, AP-1, C-Fos/Jun. TLR3 and TLR4 recruit TRIF and initiate TRIF-

dependent signaling to activate NFκB and IRF3 to induce production of pro-inflammatory and type I interferons[29].

TLR1, TLR2, TLR4, TLR5, TL6 and TLR11 are expressed on the cytoplasmic membrane, while TLR3, TLR7, TLR8 and TLR9 are expressed in intracellular vesicles, such as endosomes [25]. TLR4, together with myeloid differentiation factor 2 (MD2), recognize LPS, a component of the Gram-negative bacterial cell walls [20]. Recent studies have also identified oxidized low-density lipoprotein (Ox-LDL) and free fatty acid (FFA) as endogenous ligands of TLR4 [30]. TLR2 forms heterodimers with TLR1 or TLR6. The TLR1/2 and TLR2/6 heterodimers recognize lipoproteins derived from gram-positive bacteria [31]. TLR5 recognizes flagellin which is a conserved protein component of bacteria flagella [32]. TLRs which recognize nucleotides derived from invading pathogens including TLR3, TLR7, TLR8 and TLR9, are localized in intracellular compartments, such as endosomes and early lysosomes. Both of TLR7 and TLR 8 recognize uridine or guanosine-rich single strand (ss) RNA [24, 27, 33]. TLR3 can recognize double strand (ds) RNA, which is typically an intermediate product during replication of ssRNA viruses [34]. TLR9 is responsible for the recognition of genomic DNA derived from invading bacteria and viruses distinguished by a high abundance of unmethylated CpG nucleotides compared to mammalian genomic DNA [35]. (**Fig. 1**)

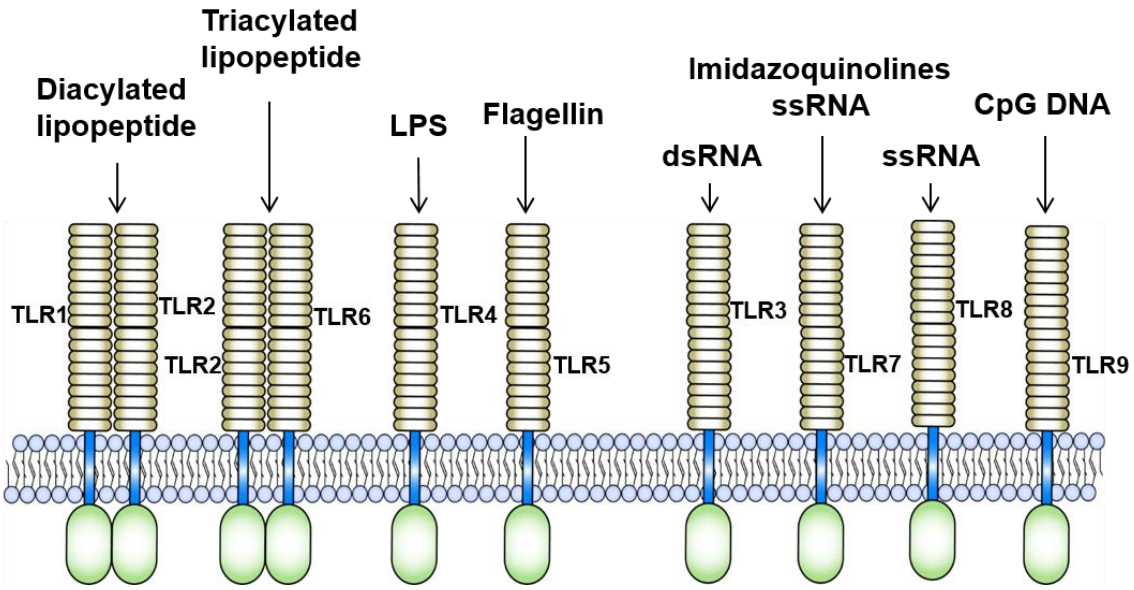

Figure 1. Toll-like receptors and their ligands.

C-type lectin receptors

C-type lectin receptor (CLR) is another important family member of PPRs. It is designed to bind to carbohydrates and named as C-type due to the requirement for calcium to bind carbohydrates initially [36, 37]. CLRs constitute a group of over 1000 members. They are characterized by a carbohydrate recognition domain (CRD) and a calcium binding motif[38]. Subsequent studies found that not all the CLRs are calcium dependent and these receptors can recognized multivalent ligands.

The N-terminal region of the genes encodes the extracellular domain which contains at least a CRD, while the C-terminal region encodes the intracellular domain[39]. Based on the features of intracellular domain, CLRs can be divided into two distinct groups: Dectin1 group (including Dectin-1 a, CLEC1, CLEC2, CLEC9A, CLEC12B, LOX1 and

MICL) and Dectin2 group (including Dectin2, Mincle, Clescsf8, BDCA-2, DCAR and DCIR)[40].

CLRs from the Dectin1 group all have a long intracellular tail including an immunoreceptor tyrosine-based activation motif (ITAM) for signaling transduction [41]. The cytoplasmic tail of Dectin1, CLEC9A, CLEC2 and LOX1 contains an immunoreceptor tyrosine-based activation motif which is required for signaling activation after ligation. In contrast, the cytoplasmic tail of CLEC12A, CLEC12B, MICL and DCIR contains an immunoreceptor tyrosine-based inhibitory motif (ITIM). The ligation of these receptors leads to a suppression of transcription factor activation.

CLRs from the Dectin2 group have the similar structure with the Dectin1 group with a notable exception: a short cytoplasmic tail [41]. The short cytoplasmic tail lacks the ability to transduce signal. Thus these receptors typically pair with an FcRγ chain which harbors an ITAM motif to activate signaling transduction.

Recent studies show that Dectin1 and Dectin2 mediated signaling activation are both critical for anti-fungal responses [42, 43]. Dectin1 is able to recognize β-glucan while Dectin2 recognizes high mannose [44, 45]. Mincle, a Dectin-2 member, has multiple ligands including cord factor of Mycobacterium tuberculosis and α-mannose on the surface of pathogenic fungus, Malassezia[46-51]. Mincle also recognized the endogenous protein SAP130, a component of small nuclear ribonucloprotein released from damaged/nectrotic cells [52]. Activation of CLRs usually leads to the activation of a tyrosine kinase SyK which transduce the signal through CARD9-Bcl10-MALT1 complex. It has been suggested that formation of this complex leads to the canonical NFκB activation through

TAK1-IKK pathway, followed by pro-inflammatory cytokine and chemokine secretion [53, 54]. Overall, CLRs are essential for host immune response and homeostasis. (**Fig. 2**)

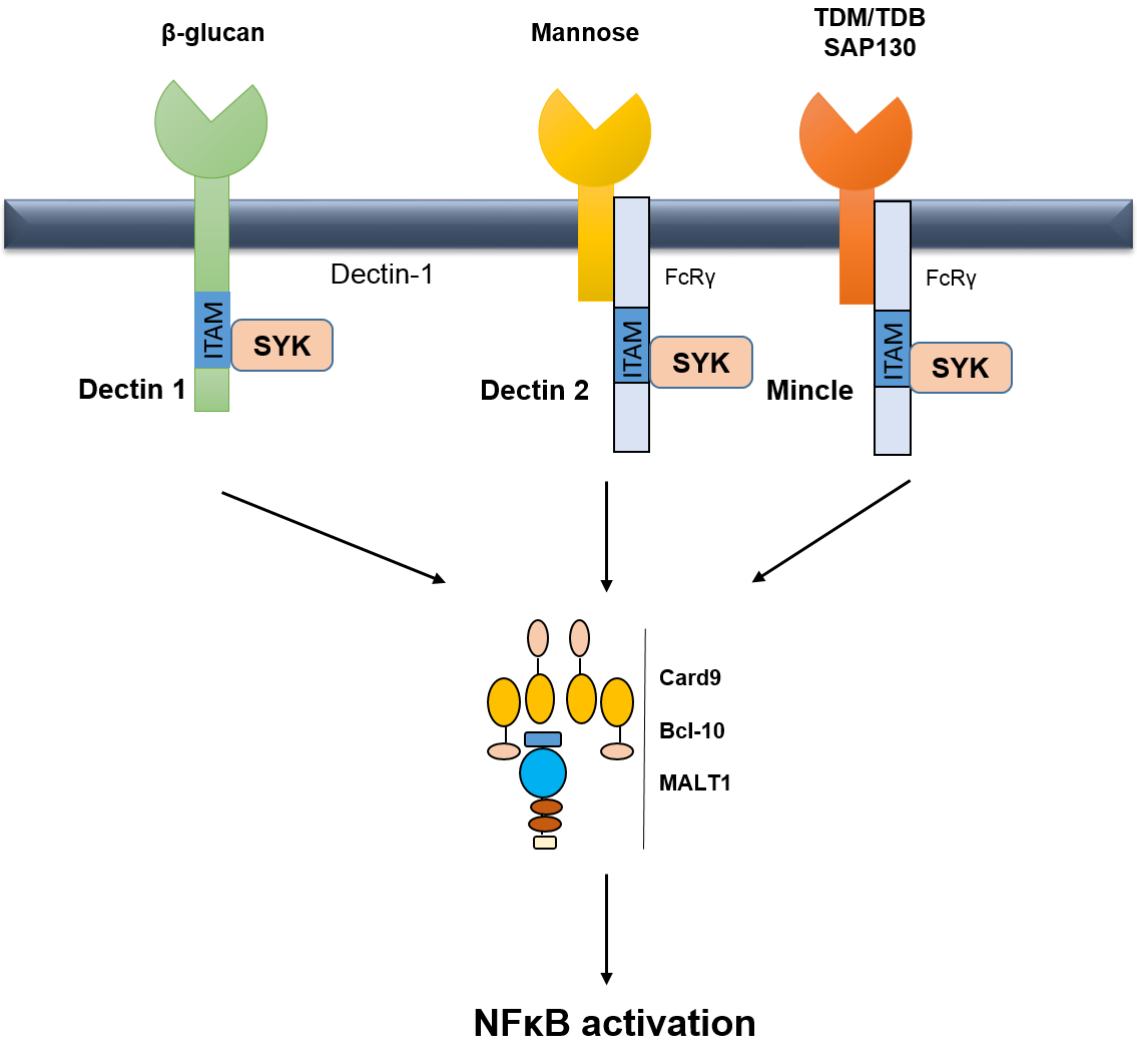

Figure 2. C-type lectins receptors and their ligands.

NOD-like receptors

NOD-like receptors (NLRs), are essential in recognizing cytosolic bacterial components. Generally, they have a leucine-rich repeat (LRR) motif that mediates ligand

recognition, a nucleotide binding oligomerization domain (NOD), and a caspase recruitment domain (CARD) to mediate the recruitment and activation of downstream signaling components. So far, at least 23 human and 34 murine NLR genes have been identified, amongst which NOD1 and NOD2 are the best-characterized members and recognize distinct structural motifs in bacterial peptidoglycans [55]. NOD1 recognizes γ-D-glutamyl-meso-diaminopimelic acid (iE-DAP) in all Gram-negative bacterial as well as several Gram-positive bacteria, while, NOD2 recognizes muramyl dipeptide (MDP) in all Gram-negative and Gram-positive bacteria [56-58]. After ligand binding, the CARD domain of NOD1 and NOD2 interacts with a serine/threonine kinase, RIP2 (RICK) that initiates a signaling cascade resulting NFκB activation, as well as the activation of MAPKs [52, 59].

RIG-I-like receptors

The RIG-I-like receptor family is another group of cytosolic PRRs which are essential for the detection of viral RNA in the cytoplasm of most cell types. It includes RIG-I, melanoma differentiation associated gene 5 (MDA5) and LGP2. RIG-I and MDA5 contain a central DExD/H-box helicase domain and a C-terminal domain (CTD), both of which are responsible for binding viral RNA [60-62]. It is well established that the signal-transducing activities of RIG-I and MDA5 are tightly regulated by a combination of phosphorylation and ubiquitination. Interferon-beta promoter stimulator 1 (IPS-1, also called MAVS, VISA or CARDIF) is an essential adaptor molecule for both RIG-I- and MDA-5- mediated signaling. It associates with RIG-I and MDA-5 through CARD domains upon viral infection, and activates downstream signaling components. The third RIG-I-

like receptor, LGP2, lacks the CARD domain and has been shown to exert a regulatory role in RLR signaling [63]. However, its precise action has not been well defined yet.

C. TLR-mediated Signaling Activation

The intracellular signaling cascades activated by PRRs results in the production of inflammatory mediators, including a variety of pro-inflammatory cytokines and chemokines. The production of pro-inflammatory cytokines, such as tumor necrosis factor alpha (TNFα), interleukin-1β (IL-1β), and IL-6, are essential to promote inflammatory responses [64].

All TLRs have a conserved intracellular TIR domain. After binding with the ligands, TLRs undergo conformational changes, and recruit adapter molecules through interaction with TIR domains [65]. Five TIR-containing adaptor molecules have been identified, including MyD88, MAL, TRIF, TIRAP and TRAM. TLRs utilize different adaptor molecules to activate downstream signaling cascades, which can be roughly divided into the MyD88-dependent pathway and the TRIF-dependent pathway [29, 66].

The MyD88-dependent pathway

MyD88 is employed by all TLRs except TLR3 as an adaptor molecule. In addition to a TIR domain, MyD88 also has a death domain (DD) [25]. Stimulation of TLRs by their respective ligands causes the recruitment of MyD88 through TIR domain interaction. After binding to the receptor complex, MyD88 interacts with the IL-1 receptor-associated kinases (IRAKs) via the respective death domains. The MyD88-IRAK4-IRAK2/1 signaling complex has been named as Myddosome [67]. Formaiton of Myddsome leads

the activation the kinase activity of IRAK4, which activates IRAK1 and IRAK2 through subsequent phosphorylation[68]. The activated IRAKs recruit TNFR-associated factor 6 (TRAF6), which is an E3-ubiquitin protein ligase. TRAF6, ubiquitination conjugating enzymes (E2) UBC13 and UEV1A add lysine 63-linked polyubiquitin chain to TRAF6 as well as to other signaling components [69]. The ubiquitinated TRAF6 recruits a protein complex that is composed of TGF-β-activated kinase 1 (TAK1) and the TAK1 binding proteins TAB1, TAB2, and TAB3. The activated TAK1 complex activates IKB kinase (IKK) complex (composed of IKKα, IKKβ and /IKKγ) and mitogen-activated protein kinase kinase (MAPKK) through phosphorylation [70]. The activated IKK complex phosphorylates NF-κB inhibitory protein (IκBα), leading to the lysine 48-linked polyubiquitination and degradation of IκBα[71]. The degradation of IκBα releases NFκB, which translocates into the nucleus and induces the transcription of a series of NFκB target genes, including pro-inflammatory cytokines and cytokines. Activation of MAP kinase leads to the activation of another transcription factor, activator protein 1 (AP-1), which also regulates the transcription of pro-inflammatory cytokine genes.

Recent studies also suggest that there is a parallel pathway which is TAK1-independent MEKK3 dependent downstream of MyD88 [65, 72, 73]. In contrast to TAK1-dependet pathway results in IKKα/β phosphorylation and IKKγ activation, leading to classical NFκB activation via IκBα phosphorylation and degradation, MEKK3-dependent pathway entails to IKKγ phosphorylation and IKKα activation, which leads to NFκB activation by IκBα phosphorylation and its subsequent dissociation from NFκB, but without IκBα degradation. IRAK4 kinase activity is not required for MEKK3-dependent pathway, suggesting by the study of IRAK4 kinase activity dead knock-in mice [65].

However, the precise mechanism of how MEKK3-dependent pathway gets activated is still not well understood. (**Fig. 3**)

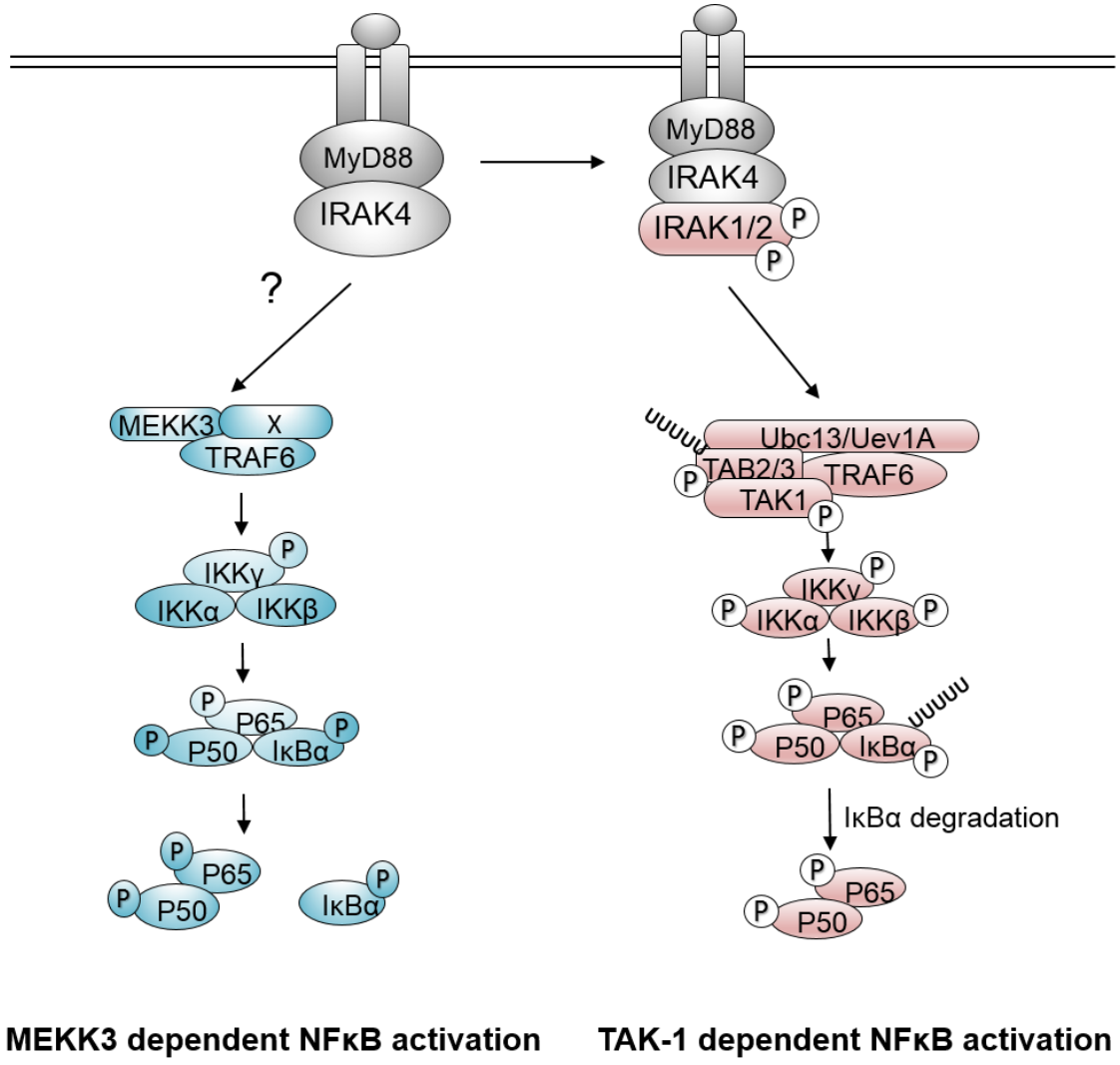

Figure 3. TLR-induced MyD88-dependent signaling pathway.

The TRIF-dependent pathway

The TLR3 signaling pathway is mediated exclusively by the TRIF adaptor [74]. TRIF-mediated activation of TRAF3 leads to the activation of the non-canonical IKKs, including TBK1 and IKKi. The subsequent phosphorylation of IRF3 by TBK1/IKKi leads to the translocation IRF3 and the induction of type I IFNs and IL-10. TRIF recruitment and activation of TRAF6 and RIP1 lead to NF-κB activity through TAK1.

TLR4 uses both the MyD88-dependent and the TRIF-dependent pathways to induce the production of pro-inflammatory cytokines [20, 26]. MyD88 and TRIF double-deficient cells show complete loss of NFκB activation in response to LPS stimulation [75]. (**Fig. 4**)

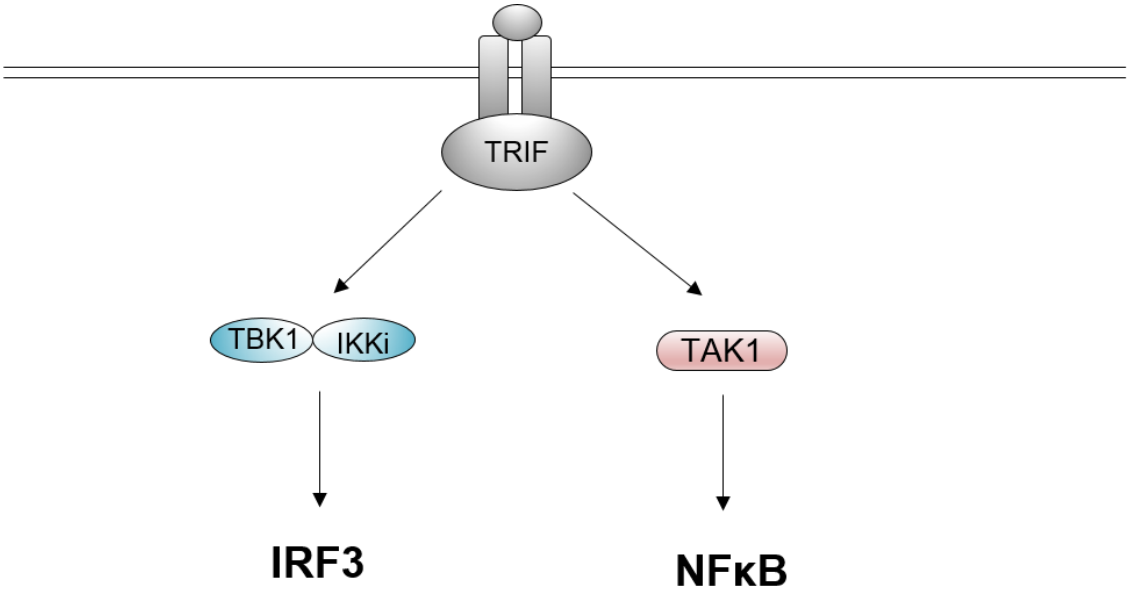

Figure 4. TLR-induced TRIF-dependent signaling pathway.

D. Post-transcriptional Regulation of Proinflammtory Cytokine Production

Although proinflammatory cytokines promote host defense against infection, their prolonged production may lead to chronic inflammation that can cause substantial tissue damage. Therefore, it is crucial to maintain tight control of proinflammatory cytokine production, not only to induce them promptly respond to infection, but also to shut them off quickly after the pathogens are eliminated.

Regulation of mRNA stability

Cellular mRNA levels are established by both mRNA synthesis and degradation. Many cytokine mRNAs have adenine and uridine-rich elements (AREs) in their 3' untranslated regions (UTRs), characterized by a pentamer "AUUUA" or a nonamer "UUAUUUAUU". It has been shown that AREs are crucial for rapid mRNA decay [76-78]. Numerous pro-inflammatory cytokines undergo ARE mediated regulation including IL-6, TNFα, IL-1β, GM-CSF, TGFβ and CXCL1. Over twenty different ARE-binding proteins have been identified which associate with AREs mediate interactions between these mRNAs and exosome complexes, the major machinery for intracellular mRNA degradation. Tristetraprolin (TTP), the prototype of an ARE binding protein, plays a critical role in inhibiting TNFα production by destabilizing TNFα mRNA [79, 80]. By contrast, the ELAV (embryonic lethal and abnormal vision) family members Hu-antigen R (HUR) and HUD stabilize their targets by competing with the destabilizing ARE-binding proteins for ARE occupancy [81].

Recently, Regnase 1 (Zc3h12a) has been identified as another negative regulator of pro-inflammatory cytokine production [82]. Regnase 1 is induced rapidly and

phosphorylated by IKKβ in response to TLR ligand stimulation. It binds to the 3'UTR regions of multiple proinflammatory cytokine mRNAs, including IL-6 and IL-20p40, and leads to mRNA degradation. Further studies indicated that Regnase 1 degrades mRNA via its endonucleolytic activity[83]. These results demonstrate that the stability of mRNA encoding different pro-inflammatory cytokines is regulated by different mechanisms.

Regulation of protein translation

In addition to stabilize mRNA, initiation of protein translation is also crucial for prompt and robust cytokine production in response to pathogen infection. Among all translation initiation factors, eukaryotic translation initiation factor 2 (eIF2) and eIF4e are most well studied in innate immunity. eIF2 forms a ternary complex with the initiator methionyl-tRNA and GTP. The binding of eIF2 complex to 40S ribosomal subunit is essential for start codon recognition, followed by recruitment of the 60S ribosomal subunit [84]. eIF4E is a cap-binding protein which interacts with 5'mRNA cap structure and the scaffold initiation factor eIF4G[51]. In most cells, eIF4E levels are limited, therefore, the regulation of its activity has strong impact on the translation efficiency. Two MAPK-interacting protein kinase, MNK1 and MNK2, are activated in response to LPS and subsequently activate eIF4E through phosphorylation which greatly promote the translation of a variety of pro-inflammatory genes [85-87].

E. Inflammasome Activation

IL-1 signaling is a key component of the immune and inflammatory responses. IL-1β is synthesized as an inactive 31-kD precursor molecule which requires cleavage by the

cysteine protease caspase-1 to release biologically active mature 17-kD IL-1β [88, 89]. Inflammasomes are multiprotein complex which contain a member of the nucleotide-binding domain leucine-rich repeat (NLR) or AIM2-like receptor (ALR) family, an adaptor molecule known as apoptosis associated speck-like protein containing a CARD (ASC) and a caspase. Inflammasomes are activated in response to a diverse range of microbial, stress and damage signals that trigger caspase-1 activation, resulting in maturation of the pro-inflammatory cytokines interleukin (IL)-1β, IL-18 and IL-33 [90-92]. A great deal of work over the past ten years has been committed to elucidating the mechanism by which the inflammasome is activated, and the particular ligands that are capable of initiating this activation.

The NOD-like receptors are a diverse family of intracellular pattern recognition receptors that contain a C-terminal leucine-rich repeat (LRR) that is thought to contribute to ligand recognition, a central NACHT nucleotide-binding domain that is involved in orchestrating oligomerization, and an N-terminal "effector" domain that, in the case of inflammasome-associated NLRs, consists of a either a caspase-1 recruitment domain (CARD) or a Pyrin domain. The adaptor molecule ASC consists of an N-terminal CARD domain and a C-terminal Pyrin domain [93]. The classical role for ASC is to function as a "bridge", linking NLRs containing an N-terminal Pyrin domain with caspase-1 via PYD-PYD and CARD-CARD interactions, respectively [94]. Caspase-1 is a member of the caspase family of cysteine proteases that function to carry out a variety of cellular programs, including programmed cell death and inflammation. The caspases, including caspase-1, are produced as zymogens and must be activated in order to commence catalytic activity. Caspase-1 exists as a tetramer comprised of two p10 and two p20 subunits, and undergoes

autoactivation following its recruitment to the inflammasome complex. Upon activation, caspase-1 functions by processing the pro-IL-1β, pro-IL-18, and pro-IL-33 to their active forms in preparation for extracellular secretion.

The NOD-like receptors (NLRs) are a large and diverse family of intracellular pattern recognition receptors (PPRs). All NLRs, with the exception of NLRP10, contain a C-terminal leucine-rich repeat (LRR) which is thought to contribute to ligand recognition. The NLRP1, NLRP3 and NLRC4 (Ipaf) inflammasomes are only inflammasome complexes that have been shown to lead to the activation of the inflammatory caspases.

Of the inflammasomes, the NLRP3 inflammasome is by far the best characterized, and is the model from which essentially all mechanistic data on inflammasome activation is derived. So far, the NLRP3 inflammasome has been found to be activated in response to a surprisingly wide variety of triggers, including pathogen-associated molecular patterns (PAMPs) such as the flagellin component of Salmonella, danger-associated molecular patterns (DAMPs) of which ATP and mitochondrial DNA are considered prototypes, and even to whole pathogens such as Staphylococcus aureus, Candida albicans, and influenza virus.

Despite much effort, the exact mechanism by which the NLRP3 inflammasome is activated remains elusive. It is known that in the resting state, NLRP3 is located in the cytoplasm and is accompanied by the chaperone molecules HSP90 and SGT1, which are thought to stabilize the inactive state. By some mechanisms, the NLRP3 molecules "senses" one of its many activators and oligomerizes, with the Pyrin domains having been shown by x-ray crystallographic studies to "stack" and therefore allow for homotypic interaction

with the Pyrin domain of the adaptor ASC [94]. Following ASC association, procaspase-1 is recruited and cleaved and forms an active caspase-1 tetramer.

At this time, there are essentially three models for the initiation of NLRP3 activation, and all three have approximately equal support in the literature. One model posits that when inflammasome agonists are phagocytosed and enter the lysosome, some property of the agonist leads to lysosomal rupture, and the presence of lysosomal enzymes or other constituents in the cytoplasm are sensed by NLRP3 [67, 95, 96] Another model hypothesizes that ATP, a powerful inflammasome activator in macrophages, signals via the P2X7-receptor, leading to potassium efflux through activation of the cell membrane channel protein Pannexin-1 [97-103]. A third model suggests that all of the inflammasome activators lead to the generation of reactive-oxygen species (ROS), and that the presence of cytoplasmic ROS, either by change in cellular redox state or another factor, leads to NLRP3 activation. This model is supported by very recent work suggesting that the mitochondria is a key mediator of ROS production, and that inflammasome components, including ASC and NLRP3, colocalize to the mitochondria during activation [92, 104].

F. Alcohol-induced Liver Diseases

Alcoholism results in about 2.5 million deaths annually worldwide and has long been associated with various liver diseases accounting for about 4% of all deaths [105-107]. Alcoholic liver disease (ALD) ranges from steatosis to hepatitis, fibrosis, cirrhosis and hepatocellular carcinoma. Hepatic steatosis is the earliest response to alcohol consumption and develops in 90% of heavy alcohol drinkers. Simple steatosis usually is asymptomatic

and reversible. 20-25% of alcoholics will develop alcoholic hepatitis, about 15% develop alcoholic cirrhosis and about 10% develop hepatocellular carcinoma [108]. Meanwhile, pharmacological treatment options are limited and the outcomes from the therapies are poor. Thus understanding the detailed mechanisms involved in the pathogenesis and progress of ALD is critical, which serves the need of developing novel and more effective pharmacological agents for treatment.

The pathogenesis of ALD is multifactorial and is still not fully understood. Emerging evidences suggest that the damage is the end result of the interplay among ethanol metabolism, inflammation and innate immunity. Acetaldehyde, a direct metabolism of ethanol, is a highly reactive and toxic chemical to hepatocytes which contributes to liver tissue damage because it forms a variety of protein and DNA adducts that promote glutathione depletion, lipid peroxidation and mitochondrial dysfunction. It also leads to the formation of reactive oxygen species (ROS), which are potent inducers of lipid peroxidation and leads to the eventual cell death of hepatocytes. Increased endotoxin levels in the serum have been documented in both ALD patients and alcohol-fed experimental animals [109]. One intriguing paradigm suggests that alcohol drinking promotes altered gastrointestinal microbiota and increased intestinal permeability. Translocation of bacterial related products from gut into blood stream arrive at the liver through the portal vein. Antibiotic treatment significantly reduced the pathologic change of livers in rats exposed to ethanol, which suggested endotoxin is a crucial mediator of ALD [110-114]. Previous studies have shown Kupffer cells, the resident macrophages of liver, express TLRs and are responsible for the uptake of gut-derived toxins such as LPS. Seki et.al showed that Kupffer cells could response to various concentrations LPS

stimulation to produce pro-inflammatory cytokines (TNFα, IL-1β, IL-6, IL-12, and IL-18) and chemokines. Notably, induction of chemokines (MIP-1α, MIP-1β, RANTES, and MCP-5) gene expression in livers from mice induced by LPS was reduced by 80–97% after selective depletion of Kupffer cells [115, 116]. Furthermore, long-term ethanol administration results in sensitization of LPS-induced liver injury and secretion of TNFα by Kupffer cells. Thus TLRs, especially TLR4 expressed on Kupffer cells, are activated by these PAMPs, resulting in pro-inflammatory cytokine and chemokine production and recruitment of other immune cells such as neutrophils. All of these inflammatory responses are critical contributors to disease progression. Consistent with this, both TLR4-mutated (C3H/HeJ) mice and TLR4-deficient mice displayed dramatically reduced levels of proinflammatory cytokines in the liver and protected mice from liver injury in a long-term intragastric ethanol feeding model. Several studies have shown the role of inflammasome-IL-1 signaling in acute and chronic liver injury including ALD [19, 26, 115]. Petrasek et.al. showed that IL-1β signaling is required for the development of alcohol-induced liver steatosis, inflammation, and injury, using mice deficient in regulators of IL-1β activation (caspase-1and ASC) or signaling (IL-1 receptor) as well as treating mice with IL-1 receptor antagonist [117]. It is suggested that IL-1R/TLRs signaling and/or inflammasome pathways are potential therapeutic targets to treat ALD.

Hepatocyte cell death is a major hallmark of ethanol-induced liver injury, reflected by increased levels of serum alanine aminotransferase (ALT) and aspartate aminotransferase (AST). It is also used to risk stratify and monitor ALD patients. Multiple forms of cell death, including necrosis, apoptosis and necroptosis, commonly exist in ALD, all of which may promote liver disease progression through distinct mechanisms. DAMPs

released from dying cells, such as high-mobility group box 1 (HMGB1), are believed to trigger sterile inflammation and thus exacerbation of injury in acute liver diseases [118]. However, the significance of DAMPs-induced sterile inflammation involved in the progression of alcohol-induced chronic liver injury is underestimated.

CHAPTER II

IRAKM MEDIATES TOLL-LIKE RECEPTRO/IL-1R-INDUCED NFKB ACTIVATION AND CYTOKINE PRODUCTION

Hao Zhou[1,2,8], Minjia Yu[5,8], Koichi Fukuda[3], Jinteak Im[1], Peng Yao[4], Wei Cui[1,6], Katarzyna Bulek[1], Jarod Zepp[1], Youzhong Wan[1], Tae Whan Kim[1], Weiguo Yin[1], Victoria Ma[1], James Thomas[7], Jun Gu[6], Jian-an Wang[5], Paul E. DiCorleto[4], Paul L. Fox[4], Jun Qin[3]and Xiaoxia Li[1,*]

[1]Department of Immunology, Cleveland Clinic Foundation, Cleveland, OH 44195

[2]Department of Biological, Geological, and Environmental Sciences, Cleveland State University, Cleveland, OH 44115

[3]Department of Molecular Cardiology, Cleveland Clinic Foundation, Cleveland, OH 44195

[4]Department of Cell Biology, Cleveland Clinic Foundation, Cleveland, OH 44195

[5]Department of Cardiology, Second Affiliated Hospital, School of Medicine, Zhejiang University, Hangzhou, Zhejiang 310009, China

[6]Department of Biochemistry and Molecular Biology, College of Life Sciences, Peking University, Beijing 100871, China

[7]Departments of Pediatrics and Molecular Biology, University of Texas Southwestern Medical Center at Dallas, Dallas, TX 75390

[8]These authors contributed equally to this work.

This work was published in the *EMBO Journal* (2013)32,583-596

A. Abstract

Toll-like receptors transduce their signals through the adaptor molecule MyD88 and members of the IL-1R-associated kinase family (IRAK1, 2, M and 4). IRAK1 and IRAK2, known to form Myddosomes with MyD88-IRAK4, mediate TLR7-induced TAK1-dependent NFκB activation. IRAKM was previously known to function as a negative regulator that prevents the dissociation of IRAKs from MyD88, thereby inhibiting downstream signaling. However, we now found that IRAKM was also able to interact with MyD88-IRAK4 to form IRAKM Myddosome to mediate TLR7-induced MEKK3-dependent second wave NFκB activation, which is uncoupled from posttranscriptional regulation. As a result, the IRAKM-dependent pathway only induced expression of genes that are not regulated at the posttranscriptional levels (including inhibitory molecules SOCS1, SHIP1, A20 and IκBα), exerting an overall inhibitory effect on inflammatory response. On the other hand, through interaction with IRAK2, IRAKM inhibited TLR7-mediated production of cytokines and chemokines at translational levels. Taken together, IRAKM mediates TLR7-induced MEKK3-dependent second wave NFκB activation to produce inhibitory molecules as a negative feedback for the pathway, while exerting inhibitory effect on translational control of cytokines and chemokines.

B. Introduction

Toll-like receptors (TLRs) detect microorganisms and protect multicellular organisms from infection by inducing the production of proinflammatory cytokines and chemokines [18, 24, 33, 119-121]. TLRs transduce their signals through the adaptor

molecule MyD88 and members of the IL-1R-associated kinase (IRAK) family, which consists of four members: IRAK1, IRAK2, IRAKM and IRAK4[122-126]. The crystal structure of the MyD88–IRAK4–IRAK2 death domain (DD) complex, referred as Myddosome complex, demonstrated their sequential assembly, in which MyD88 recruits IRAK4 and the MyD88-IRAK4 complex recruits the IRAK4 substrates IRAK2 or the related IRAK1[127]. Subsequently, the IRAK1/2 form complex with TRAF6 and dissociate from the receptor complex to activate cascades of downstream kinases, leading to the activation of transcription factor NFκB [69].On the other hand, IRAKM is believed to function as a negative regulator that prevents the dissociation of IRAK1/2 from receptor complex, thereby inhibiting downstream signaling [128].

We previously reported the co-existence of the two parallel TLR/IL-1R-mediated NFκB activation: TAK1-dependent and MEKK3-dependent, respectively. The TAK1-dependent pathway leads to IKKα/β phosphorylation and IKKγ activation, resulting in classical NFκB activation through IκBα phosphorylation and degradation [129]. The TAK1-independent MEKK3-dependent pathway involves IKKγ phosphorylation and IKKα activation, which leads to NFκB activation through IκBα phosphorylation and subsequent dissociation from NFκB but without IκBα degradation. While TLR/IL-1R regulates gene transcription, they also induce gene expression by stabilizing otherwise unstable mRNAs of pro-inflammatory genes**.** Many cytokine and chemokine mRNA exhibit very short half-lives due to the presence of AU-rich sequence elements (ARE) located within their 3’ untranslated regions [130]. Therefore, the regulation of mRNA stability is an important control of inflammatory gene expression. We have previously reported that the kinase activity of IRAK4 is required for TAK1-dependent NFκB

activation and mRNA stabilization of cytokines and chemokines, but not for MEKK3-dependent NFκB activation [131, 132]. Based on these findings, we propose that IRAK4 mediates IL-1R-TLR-induced receptor-proximal signaling events through its kinase activity to coordinately regulate TAK1-dependent NFκB activation and mRNA stabilization pathways to ensure robust production of cytokines and chemokines during inflammatory response. In addition to mRNA stabilization, TLR signaling is also necessary for efficient and sustained translation of cytokine and chemokine mRNAs [133, 134]. The ratios of LPS-induced cytokine and chemokine mRNAs in translation-active *versus* translation-inactive pools were lower in IRAK2-deficient macrophages compared with wild type macrophages, indicating the requirement of IRAK2 for sustained translation of these mRNAs[135].

In this study, we investigated the functional relationships among IRAK family members and their roles in TLR signaling by analyzing mice deficient in IRAK1, IRAK2 and/or IRAKM. We found that IRAK1 and IRAK2, substrates of IRAK4, are required for TAK1-dependent NFκB activation and mRNA stabilization of cytokines and chemokines, but not for MEKK3-dependent NFκB activation. In contrast to the direct inhibitory role of IRAKM in TLR signaling, IRAKM was able to interact with MyD88-IRAK4 to form IRAKM Myddosome to mediate TAK1-independent MEKK3-dependent NFκB activation in the absence of IRAK1 and IRAK2. This IRAKM-dependent pathway is required for the second wave of TLR7-induced NFκB activation in the presence of IRAK1/IRAK2, which is uncoupled from posttranscriptional regulation. Thus, the IRAKM-dependent pathway only induced expression of genes that are not regulated at the posttranscriptional levels (including inhibitory molecules SOCS1, SHIP1, A20 and IκBα), exerting an overall

inhibitory effect on inflammatory response. Taken together, this study for the first time demonstrates unique positive engagement of IRAKM in transmitting signaling upon TLR activation, providing important insight into the mechanistic roles of IRAKM in modulating TLR signaling.

C. Results

IRAKM mediates TLR-induced MEKK3-dependent NFκB activation in the absence of IRAK1 and IRAK2

Although IRAKM has been implicated as a negative regulator in TLR signaling, the precise molecular mechanism for how IRAKM participates and modulates TLR signaling remains unclear. We recently found that substantial TLR7-induced NFκB activation was retained in IRAK1/2-double deficient (DKO) BMDMs, whereas completely abolished in MyD88- or IRAK4-deficient BMDMs (**Fig. 5A and data not shown**). These results suggest that MyD88-IRAK4 either themselves or in conjunction with IRAKM can mediate NFκB activation in IRAK1/2-DKO-BMDMs. To determine the role of IRAKM in this process, we compared TLR7-mediated NFκB activation in IRAK1/2-DKOwith that in IRAK1/2/M-deficient (TKO) BMDMs.TLR7-mediated NFκB activation was completely abolished in IRAK1/2/M-TKO-BMDMs, indicating the importance of IRAKM in mediating TLR7-dependent NFκB activation in the absence of IRAK1 and IRAK2 (**Fig. 5A**).

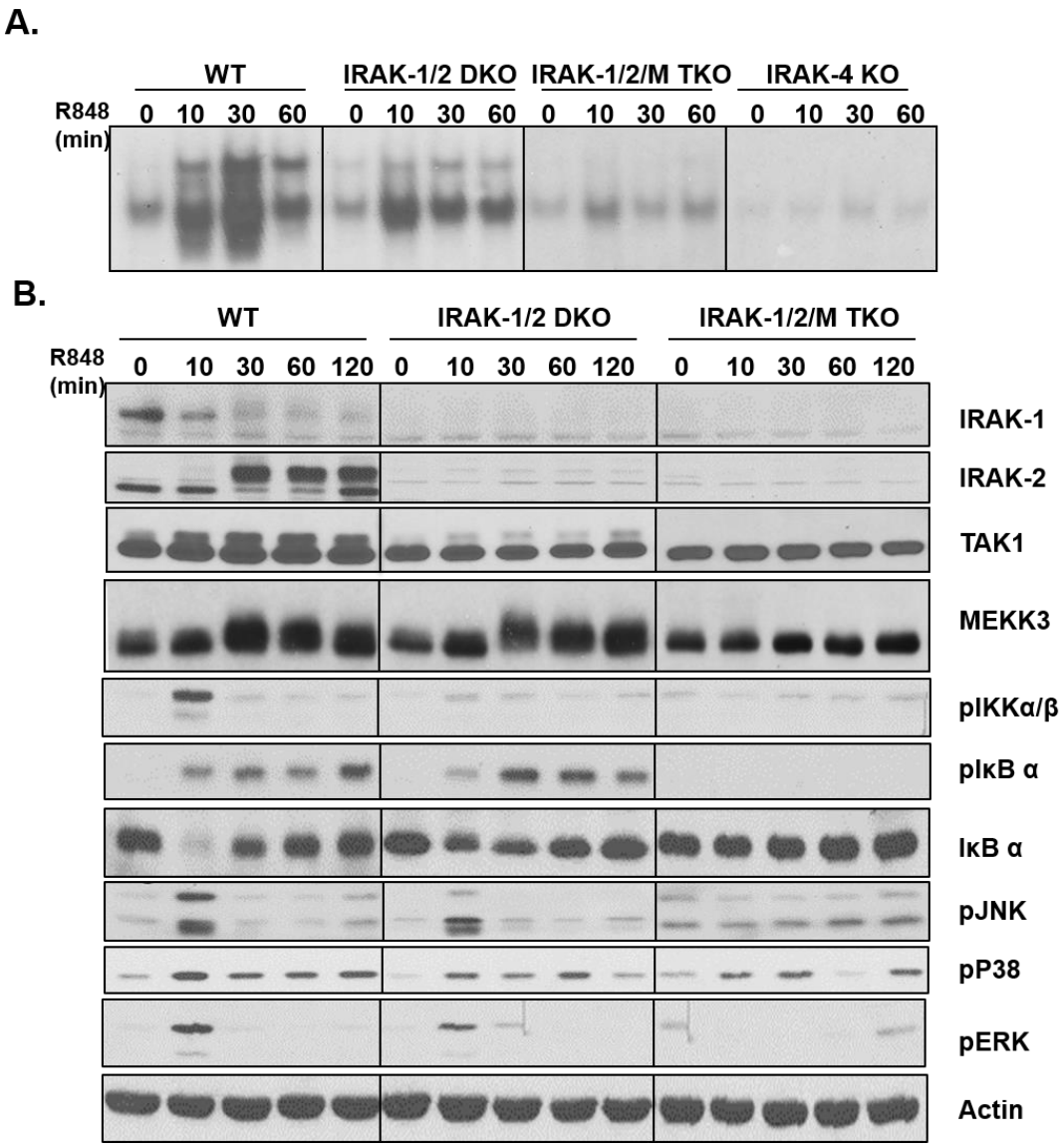

Figure 5. IRAKM mediates TLR7-induced NFκB activation in the absence of IRAK1 and IRAK2. A. Nuclear extracts prepared from wild-type (WT), IRAK1/2-double deficient (IRAK1/2 DKO), IRAK1/2/M-triple deficient (IRAK1/2/M TKO), IRAK4-deficient (IRAK4 KO) bone marrow-derived macrophages (BMDMs) untreated or treated

with TLR7 ligand R848 (1μg/ml) for the indicated times were analyzed by electrophoresis mobility shift assay using an NFκB-specific probe. **B.** Cell lysates from wild-type (WT), IRAK1/2- double deficient (IRAK1/2 DKO), IRAK1/2/M-triple deficient (IRAK1/2/M TKO) bone marrow-derived macrophages (BMDMs) untreated or treated with TLR7 ligand R848 (1μg/ml) for the indicated times were analyzed by Western blot analysis with antibodies against IRAK1, IRAK2, p-IKKα/β, TAK1, MEKK3, p-IκBα, IκBα, p-JNK, p-p38, p-ERK and actin. The experiments were repeated for five times with similar results.

We previously uncovered two parallel TLR-mediated MyD88/IRAK4-dependent signaling pathways for NFκB activation, TAK1-dependent and independent, respectively [129]. The TAK1-dependent pathway leads to IKKα/β phosphorylation and IKKα activation, resulting in classical NFκB activation through IκBα phosphorylation and degradation. The TAK1-independent pathway involves activation of MEKK3 and IKKα, resulting in NFκB activation through IκBα phosphorylation and subsequent dissociation from NFκB but without IκBα degradation. TLR7-induced TAK1 activation (shown as slower mobility shift bands) was greatly reduced in IRAK1/2-DKO-BMDMs, while IRAK1/2-double deficiency also substantially decreased TLR7-induced IKKα/β phosphorylation, indicating the important role of IRAK1/IRAK2 in mediating TAK1-dependent NFκB activation.TLR7-induced TAK1-mediated IKK activation leads to the phosphorylation and degradation of IκBα. Indeed, TLR7-induced IκBα degradation was attenuated in theIRAK1/2-DKO-BMDMs.

However, consistent with the NFκB gel-shift assay, TLR7-induced IκBα phosphorylation was still retained in IRAK1/2-DKO-BMDMs, which was completely abolished in IRAK1/2/M-TKO-BMDMs, indicating the importance of IRAKM in mediating TLR7-induced TAK1-independent NFκB activation in IRAK1/2-DKO-BMDMs (**Fig. 5B**). Importantly, through co-immunoprecipitation we found that IRAKM

formed a complex with MEKK3, but not with TAK1 (**Fig. 5A-B**). Furthermore, TLR7-induced MEKK3 modification was still retained in IRAK1/2-DKO-BMDMs, whereas abolished in IRAK1/2/M-TKO-BMDMs (**Fig. 5A**). Taken together, these results suggest that IRAKM probably mediates TLR7-induced NFκB activation through the TAK1-independent MEKK3-dependent pathway in the absence of IRAK1 and IRAK2. In addition to NFκB activation, TLR7-mediated JNK and ERK phosphorylation were completely abolished in IRAK1/2/M-TKO-BMDMs, although some levels of phosphorylation of p38 was still retained. Importantly, this positive signaling role of IRAKM was not restricted to TLR7. Similarly, TLR2- and TLR9-induced phosphorylation of IκBα were still retained in IRAK1/2-DKO-BMDMs, which was completely abolished in IRAK1/2/M-TKO-BMDMs, implicating the participation of IRAKM in TLR2- and TLR9-mediated signaling. However, it is important to point out, while TLR9-induced IκBα phosphorylation in IRAK1/2-DKO-BMDMs was comparable to that in wild-type cells, TLR2-induced IκBα phosphorylation in IRAK1/2-DKO-BMDMs was substantially reduced compared to that in wild-type cells, suggesting differential utilization of IRAKM by different TLRs (**Fig. 7**).

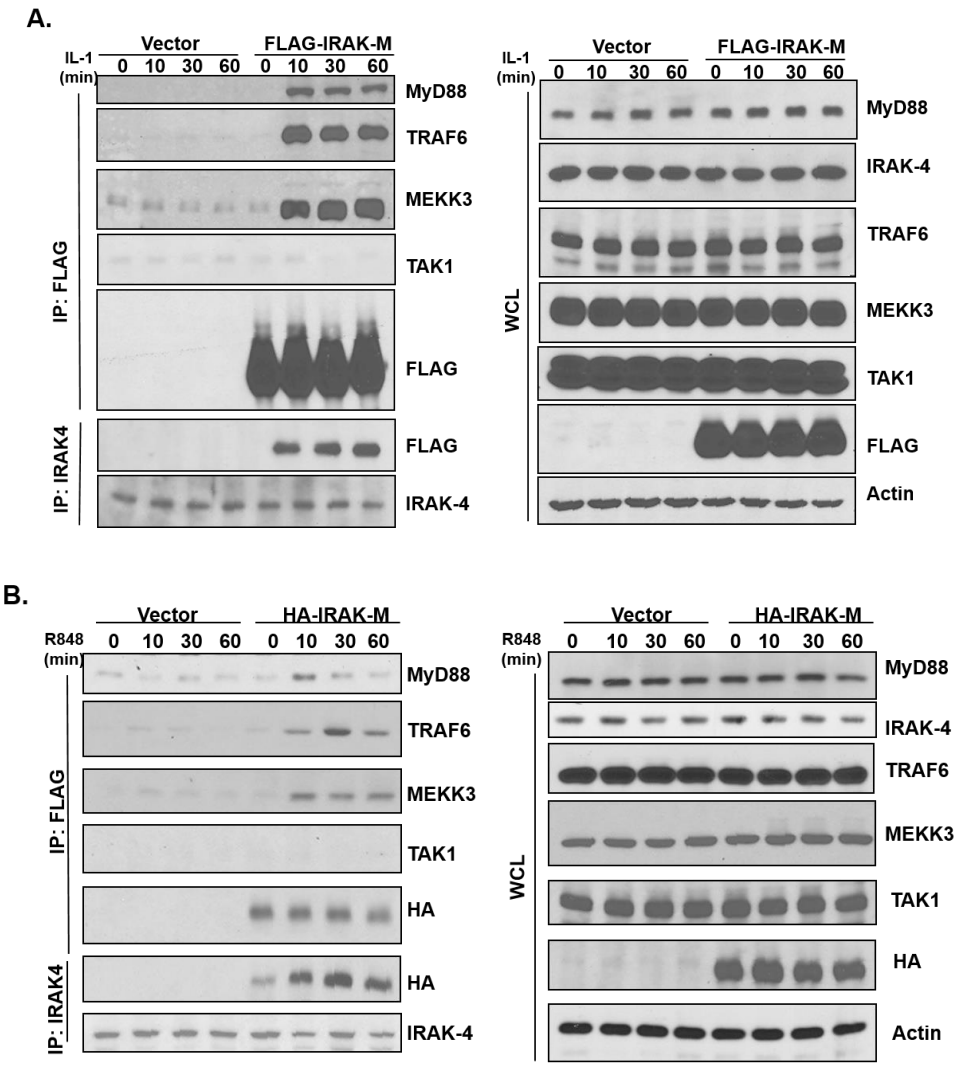

Figure 6. IRAKM forms Myddosome with MyD88-IRAK4 to mediate signaling through MEKK3 and TRAF6. A. IRAKM-deficient mouse embryonic fibroblast(MEFs) infected with retroviruses containing empty vector construct (Vector) and FLAG-IRAKM were treated with IL-1β (1ng/ml) for the indicated times, followed by immunoprecipitation (IP) with anti-FLAG antibody and analyzed by Western blot analyses using antibodies against MyD88, IRAK4, TRAF6, MEKK3, TAK1 and FLAG. The whole cell lysates (WCL) were subjected to the same Western analyses, including actin as a control. The experiments were repeated for five times with similar results. B. IRAK1/2/M-triple deficient (IRAK1/2/M TKO) BMDMs infected with adenovirus containing empty vector construct (Vector) and HA-tagged IRAKM (HA-IRAKM) were treated with R848 (1ng/ml) for the indicated times, followed by immunoprecipitation (IP) with anti-HA antibody and analyzed by Western blot analysis with antibody against MyD88, IRAK4, TRAF6,

MEKK3, TAK1 and FLAG. The whole cell lysates (WCL) were subjected to the same Western analyses, including actin as a control. The experiments were repeated for five times with similar results

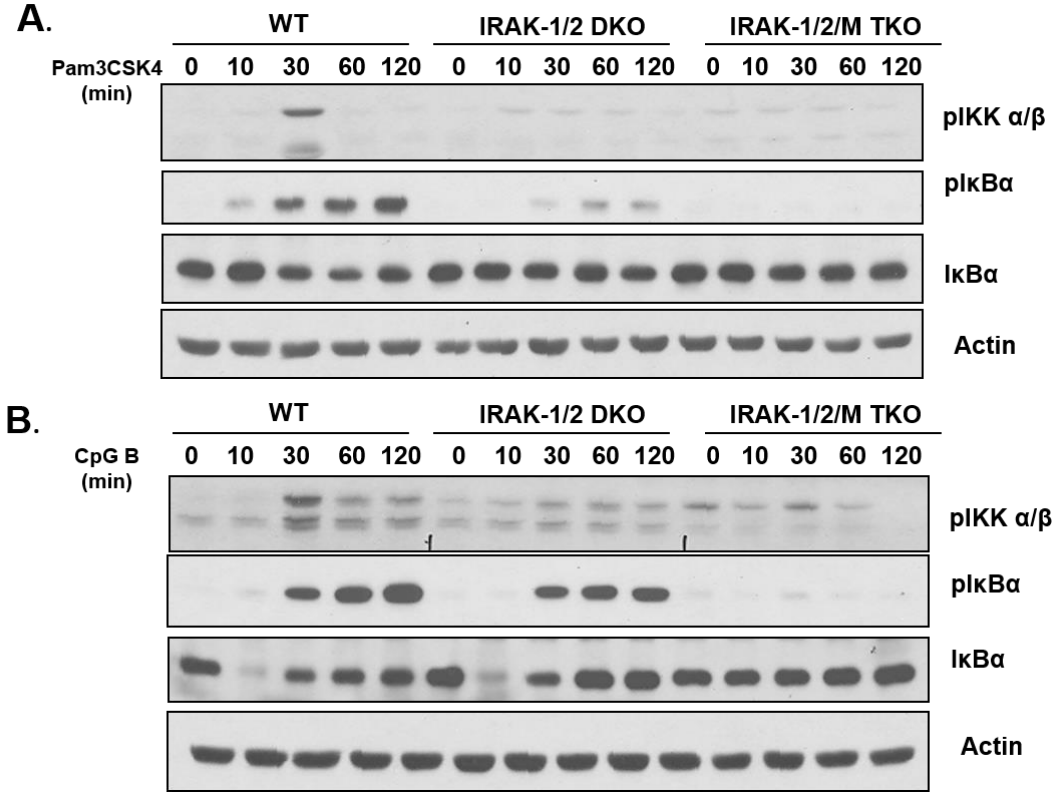

Figure 7. IRAKM mediates TLR2/9-induced NFκB activation in the absence of IRAK1 and IRAK2. A. Cell lysates from wild-type (WT), IRAK1/2- double deficient (IRAK1/2 DKO), IRAK1/2/M-triple deficient (IRAK1/2/3 TKO) bone marrow-derived macrophages (BMDMs) untreated or treated with TLR2 ligand Pam3CSK4 (200ng/ml) for the indicated times were analyzed by Western blot analysis with antibodies against p-IKKα/β, p-IκBα, IκBα, and actin. The experiments were repeated for five times with similar results. **B.** Cell lysates from wild-type (WT), IRAK1/2- double deficient (IRAK1/2 DKO), IRAK1/2/M-triple deficient (IRAK1/2/3 TKO) bone marrow-derived macrophages (BMDMs) untreated or treated with TLR9 ligand CpG B (1μg/ml) for the indicated times were analyzed by Western blot analysis with antibodies against p-IKKα/β, p-IκBα, IκBα, and actin. The experiments were repeated for five times with similar results.

IRAKM mediates IL-1R-induced NFκB activation through formation of Myddosome with MyD88-IRAK4

Lin et al recently reported the crystal structure of the MyD88–IRAK4–IRAK2 death domain (DD) complex, which revealed a left-handed helical oligomer that consists of 6 MyD88, 4 IRAK4 and 4 IRAK2 DDs[127]. This helical signaling tower is referred as Myddosome complex and its assembly is sequential, in which MyD88 recruits IRAK4 and the MyD88-IRAK4 complex recruits the IRAK4 substrates IRAK2 or the related IRAK1. This study has provided great insight into how IL-1R and also TLRs utilize adaptor molecule MyD88 to recruit IRAKs to mediate its signaling. The question here was how TLR/IL-1R utilizes IRAKM to mediate signaling in the absence of IRAK1 and IRAK2. Since MyD88- or IRAK4-deficient BMDMs had completely abolished TLR/IL-1R-mediated NFκB activation, indicating that TLR/IL-1R-induced IRAKM-mediated NFκB activation in the IRAK1/2-DKO-BMDMs must be MyD88-IRAK4-dependent. In the light of the crystal structure of MyD88-IRAK4-IRAK2 DD Myddosome, we hypothesized that IRAKM might also be capable of forming a complex with MyD88-IRAK4 to mediate signaling. We indeed detected IL-1-induced interaction of IRAKM with MyD88, IRAK4, TRAF6 and MEKK3, but not with TAK1 when we restored IRAKM-deficient MEFs with tagged-IRAKM (**Fig. 6A**). Furthermore, TLR-induced interaction of IRAKM with MyD88, IRAK4, TRAF6 and MEKK3 (but not with TAK1) can take place in the absence of IRAK1 and IRAK2 when we introduced tagged-IRAKM into the IRAK1/2/M-TKO-BMDMs (**Fig. 6B**). These data indicate the formation of IRAKM Myddosome (MyD88-IRAK4-IRAKM), which is probably responsible for TLR-induced IRAKM-mediated

NFκB activation in the absence of IRAK1 and IRAK2 through the MEKK3-dependent, but not the TAK1-dependent pathway.

The N-terminal DD of IRAKM shares a considerable sequence identity to those of other members of the IRAK family. The similarity of topologies within this region (DD) of IRAKM to the region of IRAK2 suggested that this region of IRAKM may adopt a similar protein fold. To test this prediction, we built a three-dimensional model of the region of IRAKM DD (residues 14-105). The model has secondary structure elements similar to those of other IRAK DDs with a hexahelical bundle [136]. The model places a cluster of hydrophilic residues on the surface that is reminiscent to that of IRAK2 DD when bound to IRAK4 DD[127]. IRAK4-binding residues with IRAK2 are highly conserved in IRAKM DD, suggesting that IRAKM is assembled with IRAK4 DD in a similar manner to IRAK2 (**Fig. 8**). In particular, the conserved W74 (W62 in IRAK2) in helix H4 of the IRAKM DD is likely a key residue for interacting with IRAK4 DD. The model also a conserved salt bridge between E71 (E59 in IRAK2) in helix H4 of the IRAKM and R54 in IRAK4, suggesting a critical role of the helix H4 segment in IRAKM for recognizing IRAK4. Interestingly, Q78 in IRAKM is a polar residue and distinct from the equivalent residue in IRAK2 (M66) but the hydrophobic side chain portion of Q78 seems to make the hydrophobic interaction with IRAK4 whereas the hydrophilic part of Q78 in IRAKM may interact with the backbone oxygen atoms of F25, E92, and F93 in IRAK4.

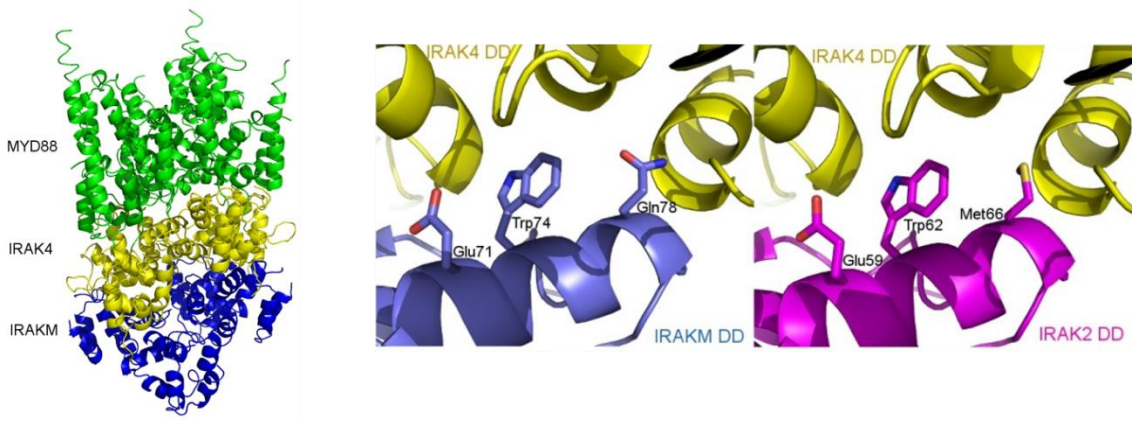

Figure 8. Computer modeling of IRAKM Myddosome complex. Conserved binding interface in the interaction of IRAKM with IRAK4 (Left). A three-dimensional model of the MyD88-IRAK4-IRAKM Myddosome complex (Middle). A putative binding interface in the death domain (DD) between IRAKM (blue) and IRAK4 (yellow), as guided by molecular modeling study. The helix H4 of IRAKM DD seems to be a critical element for the interaction with IRAK4 DD. Putative binding residues in the helix H4 in the IRAKM in the interaction with IRAK4 are highlighted. Specifically, the surface exposed E71 on the helix H4 of IRAKM makes a salt bridge with R54 from one IRAK4 DD molecule, and this salt bridge formation is conserved in the IRAK2 DD/IRAK4 DD interface. The E71-mediated IRAKM DD/IRAK4 DD interaction is further stabilized by a hydrophilic interaction with Q29 from another neighboring IRAK4 DD molecule upon the Myddosome formation. W74 of IRAKM is situated in the center of the helix H4 and packs against a hydrophobic environment that is created by two IRAK4 DD monomers upon Myddosome formation. Q78 in IRAKM may play an important role both in the hydrophilic and hydrophobic interactions with IRAK4 (see text). The significance of these side chains of IRAKM in the interaction with IRAK4 was verified by our site-directed mutagenesis study (Right). The interaction interface in the DD between IRAK2 (magenta) and IRAK4 (yellow), as evidenced by crystallographic study.

To test the proposed binding interface, we made individual and combined point mutants of IRAKM in retroviral vector. We have previously shown that IRAKM was able to restore IL-1-induced NFκB activation in 293-derived IRAK1-deficient cells (293-I1A cells), in which IRAKM and IRAK2 expression were not detectable (absent or very low) [125]. Therefore, this cell line was used to test the ability of IRAKM to form Myddosome

in response to IL-1 stimulation. Fig 2C shows that E71A and Q78G each showed partial defect whereas the combination of these two mutations (E71A/Q78G) drastically decreased the binding of IRAKM to IRAK4. Furthermore, the W74A IRAKM mutant completely lost the interaction with IRAK4 (**Fig. 9A**). We next used this cell line to examine the ability of IRAKM mutants in mediatingIL-1-dependent NFκB activation. IRAKM wild-type and mutants were co-transfected with NFκB-dependent luciferase reporter construct (E-selectin-Luc) into 293-I1A cells, followed by IL-1 treatment and luciferase assay. The W74A IRAKM mutant completely lost the ability to activate NFκB in 293-I1A cells upon IL-1 stimulation (**Fig. 9B**). On the other hand, while E71A and Q78G exhibited partial defect, the combination of these two mutations (E71A/Q78G) greatly decreased the IL-1-induced NFκB-dependent luciferase activity in 293-I1A cells (**Fig. 9B**). The same results were obtained from the analysis of the IRAKM mutants in NFκB electrophoretic mobility shift assay (**Fig. 9C**). Consistent with its ability in mediating IL-1-induced NFκB activation, IRAKM was also able to restore IL-1-induced IL-8 and TNFα gene expression in 293-I1A cells (**Fig. 9D**). Importantly, W74A and E71A/Q78G IRAKM mutants failed to restore the IL-8 and TNFα gene expression in 293-I1A cells in response to IL-1 stimulation (**Fig. 9D**). Moreover, since we predict the hydrophilic part of Q78 in IRAKM may interact with the backbone oxygen atoms of F25 in IRAK4, we generated the IRAK4 F25D mutant. When tested in IRAK4-deficient cells, this F25D mutant showed decreased interaction with IRAKM compared with wild-type IRAK4 upon IL-1 stimulation (**Fig. 10**), confirming the critical contact between Q78 in IRAKM and F25 in IRAK4.

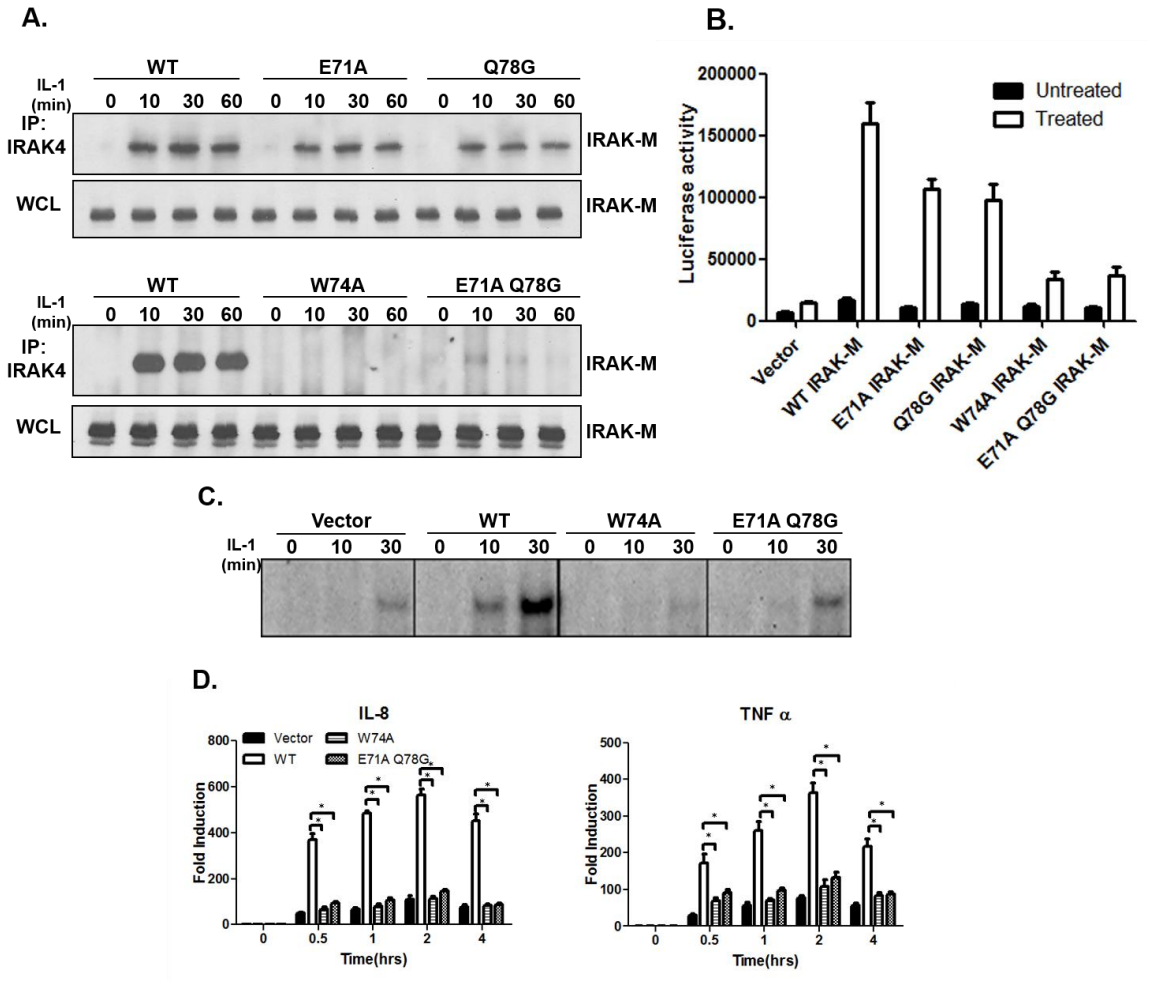

Figure 9. Restoration of IRAKM wild-type and mutants in 293-I1A cell. A. IRAK1-deficient 293-IL1R (I1A) cells transfected with empty vector, FLAG-tagged wild-type IRAKM (WT), FLAG-tagged IRAKM mutants (F18A, E71A, Q78A, W74A and E71A/Q78G) were treated with IL-1β (1ng/ml) for the indicated times, followed by immunoprecipitation (IP) with anti-IRAK4 antibody and analyzed by Western blot analysis with antibody against FLAG to detect IRAKM. **B.** IRAKM wild-type and mutants (F18A, E71A, Q78A, W74A and E71A/Q78G) were transiently co-transfected with NFκB-dependent luciferase reporter construct (E-selectin-Luc) into IRAK1-deficient 293-IL1R (293-I1A) cells, followed by IL-1 (1ng/ml) treatment for 6 hours and luciferase assay. The experiment was repeated three times. Data represent mean ± SEM; *, $p<0.05$(two tailed t-test). **C.** Nuclear extracts prepared from 293-I1A cells transiently co-transfected with wild-type (WT), W74A and E71A/Q78A untreated or treated with IL-1β (1ng/ml) for the indicated times were analyzed by electrophoretic mobility shift assay using an NFκB specific probe. **D.** IRAK1-deficient 293-IL1R (I1A) cells transiently transfected with empty expression vector, wild-type IRAKM, and IRAKM mutants (W74A and E71A/Q78G) were treated with IL-1β (1ng/ml) for the indicated times. Total RNAs from these cells were subjected to real-time PCR analysis for the levels of human IL-8 and TNFα

mRNAs. The experiments were repeated three times. Data represent mean ± SEM; *, $p<0.05$ (two tailed t-test).

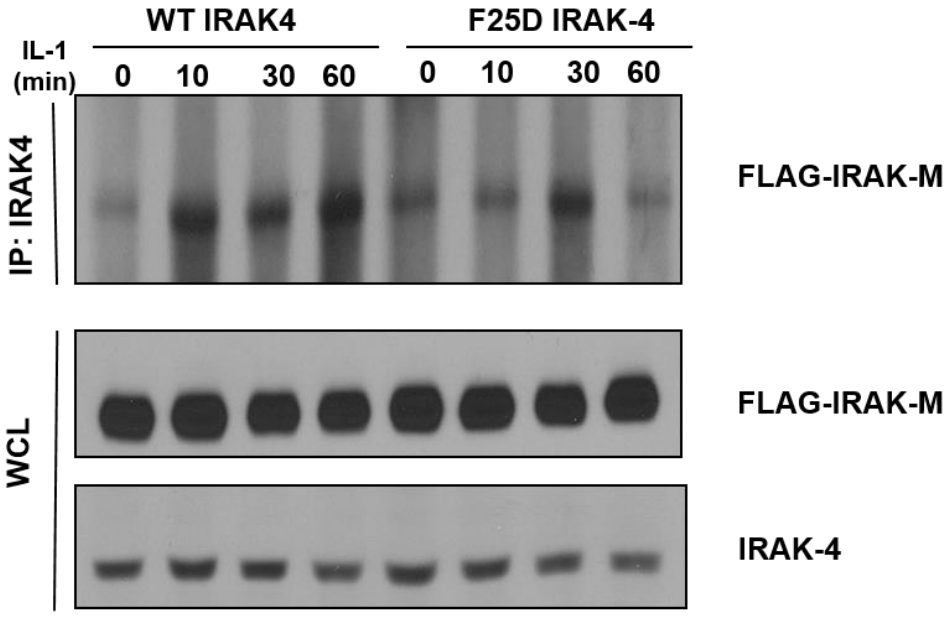

Figure 10. F25 in IRAK4 is required for the interaction with IRAKM. IRAK4 wild-type (WT) and F25D mutant (F25D) were retrovirally expressed together with FLAG-tagged IRAKM in IRAK4 deficient fibroblasts. Cells were treated with IL-1β (1ng/ml) for the indicated times, followed by immunoprecipitation (IP) with IRAK4 antibody and analyzed by Western blot analyses using antibodies against FLAG and IRAK4. WCL (whole cell lysates). The experiments were repeated for five times with similar results.

We then confirmed the binding interface of IRAKM with IRAK4 in response to TLR7 stimulation. IRAKM wild-type and mutants were expressed in IRAK1/2/M-TKO-BMDMs by adenovirus infection. Consistent with the results for the IL-1 response, wild-type IRAKM was able to interact with IRAK4 and restored TLR7-induced NFκB activation in IRAK1/2/M-TKO-BMDMs, whereas W74A mutant lost its ability to interact with IRAK4 and failed to mediate NFκB activation. While E71 and Q78G showed partial reduction, the combinational mutant E71A/Q78G was unable to interact with IRAK4 with abolished TLR7-induced NFκB activation (**Fig. 11A-B**). Furthermore, W74A and

E71A/Q78G mutants also failed to restore CXCL1, TNFα and IL-6 gene expression in IRAK1/2/M-TKO-BMDMs upon TLR7 stimulation (**Fig. 11C**). Taken together, these results provide strong supporting evidence for the interaction between DDs of IRAKM and IRAK4 and demonstrate that this interaction is critical for IRAKM to mediate IL-1R/TLR-induced NFκB activation.

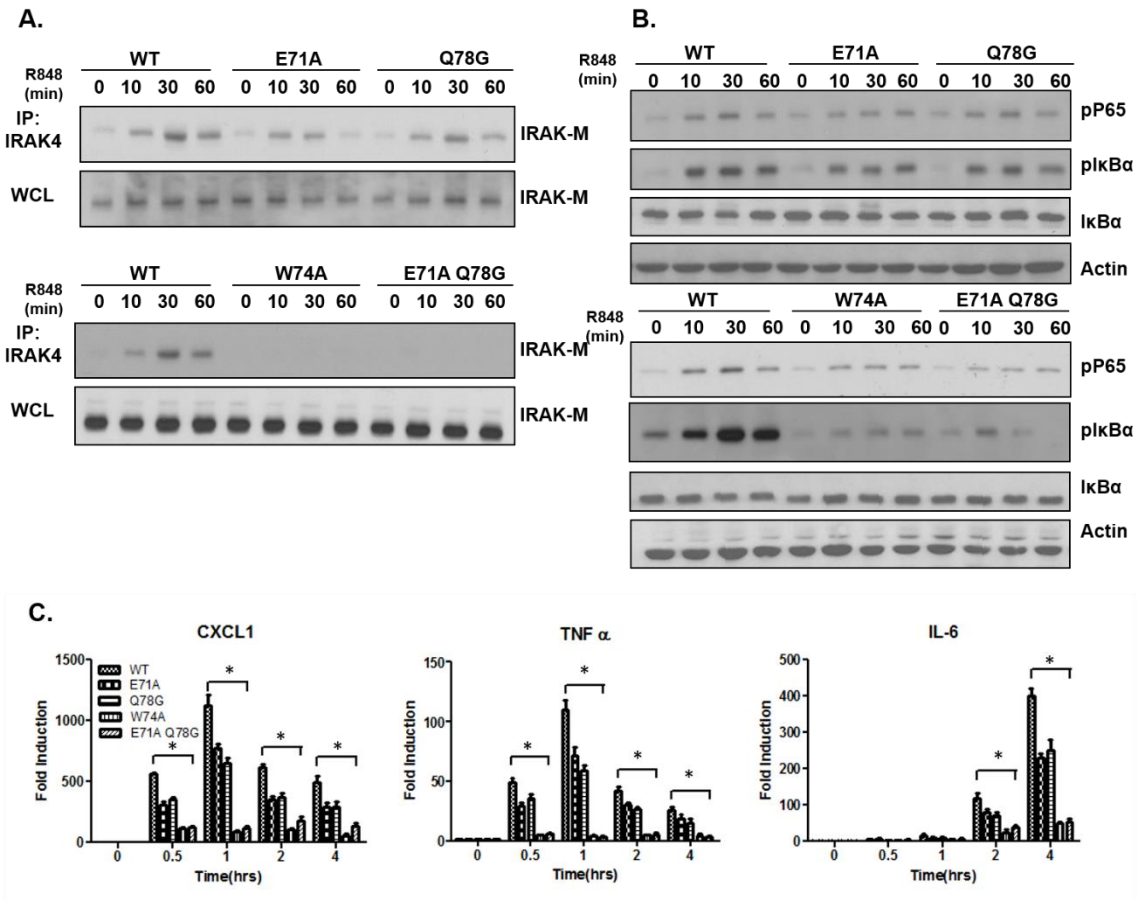

Figure 11. Restoration of wild-type and IRAKM mutants in IRAK1/2/M-triple deficient cells. A. IRAK1/2/M-triple deficient (IRAK1/2/M TKO) BMDMs infected with adenovirus expressing HA-tagged wild-type IRAKM (WT) and HA-tagged IRAKM mutants (F18A, E71A, Q78A, W74A and E71A/Q78G) were treated with R848 (1ng/ml) for the indicated times, followed by immunoprecipitation (IP) with anti-IRAK4 antibody and analyzed by Western blot analysis with antibody against HA to detect IRAKM. The experiments were repeated for five times with similar results. **B.** IRAK1/2/M-triple deficient (IRAK1/2/M TKO) BMDMs infected with adenovirus expressing HA-tagged wild-type IRAKM (WT) and HA-tagged IRAKM mutants (F18A, E71A, Q78A, W74A

and E71A/Q78G) were treated with R848 (1ng/ml) for the indicated times, followed by Western blot analyses with antibodies against p-p65 p-IκBα, IκBα, and actin. The experiments were repeated for five times with similar results. **C.** IRAK1/2/M-triple deficient (IRAK1/2/M TKO) BMDMs infected with adenovirus expressing HA-tagged wild-type IRAKM (WT) and HA-tagged IRAKM mutants (F18A, E71A, Q78A, W74A and E71A/Q78G) were treated with R848 (1ng/ml) for the indicated times. Total RNAs from these cells were subjected to real-time PCR analysis for the levels of mouse CXCl1, TNFα and IL-6 mRNAs. The experiment was repeated three times. Data represent mean ± SEM; *, $p<0.05$(two tailed t-test).

IRAKM deficiency resulted in decreased second wave TLR7-induced NFκB activation in the presence of IRAK1 and IRAK2

Previous studies suggested that IRAKM functions as a negative regulator that prevents the dissociation of IRAKs from MyD88, thereby inhibits all downstream signaling events including NFκB activation [128]. Considering how IRAKM can form Myddosome and is capable of mediating TLR/IL-1R signaling in the absence of IRAK1/IRAK2, we decided to re-investigate the impact of IRAKM single deficiency on TLR7-mediated signaling. To our surprise, IRAKM deficiency decreased TLR7-induced late phase NFκB activation (after 0.5h) in a gel-shift assay (**Fig. 12A**). The TAK1-dependent downstream signaling events (phosphorylation of TAK1 and IKKα/β and IκBα degradation) were similar or slightly enhanced in IRAKMKO-BMDMs compared to that in control cells. However, whereas TLR7-induced IκBα and p65 phosphorylation were comparable at early times (within 10min), they were substantially reduced at later times (after 30min) (**Fig. 12B**). These results suggest that IRAKM Myddosome contributes to the second wave of TLR7-induced NFκB activation in the presence of IRAK1 and IRAK2, probably through the TAK1-independent pathway.

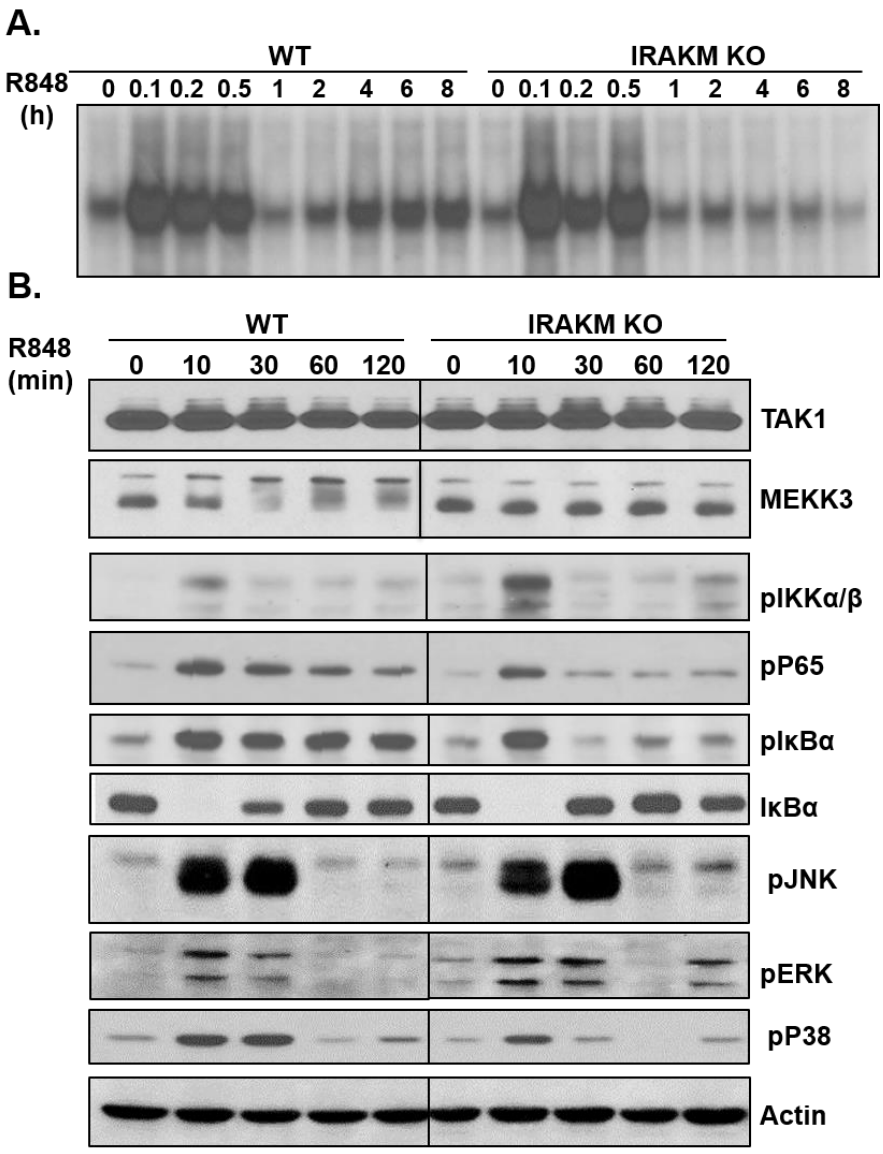

Figure 12. The role of IRAKM in second wave of TLR-mediated NFκB activation. A. Nuclear extracts prepared from wild-type (WT), and IRAKM deficient (MKO) BMDMs untreated or treated with R848 (1μg/ml) for the indicated times were analyzed by electrophoretic mobility shift assay using an NFκB specific probe. The experiments were repeated for five times with similar results. **B.** Cell lysates from wild-type (WT), and IRAKM deficient (MKO) BMDMs untreated or treated with R848 (1μg/ml) for the indicated times were analyzed by Western blot analyses with antibodies against TAK1, MEKK3, p-IKKα/β, p-p65, p-IκBα, IκBα, p-JNK, p-ERK, p-p38 and actin. The experiments were repeated for five times with similar results.

Our previous studies showed MG132, which inhibits proteasome-dependent protein degradation, can block TLR-mediated TAK1-depenent pathway (phosphorylation of TAK1 and IKKα/β and IκBα degradation), since IRAK1 ubiquitination and degradation is critical for TAK1-dependent downstream signaling [137] (**Fig. 13A**). On the other hand, MG132 does not block the TLR-induced MEKK3-dependent pathway, as evident by intact TLR-induced phosphorylation of MEKK3 and IκBα; and substantial residual JNK, p38 and ERK activation after MG132 treatment. Therefore, to confirm the role of IRAKM in TLR7-induced TAK1-independent MEKK3-dependent signaling, we examined the impact of MG132 on TLR7-induced signaling in IRAKMKO BMDMs. We indeed found that pretreatment of MG132 greatly reduced TLR7-induced phosphorylation of MEKK3, IκBα, JNK, p38 and ERK in IRAKM-deficient BMDMs compared to its impact on wild-type control cells. These results showed that IRAKM-mediated signaling becomes the dominant pathway when the TAK1 pathway is blocked by MG132, supporting that IRAKM Myddosome might mediate the second wave of TLR7-induced NFκB activation through the TAK1-independent MEKK3-dependent pathway (**Fig. 13B**). To confirm the role of MEKK3 in IRAKM-mediated NFκB activation, IRAKM was co-transfected with NFκB-dependent luciferase reporter construct (E-selectin-Luc) into scramble shRNA-transfected or MEKK3 knock-down 293-I1A cells, followed by IL-1 treatment and luciferase assay. IL-1-induced IRAKM-mediated NFκB activation was greatly reduced in MEKK3 knock-down cells compared to that in the control cells (**Fig. 14C&D).** Taken together, these data support that IRAKM Myddosome-mediated NFκB activation is through the MEKK3-dependent pathway.

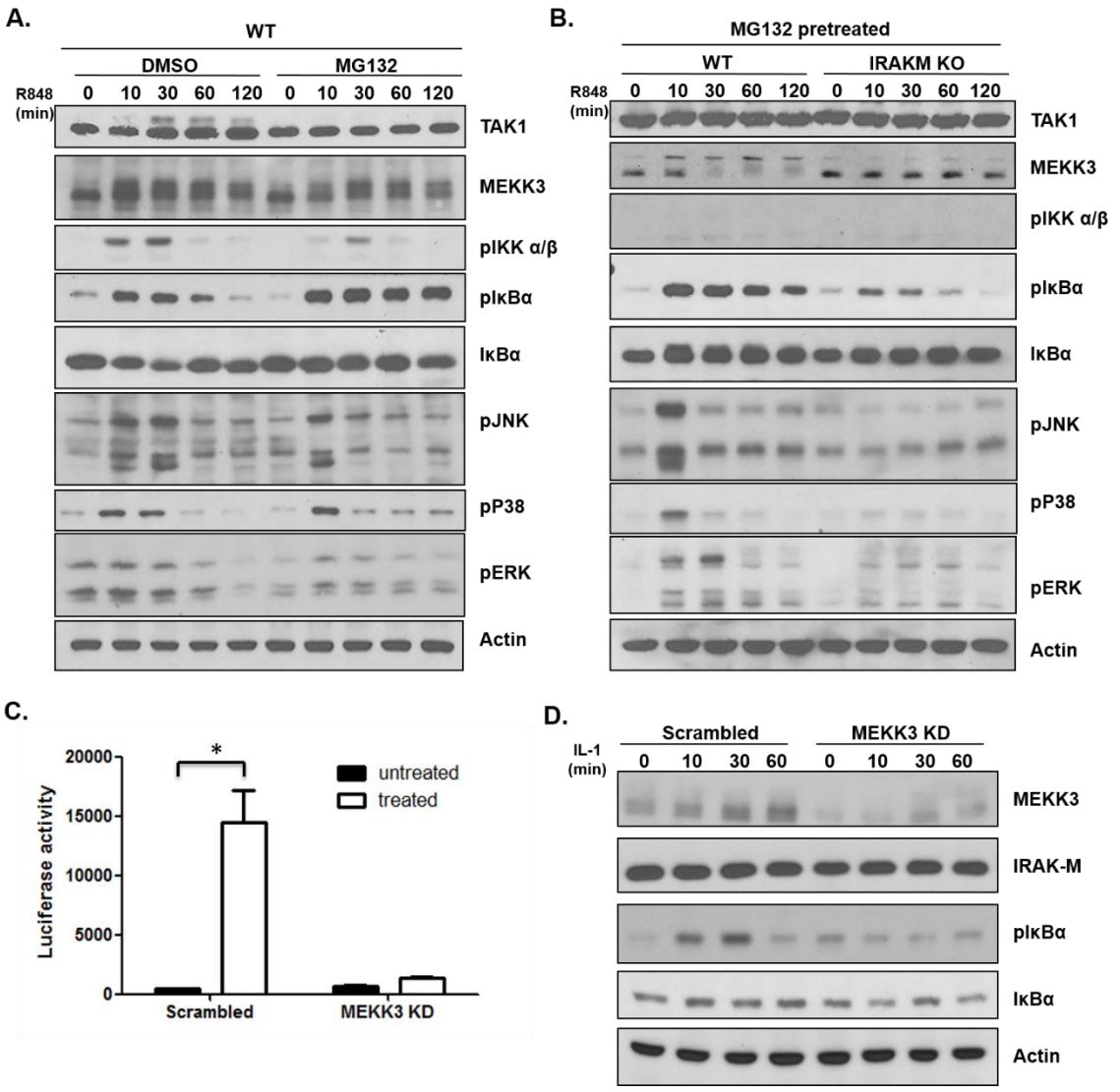

Figure 13. IRAKM-mediated NFκB activation is dependent on MEKK3. A. BMDMs from wild-type (WT) were pre-treated with/without MG132 (20μM) for 2 hours followed by R848 (1μg/ml) treatment for the indicated time. **B.** BMDMs from wild-type (WT) and IRAKM deficient (MKO) mice were pre-treated with MG132 (20μM) for 2 hours followed by R848 (1μg/ml) treatment for the indicated time. Western blot analysis was performed by antibodies againstTAK1, MEKK3, p-IKKα/β, p-IκBα, IκBα, p-JNK, p-ERK, p-p38 and actin. The experiments were repeated for five times with similar results. **C.** MEKK3 knock-down (MEKK3 KD) cells and control (Scrambled) cells were transiently co-transfected with IRAKM and NFκB-dependent luciferase reporter construct (E-selectin-Luc) followed by IL-1 (1ng/ml) treatment for 6 hours and luciferase assay. The experiments were repeated three times. Data represent mean ± SEM; *, $p<0.05$(two tailed t-test). **D.** FALG-tagged IRAKM transfected MEKK3 knock-down (MEKK3 KD) cells and control (Scrambled) cells were treated with IL-1 (1ng/ml) for indicated time, followed by Western blot

analyses with antibodies against MEKK3, FLAG, p-IκBα, IκBα and actin. The experiments were repeated for five times with similar results.

IRAKM is required for TLR7-induced expression of inhibitory molecules SHIP1, SOCS1, A20 and IκBα

One important question is then whether TLR-induced IRAKM-mediated signaling has any impact on gene expression.IRAK1/IRAK2 double deficiency results insubstantial impairment of TLR-mediated production of pro-inflammatory cytokines and chemokines [138]. It is important to note that the TLR-induced IRAKM-mediated signaling events in IRAK1/2-DKO-BMDMs allowed the induction of cytokines and chemokines mRNAs at early times (peak at 30min), such as TNFα and CXCL1 (KC), which was completely abolished in IRAK1/2/M-TKO-BMDMs (**Fig. 14A**). However, since IRAK2 is required for posttranscriptional control of the TNFα and CXCL1 (KC) mRNAs, we failed to detect TNFα and CXCL1 (KC) mRNAs at later times (after 1 hour) and thus little protein production of TNFα and CXCL1 (KC) in IRAK1/2-DKO-BMDMs (**Fig. 14B**).Therefore, the IRAK1/IRAK2-mediated coupling of the TAK1-dependent NFκB activation and posttranscriptional regulation plays an essential role in the production of these pro-inflammatory cytokines and chemokines. Although TLR7-induced IRAKM-mediated signaling in IRAK1/2 DKO-BMDMs can mediate the induction of cytokines and chemokines mRNAs at early times, this IRAKM-mediated pathway alone in the absence of IRAK1 and IRAK2 is insufficient to induce the production of cytokines and chemokines that are under the posttranscriptional control. Similar results were obtained for TLR2 and TLR9 signaling pathways (**Fig. 15**).

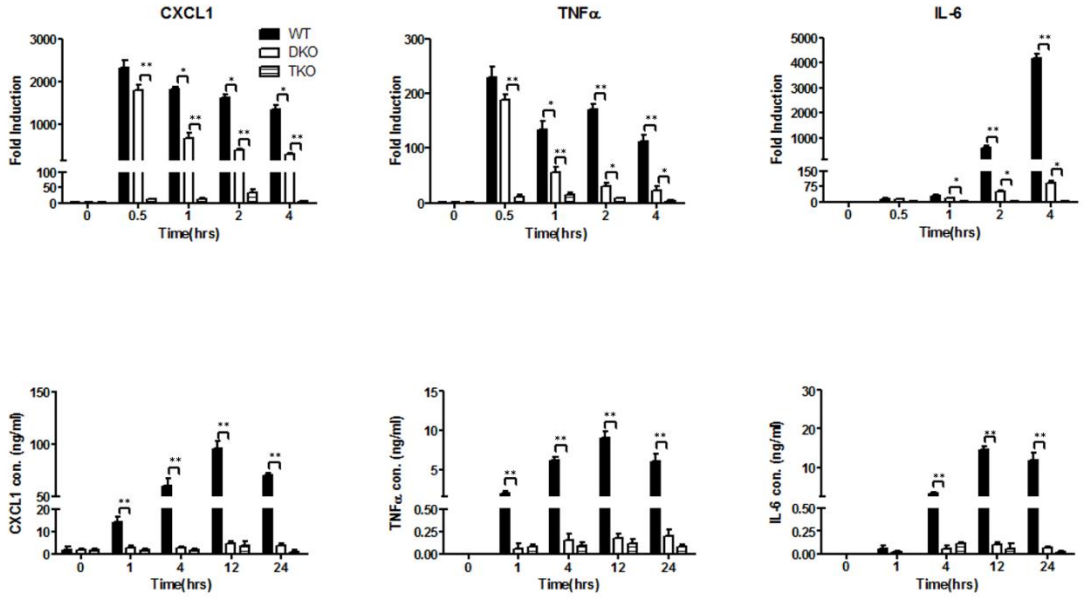

Fig. 14. IRAK1 and IRAK2 are required for TLR7-induced pro-inflammatory gene expression. A. Total mRNAs from BMDMs of wild-type (WT), IRAK1/2-double deficient (DKO) and IRAK1/2/M-triple deficient (TKO) mice treated with R848 (1μg/ml) for the indicated times, were subjected to RT-PCR analyses for the levels of CXCL1, IL-6 and TNFα expression. **B.** BMDMs from wild-type (WT), IRAK1/2 double deficient (DKO) and IRAK1/2/M triple deficient (TKO) mice were treated with R848 (1μg/ml) for the indicated time. CXCL1, IL-6 and TNFα concentrations in the supernatant were measured by ELISA. The experiments were repeated three times. Data represent mean ± SEM; **, P<0.01; *, p<0.05(two tailed t-test).

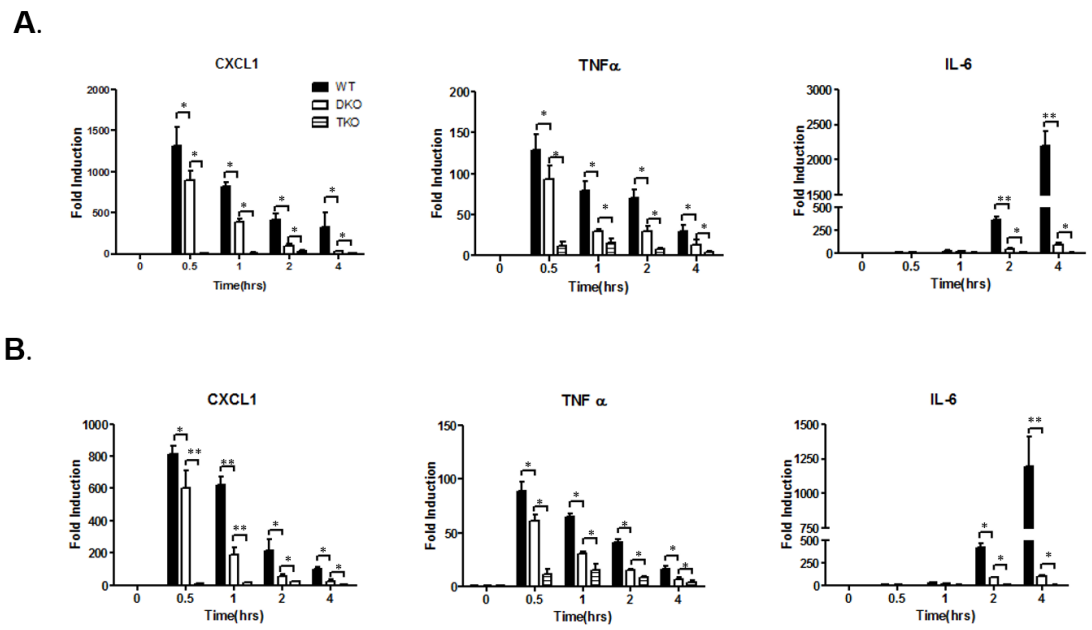

Figure 15. IRAK1 and IRAK2 are required for TLR2/9-induced pro-inflammatory gene expression. A. Total mRNAs from BMDMs of wild-type (WT), IRAK1/2-double deficient (DKO) and IRAK1/2/M-triple deficient (TKO) mice treated with Pam3CSK4 (200ng/ml) for the indicated times, were subjected to RT-PCR analyses for the levels of CXCL1, IL-6 and TNFα expression. **B.** Total mRNAs from BMDMs of wild-type (WT), IRAK1/2-double deficient (DKO) and IRAK1/2/M-triple deficient (TKO) mice treated with CpG B (1μg/ml) for the indicated times, were subjected to RT-PCR analyses for the levels of CXCL1, IL-6 and TNFα expression. The experiments were repeated three times. Data represent mean ± SEM; **p<0.01, *p<0.05 (two tailed t-test).

We have previously also identified a group of TLR-induced genes that are not regulated at posttranscriptional levels [131]. The TLR7-induced IRAKM-mediated signaling events in IRAK1/2-DKO-BMDMs allowed sustained induction of these genes, which was completely abolished in IRAK1/2/M-TKO-BMDMs (**Fig. 16A**).Furthermore, the expression of these genes was also substantially reduced in IRAKM-KO-BMDMs compared to that in wild-type cells (**Fig. 16B**). Several of the genes are important for the activation and homeostasis of the macrophages (including ETS2, SOD2, Bcl-2A1D and GPR84) (**Fig. 16A-B**). Another group of IRAKM-dependent genes is inhibitory molecules, including A20, SOCS1, SHIP1 and IκBα (**Fig. 16A-B, Fig. 17**). The gene expression data were consistent with the role of IRAKM in TLR7-induced second wave NFκB activation, since most of the IRAKM-dependent genes were late genes (induced after 1 hour). Although A20 was readily induced at 30 min, its expression peaked at 4 hours of treatment. Taken together, these results suggest that at least one potential importance of TLR7-induced IRAKM-mediated signaling is to induce the expression of several inhibitory molecules (SHIP1, SOCS1, A20 and IκBα, which might serve as a negative feedback control, implicating a novel inhibitory mechanism by which IRAKM modulates TLR signaling.

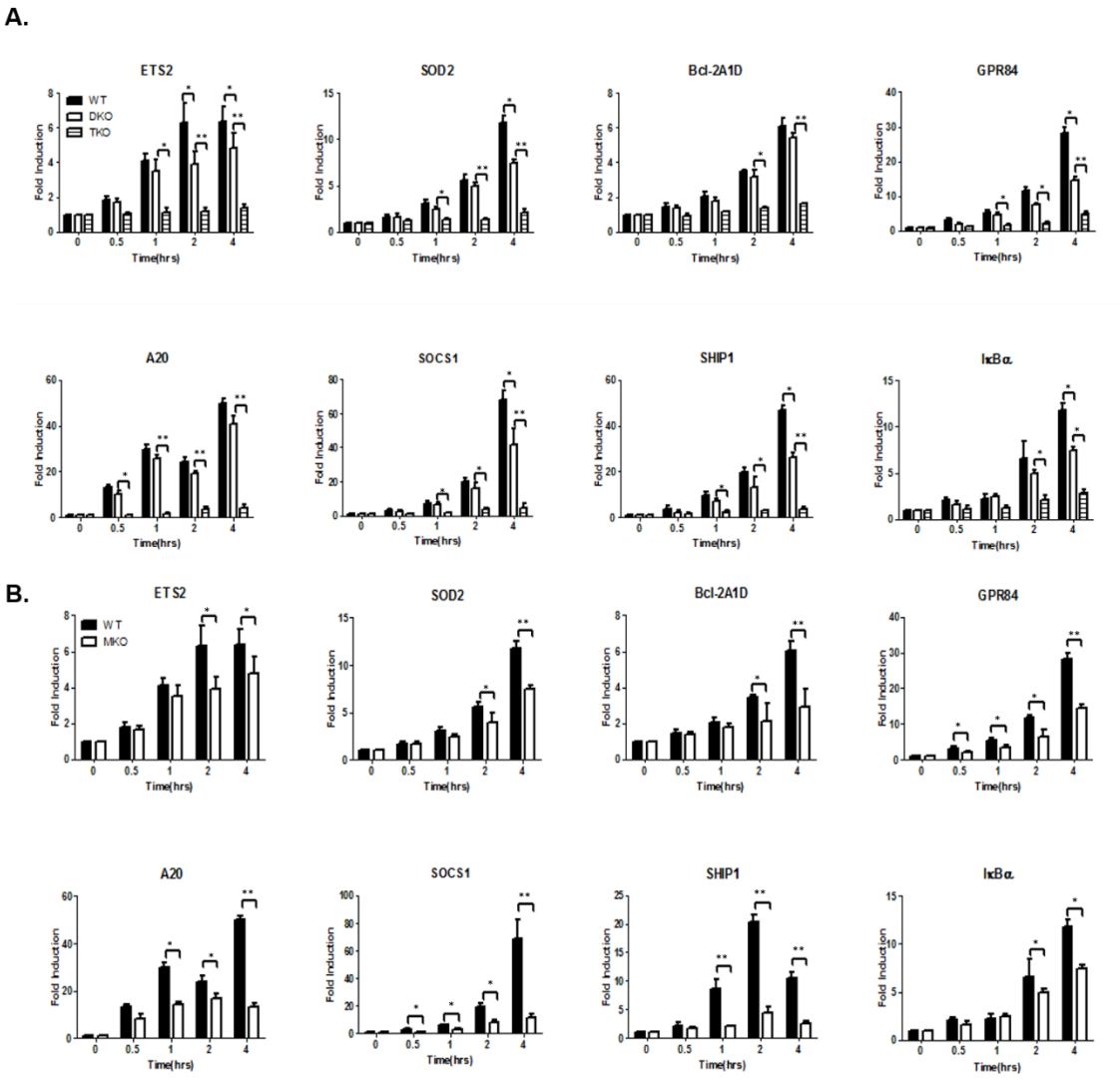

Figure 16. IRAKM is required for TLR7-induced expression of inhibitory molecules SHIP-1, SOCS1, A20 and IκBα. A. Total mRNAs from BMDMs of wild-type (WT), IRAK1/2-double deficient (DKO) and IRAK1/2/M-triple deficient (TKO) mice treated with R848 (1μg/ml) for the indicated times, were subjected to RT-PCR analyses for the levels of ETS2, SOD2, Bcl-2A1D, GPR84, SHIP-1, SOCS1, A20 and IκB expression. **B.** Total mRNAs from BMDMs of wild-type (WT) and IRAKM-deficient (MKO) mice treated with R848 (1μg/ml) for the indicated times, were subjected to RT-PCR analyses for the levels of ETS2, SOD2, Bcl-2A1D, GPR84, SHIP-1, SOCS1, A20 and IκBαexpression. The experiments were repeated three times. Data represent mean ± SEM; **, P<0.01;*, p<0.05(two tailed t-test).

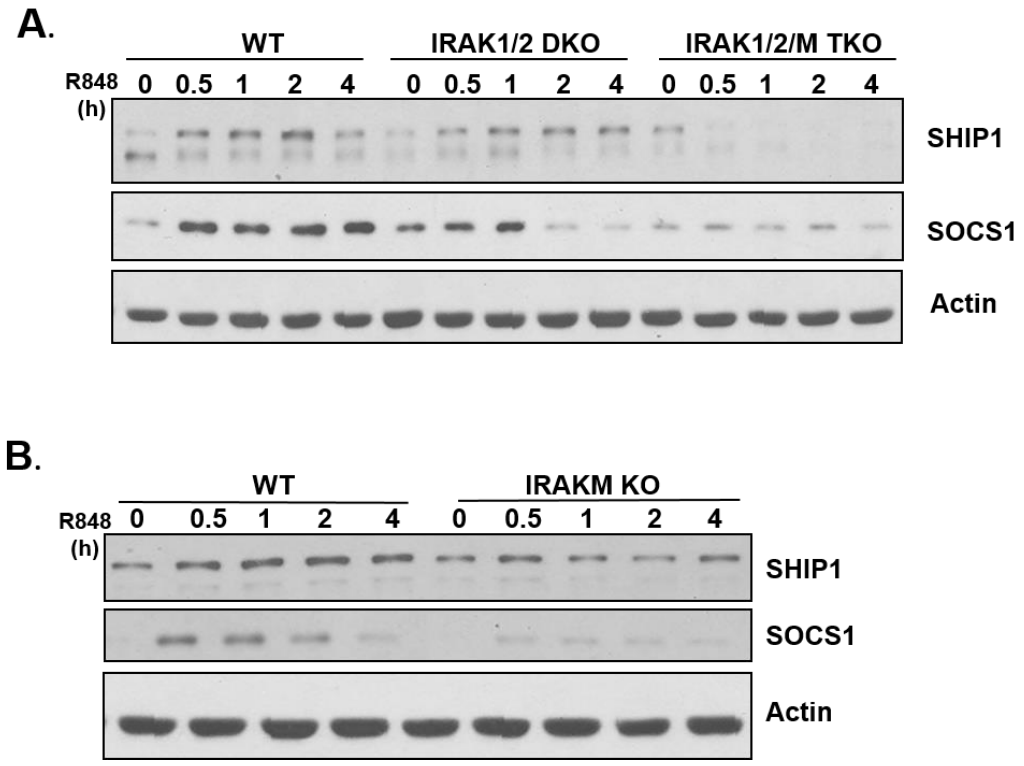

Figure 17. IRAKM is required for TLR7-induced protein translation of SHIP1 and SOCS1. A. Cell lysates from wild-type (WT), IRAK1/2- double deficient (IRAK1/2 DKO), IRAK1/2/M-triple deficient (IRAK1/2/3 TKO) bone marrow-derived macrophages (BMDMs) untreated or treated with R848 (1μg/ml) for the indicated times were analyzed by Western blot analysis with antibodies against SHIP1, SOCS1, and actin. The experiments were repeated for five times with similar results. **B.** Cell lysates from wild-type (WT), and IRAKM deficient (MKO) BMDMs untreated or treated with R848 (1μg/ml) for the indicated times were analyzed by Western blot analyses with antibodies against SHIP1, SOCS1, and actin. The experiments were repeated for five times with similar results.

IRAKM inhibits translational control of proinflammatory cytokines via its interaction with IRAK2

Although it is clear that IRAKM contributes to TLR7-induced gene transcription through the activation of second wave of NFκB activation, the production of somepro-inflammatory cytokines and chemokines(including CXCL1, TNFα and IL-6) was actually

enhanced in the IRAKMKO-BMDMs compared to that in the control cells [128](**Fig. 18B**). Since the mRNAs of these pro-inflammatory genes were induced at similar or reduced levels in IRAKMKO-BMDMs as compared to wild-type cells (**Fig. 18A**), we investigated the possible role of IRAKM in regulation of cytokine and chemokine translation. BMDMs from IRAKM-deficient mice and wild-type mice were treated with TLR7 ligand R848 for 1.5 hours and a sucrose gradient was used to separate the mRNA translation-inactive pool (free ribosome) and translation-active pool (poly-ribosomes) **(Fig. 19A)**. Compared with wild-type BMDMs, IRAKM KO BMDMs had more cytokine and chemokine mRNAs (IL-6, KC and TNFα) in the translation-active pool. IRAKM deficiency thus resulted in the increased ratios of TLR-induced cytokine and chemokine mRNAs in translation-active pool versus translation-inactive pool (**Fig. 19B&E**). On the other hand, IRAKM deficiency had no impact on the translation of mRNAs that are not regulated at the post-transcriptional levels, including the inhibitory molecules (ETS2, SOD2, Bcl-2A1D, GPR84, SHIP1, SOCS1, A20 and IκBα (**Fig. 19C-D&E**).

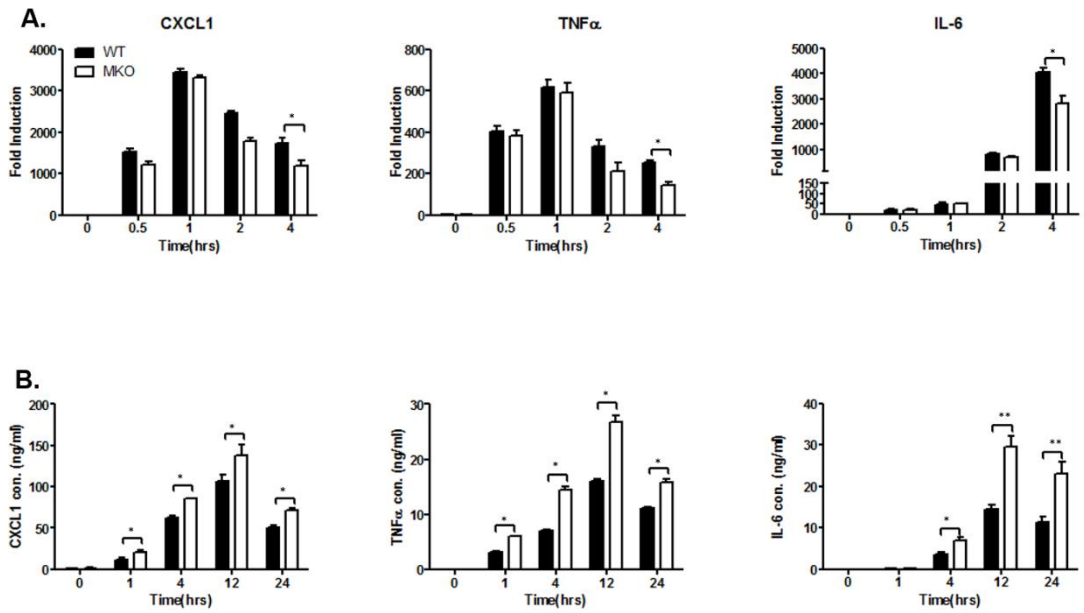

Figure 18. IRAKM inhibits TLR7-induced pro-inflammatory gene expression. A. Total mRNAs from BMDMs of wild-type (WT) and IRAKM-deficient (MKO) mice treated with R848 (1μg/ml) for the indicated times, were subjected to RT-PCR analyses for the levels of CXCL1, IL-6 and TNFα expression. **B.** BMDMs from wild-type (WT) and IRAKM-deficient (MKO) mice were treated with R848 (1μg/ml) for the indicated time. CXCL1, IL-6 and TNFα concentrations in the supernatant were measured by ELISA. The experiments were repeated three times. Data represent mean ± SEM; **P<0.01. *p<0.05(two tailed t-test).

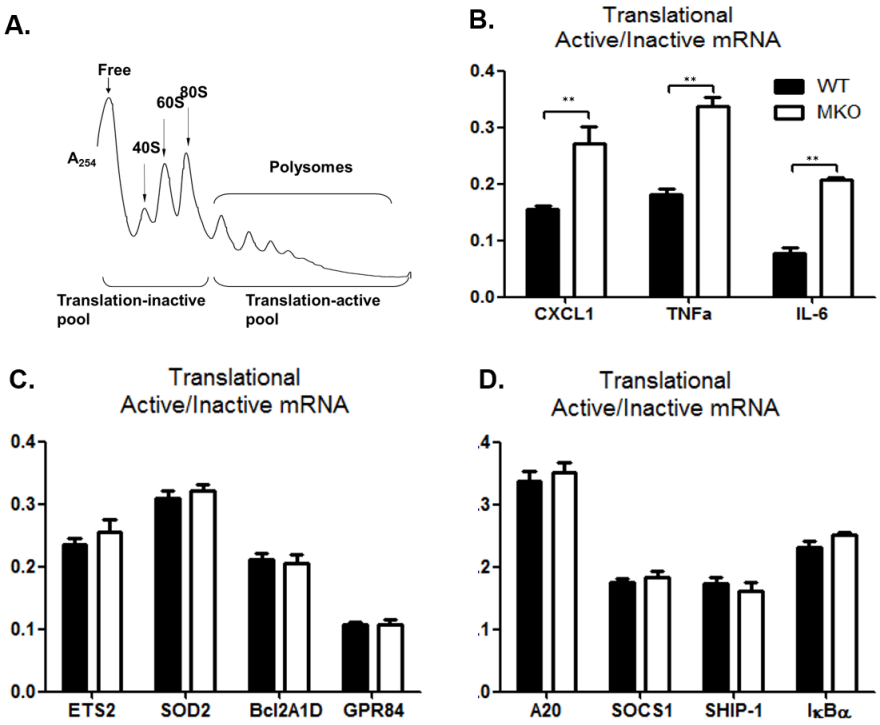

E.

mRNA	Cell type	Total	Translation-inactive	Translation-active	Ratio: Translation-active/-inactive
IL-6	WT	1.22	1.145	0.075	0.066
IL-6	MKO	1	0.832	0.168	0.202
KC	WT	1.58	1.373	0.197	0.151
KC	MKO	1	0.805	0.194	0.241
TNFα	WT	2.46	1.861	0.599	0.191
TNFα	MKO	1	0.746	0.254	0.341
A20	WT	1.38	1.045	0.335	0.321
A20	MKO	1	0.749	0.251	0.334
SOCS1	WT	2.34	1.980	0.360	0.182
SOCS1	MKO	1	0.852	0.148	0.174
SHIP1	WT	3.58	3.073	0.507	0.165
SHIP1	MKO	1	0.851	0.149	0.175
IκBα	WT	1.36	1.096	0.264	0.241
IκBα	MKO	1	0.801	0.199	0.248
GAPDH	WT	1	0.67	0.33	0.492
GAPDH	MKO	1	0.69	0.31	0.449

Figure 19. IRAKM inhibits the translation of TLR7-induced pro-inflammatory genes. **A.** Translation-active and –inactive mRNAs from R848-treated BMDMs were isolated by sucrose gradient fraction. **B-D.**BMDMs from wild-type (WT) and IRAKM deficient (MKO) mice were treated with R848 (1μg/ml) for 90 min. **(B)** IL-6, KC and TNFα; **(C)**ETS2, SOD2, Bcl2A1D and GPR84; **(D)**A20, SOCS1, SHIP1 and IκBα and glyceraldehyde-3-phosphate dehydrogenase (GAPDH) mRNAs from unfractionated cell lysates, translation-active pools, and translation-inactive pools were analyzed by quantitative RT-PCR and normalized to β-actin (see supple. Fig. 4). The ratios of mRNAs from R848-treated translation-active and –inactive pools are shown in B-D. The experiments were repeated three times. Data represent mean ±SEM; **P<0.01. *p<0.05(two tailed t-test). **E.**IL-6, KC, TNFα, A20, SOCS1, SHIP1, IκBα and glyceraldehyde-3-phosphate dehydrogenase (GAPDH) mRNAs from unfractionated cell lysates, translation-active pools, and translation-inactive pools were analyzed by quantitative RT-PCR and normalized to β-actin. Similar results were obtained in three independent experiments. One representative is shown.

We previously reported that IRAK2 plays an important role in the regulation of TLR-mediated protein translation of cytokines and chemokines, including IL-6, CXCL1 (KC) and TNFα. Through co-immunoprecipitation experiment, we found that IRAKM specifically bound to IRAK2, not IRAK1 (**Fig. 20A**). Furthermore, we have previously reported that IRAK2 is required for TLR-induced phosphorylation of MNK1, MK2 and eIF4e, which are involved in protein translational control. Interestingly, IRAKM deficiency resulted in increased TLR7-induced phosphorylation of MNK1, MK2 and eIF4e (**Fig. 20B**), supporting the role of IRAKM in inhibition of TLR7-induced proinflammatory cytokine and chemokine translation through its interaction with IRAK2.

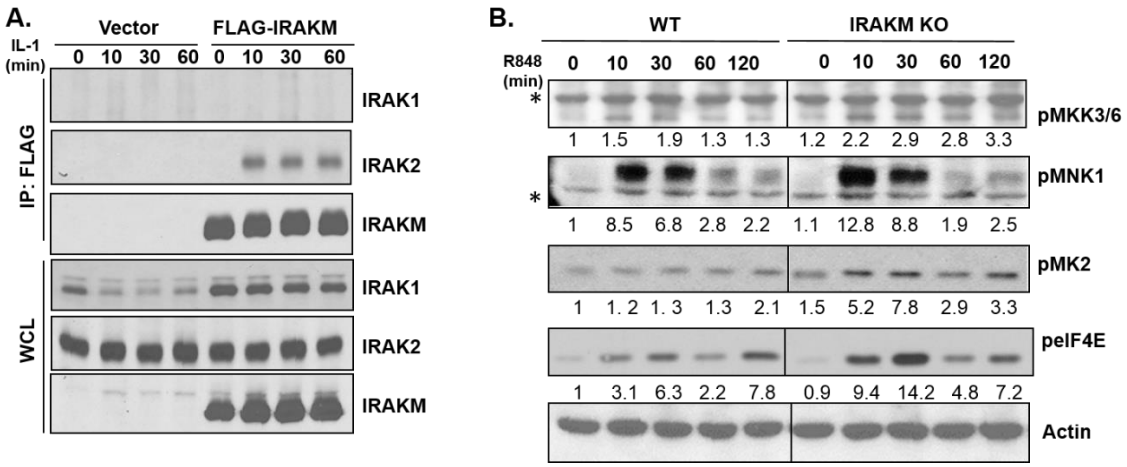

Figure 20. IRAKM inhibits the translation of TLR7-induced pro-inflammatory genes through its interaction with IRAK2. A. IRAKM-deficient mouse embryonic fibroblast (MEFs) infected with retroviruses containing empty vector construct (Vector) and FLAG-IRAKM were treated with IL-1β (1ng/ml) for the indicated times, followed by immunoprecipitation (IP) with anti-FLAG antibody and analyzed by Western blot analyses using antibodies againstIRAK1, IRAK2 and FLAG. WCL (whole cell lysates). The experiments were repeated for five times with similar results. **B.** Cell lysates from wild-type (WT), and IRAKM deficient (MKO) BMDMs untreated or treated with R848 (1μg/ml) for the indicated times were analyzed by Western blot analyses with antibodies against p-MKK3/6, p-MNK1, p-MK2, p-eIF4F and actin. The levels of the phosphorylated proteins were analyzed by ImageJ 1.43u and normalized to actin. * indicates non-specific band. The experiments were repeated for five times with similar results.

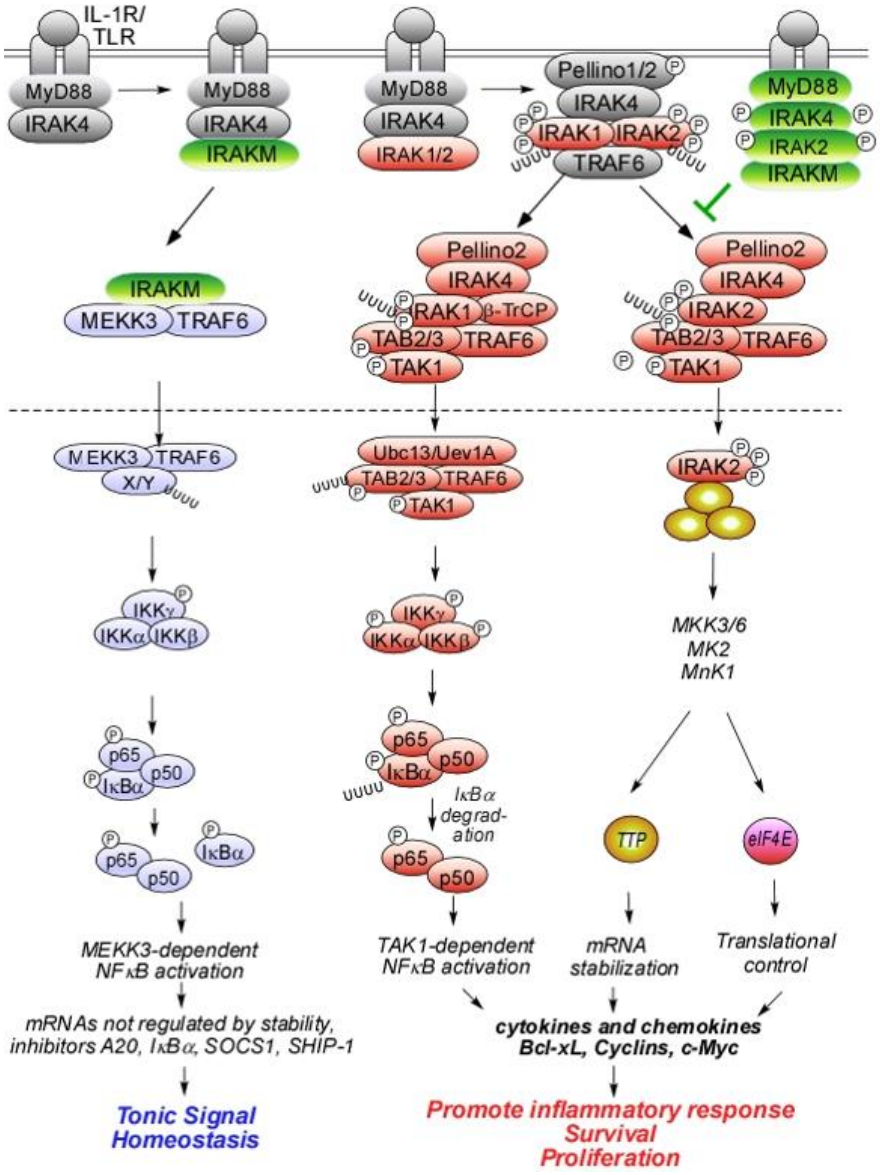

Figure 21. Model for the regulatory role of IRAKM in TLR-IL-1R signaling. IRAKM is able to function as an intermediate signaling component to transmit signaling upon TLR-IL-1R activation. IRAKM interacts with MyD88-IRAK4 to form IRAKM Myddosome to mediate TLR-IL-1R-induced MEKK3-dependent second wave NFκB activation. However, this IRAKM-dependent pathway only induces expression of genes that are not regulated at the posttranscriptional levels (including inhibitory molecules SOCS-1, SHIP-1, A20 and I B), exerting an overall inhibitory effect on inflammatory response. On the other hand, IRAKM specifically interacts with IRAK2, but not IRAK1, and suppresses TLR-IL-1R-induced IRAK2-mediated translation of cytokines and chemokines.

D. Discussion

Although previous studies suggested that IRAKM prevents the dissociation of IRAKs from MyD88, suppressing all downstream signaling, there have not been sufficient experimental evidences to fully support this hypothesis. In this manuscript, we provided two novel mechanisms for the regulatory role of IRAKM in TLR signaling (**Fig. 21**). First, IRAKM is able to function as an intermediate signaling component to transmit signaling upon TLR activation. IRAKM interacts with MyD88-IRAK4 to form IRAKM Myddosome to mediate TLR7-induced MEKK3-dependent second wave NFκB activation. However, this IRAKM-dependent pathway only induces expression of genes that are not regulated at the posttranscriptional levels (including inhibitory molecules SOCS-1, SHIP-1, A20 and IκBα), exerting an overall inhibitory effect on inflammatory response. The second novel mechanism is that IRAKM specifically interacts with IRAK2, but not IRAK1, and suppressesTLR7-induced IRAK2-mediated translation of cytokines and chemokines. These findings present a new outlook for how IRAKM modulates TLR signaling and TLR-mediated inflammatory responses.

The role of IRAKM in MEKK3-dependent NFκB activation was best demonstrated in IRAK1/2-DKO- versus IRAK1/2/M-TKO-BMDMs. While IRAK1/2 double deficiency abolished TAK1-, but not MEKK3-dependent pathway, TLR7-induced NFκB activation was no longer detectable in IRAK1/2/M-TKO-BMDMs. It is intriguing that IRAKM single deficiency resulted in loss of TLR7-induced late NFκB activation (after 30min), implicating the role of the IRAKM-MEKK3 pathway in second wave of NFκB activation in the presence of IRAK1/2. The importance of IRAKM in NFκB activation was further demonstrated in the MG132 treatment experiment, in which IRAKM deficiency greatly

diminished TLR7-induced NFκB activation, since MG132 treatment was shown to block the TAK1-dependent pathway, mimicking IRAK1/2 deficiency [137]. These mouse genetic experiments on the novel role of IRAKM were nicely supported by biochemical studies. IRAKM-mediated NFκB activation was almost abolished in MEKK3 knock-down cells and IRAKM specifically interacted with MEKK3, but not TAK1, providing direct biochemical evidence for the role of IRAKM in MEKK3-, but not TAK1-dependent pathway. IRAK1 and IRAK2 are known to form Myddosomes with MyD88-IRAK4 to mediate TLR7-induced TAK1-dependent NFκB activation. Since IRAKM was able to mediate NFκB activation in the absence of IRAK1 and IRAK2, and interacted with MyD88 and IRAK4, we proposed the formation of IRAKM Myddosome. Through protein modeling, we predicted the critical residues for interaction interface between death domains of IRAKM and IRAK4. Mutations in the conserved W74, E71 and Q78 in helix H4 of the IRAKM DD greatly reduced the interaction of IRAKM with IRAK4 and also diminished the ability of IRAKM to mediate NFκB activation. These results strongly suggest that IRAKM probably indeed has the ability to directly interact with MyD88-IRAK4, like IRAK1/2, acting as an intermediate signaling component to transmit signal from the receptor to downstream signaling cascade (interaction with TRAF6-MEKK3) to mediate NFκB activation.

One important question is what is the biological significance of the IRAK1/2-mediated TAK1- versus IRAKM-mediated MEKK3-dependent pathway? We have previously shown that the kinase activity of IRAK4 is required TAK1-, but not MEKK3-dependent NFκB activation [131, 132]. Furthermore, IRAK4 coordinately regulates TAK1-dependent NFκB activation and mRNA stabilization pathways to ensure robust

production of cytokines and chemokines during inflammatory response [139]. In addition to mRNA stabilization, TLR signaling is also necessary for efficient and sustained translation of cytokine and chemokine mRNAs. We have previously reported that IRAK2 is essential for sustained translation of TLR-induced cytokine and chemokine mRNAs [135].Therefore, it is logical to find that IRAK1/2 (substrates of IRAK4) are required for TAK1- (not MEKK3-) dependent NFκB activation, which is coupled with posttranscriptional control to promote the production of pro-inflammatory cytokines and chemokines. On the other hand, the IRAKM-induced MEKK3-dependent pathway is uncoupled from posttranscriptional regulation. Therefore, the IRAKM-dependent pathway only induced expression of IRAK4-kinase-independent genes that are not regulated at the posttranscriptional levels, including inhibitory molecules SOCS1, SHIP1, A20 and IκBα. The important concept is that IRAKM is wired to engage an alternative NFκB activation pathway to produce inhibitory molecules, which can in turn to exert an overall inhibitory effect on inflammatory response. The advantage for such inhibitory mechanism could be that through the production of these inhibitory molecules, IRAKM could exert broader inhibitory effects not just on TLR-IL-1R but also on other cytokine signaling cascades, so that the inflammatory response can be effectively controlled.

It is important to point out that IRAKM also has the ability to directly impact on TLR-induced production of cytokines and chemokines. Although IRAKM deficiency did not have much impact on TLR-induced mRNA levels of cytokines and chemokines, their protein production was enhanced in IRAKM-KO-BMDMs as early as 1 hour after stimulation. Through polysomal fractionation, we found that the mRNAs of cytokines and chemokines were more actively translated in the absence of IRAKM, indicating the critical

role of IRAKM in translational control. Consistent with the previous finding about the essential role of IRAK2 in TLR-mediated translational control, we found IRAKM specially interacts with IRAK2, but not IRAK1. These results suggest that in addition to the formation of IRAKM Myddosome, IRAKM probably has the ability to dock onto IRAK2 Myddosome, thereby interfering IRAK2-dependent downstream signaling.

While this study has provided important insight into the mechanistic roles of IRAKM in TLR signaling, many questions still remain regarding the functional relationship of the IRAK family members. Future studies are needed to determine how IRAKM specifically interacts with IRAK2, but not IRAK1 and what determines the distribution and dynamics of IRAKM in IRAKM Myddosome versus IRAK2 Myddosome. It will be important to determine how the newly found functions of IRAKM will impact on the interpretation of the role of IRAKM in inflammatory responses in vivo and the drug development of inhibitors for different IRAKs.

E. Materials and Methods

Biological reagents and cell Culture—Recombinant human IL-1 was purchased from R&D system. CpG Boligodeoxynucleotide (ODN) and Pam3CSK4 were purchased from Invivogen. LPS (Escherichia coli 055:B5) was purchased from Sigma-Aldrich and R848 was obtained from GLSynthesis company. Antibodies against phosphorylated IκBα(Ser32/S36), JNK, IKKα/β(Ser176/180), Mnk1 (Thr179/202), MK2 (Thr334), eIF4E(Thr70), MKK3(Ser189)/MKK6(Ser207), total IκBα and SOCS1 were purchased from Cell signaling. Antibody to IRAK2 was purchased from Abcam. Antibody to IRAK4 was purchased from Enzo. Antibody to FLAG (anti-FLAG) and hemagglutinin (anti-HA) were purchased from Sigma. Antibody to MEKK3 was purchased from BD Bio-sciences

Pharmingen. Antibodies against IRAK, TAK1, SHIP1 and Actin were from Santa Cruz Biotechnologies. MG132 was purchased from Calbiochem. 293-derived IRAK1-deficient cells (293-I1A cells), and mouse embryonic fibroblast (MEFs) were maintained in Dulbecco's modified Eagle's medium, supplemented with 10% fetal bovine serum, penicillin G (100 μg/ml), and streptomycin (100 μg/ml). Bone-marrow derived macrophages were obtained from the bone marrow of tibia and femur by flushing with DMEM. The cells were cultured in DMEM supplemented with 20% fetal bovine serum (FBS), and 30% L929 supernatant for 5 days.

Knock-down of MEKK3— Oligonucleotides encoding either scrambled or MEKK3-specific small hairpin RNAs were cloned into pSUPER to generate pSUPER-scrambled or pSUPER-MEKK3 respectively. 1 μg of pSUPER-scrambled or pSuper-MEKK3 was transfected into 293-I1A cells along with 0.1 μg of pBabe-puromycin by FuGENE 6 (Roche Applied Science). Two days after transfection, puromycin (1 μg/ml) containing DMEM was added to the cells to select for puromycin-resistant clones. After 10 days of puromycin selection, single clones were picked and subjected to Western analysis to determine the levels of MEKK3. Clones with over 85% knock-down of MEKK3 were pooled as MEKK3 knock down cells and used for experiments.

Transfection and luciferase assay—Transfection of the 293-I1A cells was performed using the FuGENE 6 transfection reagent as recommended by the manufacturer (Roche Diagnostics). After 24 h, the cells were stimulated with IL-1β or left untreated for 6 h before harvest. Luciferase activity was determined by using the luciferase assay system and chemiluminescent reagents from Promega.

Plasmids and retroviruses—Mouse IRAKM and IRAK4 cDNA were purchased from Open Biosystems. The IRAKM mutants and IRAK4 mutant were generated by site-directed mutagenesis polymerase chain reaction (PCR). The wild-type and mutants of IRAKM and IRAK4 were cloned into pMX retroviral expression vector and transfected into phoenix cell for viral packaging. Cells were infected by the packaged retrovirus for 3 days and selected by puromycin (2μg/ml) for 2days for stable viral integration. For all PCR reactions high fidelity Pfu Turbo polymerase was used (Stratagene).

Adenovirus infection—IRAKM wild-type and mutants were cloned into pENTR™⁄D-TOPO® Vector (Invitrogen). The pENTER clones were packaged into an adenovirus destination vector pAd/CMV/V5-DEST™ using Gateway® Vector Kit according to manufacturer's guidelines (Invitrogen). The adenoviral stocks were prepared using ViraPower™ Adenoviral Expression System according to manufacturer's guidelines (Invitrogen). The BMDMs were infected at multiplicity of infection (MOI) of 200. After sixteen hours of infection, the cells were changed to fresh L929 conditioned medium. Forty-eight hours after infection, the cells were used for experiments.

Immunoblotting—Cell were harvested and lysed in a Triton-containing lysis buffer (0.5% Triton X-100, 20 mM HEPES (pH 7.4), 150 mM NaCl, 12.5 mM β-glycerophosphate, 1.5 mM $MgCl_2$, 10 mM NaF, 2 mM dithiothreitol, 1 mM sodium orthovanadate, 2mM EGTA, 1 mM phenylmethylsulfonyl fluoride and complete protease inhibitor cocktail from Roche). Cell lysates were then separated by 10% SDS-PAGE, transferred to Immobilon-P membranes (Millipore), and subjected to immunoblotting.

Quantitative real-time PCR—Total RNA was isolated using TRIzol reagent (Invitrogen). 3μg of total RNA was then used for reverse transcription reaction using

SuperScript-reverse transcriptase (Invitrogen). Q-PCR was performed in AB 7300 RealTime PCR System, and the gene expression of human IL-8, TNFα, actin and mouse CXCL1 (KC), TNFα, IL-6, A20, SHIP1, SOCS1, IκBα, GPR84, ETS2, SOD2, Bcl-2AD1 was examined by SYBR® GREEN PCR Master Mix (Applied Biosystems). PCR amplification was performed in triplicate, and water was used to replace cDNA in each run as a negative control. The reaction protocol included preincubation at 95℃ to activate FastStart DNA polymerase for 10 min, amplification of 40 cycles that was set for 15 s at 95℃, and annealing for 60 s at 60℃. The results were normalized with the housekeeping gene human or mouse β-Actin. Primer sequences were designed using AlleleID 6.0. The following primers were used: mouse TNFα forward, CAAAGGGAGAGTGGTCAGGT; mouse TNFα reverse, ATTGCACCTCAGGGAAGAGT; mouse actin forward, GGTCATCACTATTGGCAACG; mouse actin reverse, ACGGATGTCAACGTCACACT; mouse CXCL1 forward, TAGGGTGAGGACATGTGTGG; mouse CXCL1 reverse, AAATGTCCAAGGGAAGCGT; mouse IL-6 forward, GGACCAAGACCATCCAATTC; mouse IL-6 reverse, ACCACAGTGAGGAATGTCCA; mouse SOCS1 forward, TGACTACCTGAGTTCCTTCC; mouse SOCS1 reverse, ATCTCACCCTCCACAACC; mouse SHIP1 forward, GAGGAGACAGGCAACATC; mouse SHIP1 reverse, TCTTGACACTGAAGGAACC; mouse GPR84 forward, TCAACCCTGTGCTCTATGC; mouse GPR84 reverse, GCCTGTCCTGGTGAATGG; mouse Bcl2A1D forward, GGAATGGAGGTTGGGAAGATGG; mouse Bcl2A1D reverse, CTGGTCCGTAGTGTTACTTGAGG; mouse SOD2 forward,

ACAACTCAGGTCGCTCTTCAG; mouse SOD2 reverse, GATAGCCTCCAGCAACTCTCC; mouse ETS2 forward, AGTGTGGTGCTTCCTGTCTTG; mouse ETS2 reverse, TTGCTCTGTCTGTGCTTCTGG; A20 forward, TGAGCAAGTAGGCAAGATAAG; A20 reverse, GTAGACGAGCAGCAATAGC; mouse IκBα forward, TGGAAGTCATTGGTCAGG; mouse IκBα reverse, ACAGGCAAGATGTAGAGG; human IL-8 forward, AGAGACAGCAGAGCACAC; human IL-8 reverse, GTTCTTTAGCACTCCTTGGC; human TNFα forward, TCAGCAAGGACAGCAGAG; human TNFα reverse, GTATGTGAGAGGAAGAGAACC; human actin forward, GTCGGTATGGGTCAGAAAG; human actin reverse, CTCGTTGTAGAAGGTGTGG.

ELISA assay—Supernatants from cell cultures were collected and measured for the level of mouse cytokines CXCL1, IL-6 and TNFα using Duoset ELISA kits (R&D system) according to manufacturer's instructions.

Molecular modeling—A theoretical three-dimensional model of the IRAKM DD region (residues 14-105) was generated via a web-based molecular modeling server [140]. The crystal structure of the IRAK2 DD segment (PDB 3MOP) was used as a template because it shares a considerable sequence identity (30%) and topology with IRAKM DD, as analyzed by the structure prediction. The complex of the MyD88 DD-IRAK4 DD-IRAKM DD was constructed via two steps. First, four homology models of the IRAKM DD were superposed onto each IRAK2 DD segment (chains K to N) in the Myddosome complex (PDB 3MOP) using the secondary structure matching algorism [141], as implemented in COOT [142]. Second, these four IRAKM DD models were assembled into the coordinates of the MyD88 DD-IRAK4 DD complex in the Myddosome complex after

removal of the regions of IRAK2 DD. Thus, the integrity and physicochemical property of the MyD88 DD-IRAK4 MM complex were maintained. The hypothetical IRAK4 DD-IRAKM DD interface was examined by the server PISA [143] and inspected by the program PYMOL (www.pymol.org).

Co-immunoprecipitation and immunoblotting—Bone marrow-derived macrophages and 293-I1A cells were cultured as indicated above. After stimulation with R848 (1μg/ml) or IL-1β (1ng/ml), the cells were harvested and co-immunoprecipitation and immunoblotting were performed as previously descried [144].

Electrophoretic mobility shift assay (EMSA) — Bone marrow-derived macrophages and 293-I1A cells were cultured as indicated above. After stimulation with R848 (1 μg/ml) or IL-1β (1 ng/ml), the cells were harvested and nuclear extracts were prepared with the NE-PER Nuclear and Cytoplasmic Extraction Reagent (Thermo). Labeling of NFκB specific oligonucleotides (Santa Cruz) was performed with [γ-^{32}P]-ATP (PerkinElmer) by using T4 polynucleotide kinase (NEB) following manufacturer's guideline. After purification over a Sephadex G-25 column (Amersham), radiolabelled oligonucleotides (around 20,000 cpm) were incubated with nuclear extracts at room temperature for 30 min in binding buffer containing 12 mM HEPES (pH 7.9), 4 mM Tris HCl (pH 7.8), 60 mM KCl, 1 mM ethylenediamine tetraacetic acid (EDTA), 1 mM dithiothreitol (DTT), 1 mM PMSF, 12% glycerol, 5 μg of bovine serum albumin (BSA) and 2 μg poly(dI-dC) (Sigma). The same amount of nuclear protein (around 5 μg) was used in each experiment. The protein concerntraction was measured using Quick Start Bradford Protein Assay Kit (Biorad) following manufacturer's guideline. DNA–protein complexes

were separated using 6% non-denaturing polyacrylamide gel electrophoresis. Signals were visualized by exposing the dried gel to autoradiography film.

Polysome fractionation analysis—Wild-type and IRAKM deficient macrophages were stimulated with R848 (1μg/ml) for 1.5h. Cytoplasmic extracts were prepared from BM-derived macrophages stimulated with R848 (1μg/ml) as described [144]. Cytoplasmic exacts were carefully layered over 10–50% linear sucrose gradients in polysome buffer (10 mM HEPES, pH 7.5, 100 mMKCl, 2.5 mM MgCl2, 1 mM dithiothreitol, 50 units of recombinant RNasin (Promega), and 0.1% Igepal-CA630 (Sigma)) and centrifuged at 17,000 rpm in a Beckman SW32.1 Ti rotor for 4h at 4°C. Gradients were fractioned by using an ISCO gradient fractionation system equipped with a UA-6 detector. Light RNP fractions, 40S, 60S, and 80S and heavy polysome fractions were monitored by the continuous UV absorption profile at A254, and 12 tubes of 750 μl fractions were collected. The fractions representing light RNP and free ribosomes were used to isolate the translation-inactive pool of mRNAs, and the fractions presenting heavy polysomes were used to isolate the translation-active mRNAs. RNAs were isolated from these fractions by extraction with TRIzol.

CHAPTER III

IRAKM-MINCLE AXIS CONTRIBUTES TO ALCOHOL-INDUCED LIVER INJURY VIA INFLAMMASOME ACTIVATION

Hao Zhou[1,2], Minjia Yu[1], Junjie Zhao[1], Bradly N. Martin[1], Sanjoy Roychowdhurya[3], Megan R. McMullen[3], Jazmine Dannera[3], Doug Czarnecki[3], Christine A. Wells[4], Sho Yamasaki[5], Laura E. Nagy[3,6], Xiaoxia Li[1,]

[1]Department of Immunology, Lerner Research Institute, Cleveland Clinic Foundation, Cleveland, Ohio, USA

[2]Department of Biological, Geological, and Environmental Sciences, Cleveland State University, Cleveland, Ohio, USA

[3]Center for Liver Disease Research, Department of Pathobiology, Lerner Research Institute, Cleveland Clinic Foundation, Cleveland, Ohio, USA

[4]The Australian Institute for Bioengineering and Nanotechnology, University of Queensland, Brisbane, Australia

[5]Division of Molecular Immunology, Research Center for Infectious Diseases, Medical Institute of Bioregulation, Kyushu University, 3-1-1 Maidashi Higashiku, Fukuoka, Japan

[6]Department of Gastroenterology, Lerner Research Institute, Cleveland Clinic Foundation, Cleveland, Ohio, USA

A. Abstract

Alcohol-induced liver injury is induced by necrosis of hepatocytes and increased translocation of endotoxin from the intestinal tract into hepatic portal system, which trigger chronic inflammation that is damaging to the liver together. In this study, we found that mice deficient of a Toll-like receptor proximal molecule, IRAKM, are protected from alcohol-induced liver injury. IRAKM mediates the up-regulation of Mincle, a receptor for danger signals release by damaged cells, in response to low dose of LPS. Biochemical analysis revealed that low-dose LPS preferentially induces the formation of IRAKM Myddosome, leading to MEKK3-dependent NFκB activation. Mincle-deficient mice are also protected from alcohol-induced liver injury. We found IRAKM deficiency and Mincle deficiency drastically reduced alcohol feeding induced inflammasome activation in the mouse liver. *Ex vivo* studies showed that both IRAKM and Mincle are required for inflammasome activation by endogenous Mincle ligand, SAP130, which is a danger signal release by damaged hepatocytes. Taken together, this study identifies an IRAKM-Mincle axis critical for the pathogenesis of alcohol induced liver disease through the activation of inflammasome.

B. Introduction

Alcoholic liver disease (ALD) ranges from simple steatosis to alcoholic hepatitis, fibrosis, cirrhosis and hepatocellular carcinoma [105-108]. Alcohol exposure induces endoplasmic reticulum (ER) stress and mitochondrial dysfunction in hepatocytes, which leads to hepatocyte apoptosis, necrosis and inflammation [145-147]. Alcohol disrupts the balance gut microflora associated with an increased intestinal permeability, resulting in increased translocation of bacterial products into the circulation [46, 51, 106, 114].

Increased levels of LPS were indeed detected in alcoholic patients and alcohol-treated experimental animals [113, 148]. The activation of hepatic macrophages (Kupffer cells) to portal endotoxin/lipopolysaccharide (LPS) plays a key role in the early pathogenesis of alcohol-induced liver injury. LPS recognition by Toll-like receptor 4 (TLR4) on hepatic macrophages results in the release of inflammatory cytokines such as TNF and IL-1 that can impact on the function of hepatocytes. Mice deficient in TLR4 or IL-1R indeed showed reduced alcohol-induced liver diseases [115-117]. Conversely, previous studies have shown that signals from injured hepatocytes induced by alcohol are also critical to the activation of hepatic macrophages. Thus, one important question is how TLR-dependent inflammatory response and alcohol-induced cell damage coordinately lead to the pathogenesis of ALD.

Toll-like receptors (TLRs) are molecules of the innate immune system that detect invading pathogens and protect multicellular organisms against infection by using proinflammatory chemokines and cytokines [149]. TLRs transduce signals through the adaptor molecule MyD88 and IL-1R-associated kinase (IRAK) family members, which include: IRAK1, IRAK2, IRAKM (also known as IRAK3) and IRAK4 [123-126]. The MyD88–IRAK4–IRAK2 death domain (DD) complex's crystal structure, referred to as the Myddosome complex, is constructed in a sequential manner, in which MyD88 recruits first IRAK4 and then MyD88-IRAK4 complex recruits the IRAK4 substrates IRAK2 or the related IRAK1[127]. Subsequently, the IRAK1/2 creates a complex with TRAF6 and dissociates from the receptor complex, activating cascades of downstream kinases, thus resulting in the activation of the transcription factor NFκB [69]. However, on the other hand, IRAKM is believed to act as a negative regulator that suppress Myddosome

complexes from disassociating with the receptor complex, therefore preventing signaling downstream [128].

Previously, we had reported the presence of two parallel TLR/IL-1R-mediated NFκB activation pathways: TAK1-dependent and MEKK3-dependent. The activation of TAK1-dependent pathway results in IKKα/β phosphorylation and IKKγ activation, leading to classical NFκB activation via IκBα phosphorylation and degradation. The TAK1-independent MEKK3-dependent pathway entails IKKγ phosphorylation and IKKα activation, which leads to NFκB activation by IκBα phosphorylation and its subsequent dissociation from NFκB, but without IκBα degradation [73, 129, 132]. We have recently been researching the functional relationships among IRAK family members and their roles in TLR signaling by analyzing mice with deficiencies in IRAK1, IRAK2 and/or IRAKM. We discovered that certain substrates of IRAK-4, specifically IRAK1 and IRAK2, are necessary for TAK1-dependent NFκB activation and mRNA stabilization of chemokines and cytokines, but not for MEKK3-dependent NFκB activation [135, 150-152]. IRAKM is able to interact with MyD88-IRAK4 to form IRAKM Myddosome, allowing it to control TAK1-independent MEKK3-dependent NFκB activation [153]. This IRAKM-dependent pathway is necessary for the second wave of TLR-induced NFκB activation in the company of IRAK1/IRAK2, a process which is independent on posttranscriptional regulation. Thus, the IRAKM-dependent pathway only induces expression of genes which are not controlled at posttranscriptional levels (including the inhibitory molecules SOCS1, SHIP1, A20 and IκBα), exerting an overall inhibitory effect on responses of inflammation.

In this study, we were surprised to discover that IRAKM-deficient mice were protected from ethanol-induced liver injury and inflammation. Mechanistically, we found

that with low doses of LPS (100pg-1ng/ml), IRAKM-MEKK3-dependent NFκB activation is the dominant pathway in macrophages; the IRAK1-mediated TAK1 pathway is not activated. These results suggest that this IRAKM-dependent pathway induced by low concentration of TLR ligands might contribute to the pathogenesis of ALD, since alcohol-induced increases in gut permeability result in low concentrations of TLR ligands in the circulation and liver. One of TLR4-induced IRAKM-dependent genes was Mincle (a C-type lectin receptor) that senses non-homeostatic cell death [52]. Spliceosome-associated protein (SAP) 130, which was identified as the endogenous ligand of Mincle, was released from hepatocytes after exposing to alcohol, while recombinant SAP130 was able to activate the inflammasome and IL-1 production in macrophages. Importantly, we found Mincle expression was induced in liver of ALD patients, as well as in mice after ethanol feeding. Induction of Mincle was ablated in liver of IRAKM-deficient mice and Mincle-deficient mice were protected from ethanol-induced liver injury, accompanied by reduced inflammasome activation and IL-1 production. Since Mincle is a sensor for cell death and its expression is IRAKM-dependent, these results suggest that TLR-induced IRAKM-dependent Mincle up-regulation in macrophages provides a critical link between alcohol-induced cell death and onset of inflammatory responses, contributing to the pathogenesis of ALD.

C. Results

IRAKM is required for low concentration LPS-mediated NFκB activation

IRAKM has been known as a negative regulator of innate immune response. Our recent studies showed that IRAKM also interacts with MyD88-IRAK4 to form an IRAKM Myddosome to mediate TLR-induced MEKK3-dependent second wave NFκB activation. In response to normal does LPS (1 μg/ml), MEKK3 modification and second wave of IκBα phosphorylation were ablated in IRAKM-deficient macrophages, whereas LPS-induced IRAK1 and TAK1 modification and IKKα/β phosphorylation were not affected ([153] **and Fig. 22**).

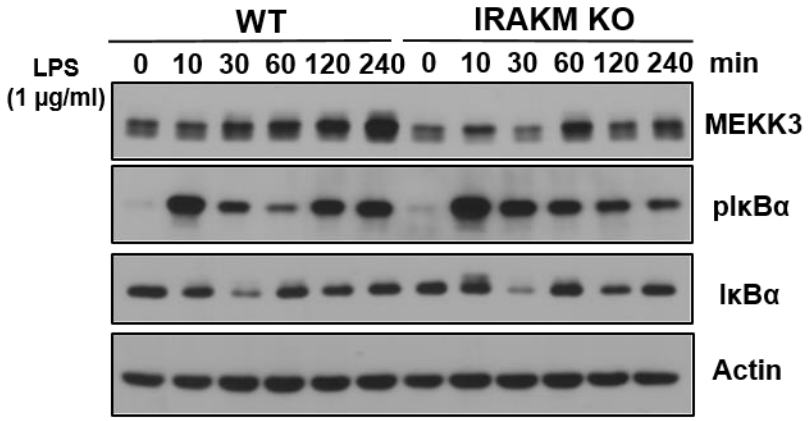

Figure 22. IRAKM is required for late phase high dose LPS-mediated NFκB activation. Cell lysates from wild-type (WT) and IRAKM KO bone marrow-derived macrophages (BMDMs) untreated or treated with high dose LPS (1 μg/ml) for the indicated times were analyzed by Western blot analysis with antibodies against, MEKK3, p-IκBα, IκBα, and actin.

This IRAKM-dependent second wave of NFκB activation only induces expression of genes that are not regulated at the posttranscriptional levels (including inhibitory molecules SOCS-1, SHIP-1, A20 and IκBα), further exerting an overall inhibitory effect on inflammatory response.

Interestingly, we now found that upon stimulation with low dose LPS (100pg-1ng/ml versus 1ug/ml, the commonly used dosage), the IRAKM-MEKK3-dependent NFκB activation is the dominant pathway. In bone marrow derived macrophages (BMDMs) treated with low dose LPS (100pg/ml), IRAK1 modification/degradation and IKKα/β phosphorylation were not observed, accompanied by the typical of MEKK3-dependent NFκB activation, evident by IκBα phosphorylation without IκBa degradation. Importantly, IκBα phosphorylation and MEKK3 modification induced by low LPS were completely abolished in IRAKM-deficient cells (**Fig. 23A**). Based on these results, we hypothesized that IRAKM is dominantly activated to mediate the MEKK3-dependent NFκB activation, whereas IRAK1-TAK1-dependent pathway was not activated by low dose of LPS (100pg/ml). In support of this, we found that inflammatory genes CXCL1, TNFα and IL-6 mRNA induction in response to low dose of LPS (100pg/ml) was not affected in IRAK1/2 double KO macrophages, but greatly reduced in IRAKM-deficient cells (**Fig. 23B**). Thus, these data suggest that low-dose LPS preferentially induces the formation of IRAKM Myddosome, leading to MEKK3-dependent NFκB activation.

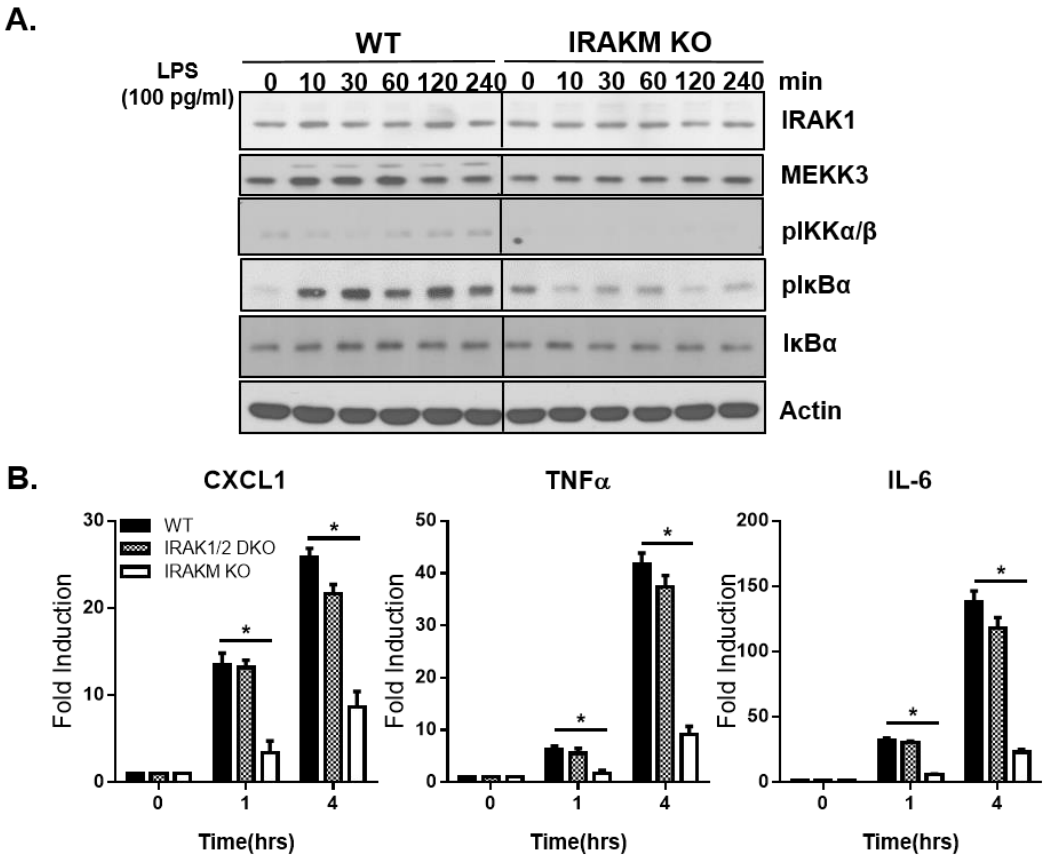

Figure 23. IRAKM is required for low dose LPS-mediated NFκB activation. A. Cell lysates from wild-type (WT) and IRAKM KO bone marrow-derived macrophages (BMDMs) untreated or treated with low dose LPS (100 pg/ml) for the indicated times were analyzed by Western blot analysis with antibodies against IRAK1, p-IKKα/β, MEKK3, p-IκBα, IκBα, and actin. **B.** Total mRNAs from BMDMs of WT, IRAK1/2-DKO and IRAKM KO mice treated with low dose LPS (1μg/ml) for the indicated times, were subjected to RT-PCR analyses for the levels of CXCL1, IL-6 and TNFα expression. Data represent mean ± SEM; *, P<0.05.

Low-dose LPS preferentially induces the formation of IRAKM Myddosome via the death domain of IRAKM

One important question is how low dose LPS activates the IRAKM-MEKK3 pathway. We previously reported that upon high dose ligand stimulation, the kinase activity

of IRAK4 is required for TLR-induced TAK1-, but not MEKK3-dependent NFκB activation [73, 132]. IRAK1 and its phosphorylation is required for TLR-induced TAK1-, but not MEKK3-dependent NFκB activation [150, 151]. These results suggest that high dose of LPS might lead to quick clustering/aggregation of the TLR-MyD88-IRAK4 complex and activation of IRAK4, which then recruits and phosphorylates IRAK1 thereby stabilizing the IRAK1 Myddosome, leading to TAK1-dependent NFκB activation. In support of this, our recent study showed that IRAK4 dimerization is required for its autophosphorylation and activation of the kinase activity. Thus, we hypothesize that the formation of TLR4 receptor complex induced by low dose LPS may not trigger the aggregation of IRAK4, which can then only attract IRAKM, but not IRAK1, leading to specific formation of IRAKM Myddosome and subsequent MEKK3-dependent NFκB activation. We indeed found that upon low dose LPS stimulation (100pg/ml), IRAKM, but not IRAK1 was recruited to IRAK4-MyD88 complex, whereas both IRAK1 and IRAKM interacted with IRAK4 upon high dose LPS stimulation (1ug/ml) (**Fig. 25A**). Furthermore, compared to BMDMs from wild-type control mice, low dose LPS-induced MEKK3 modification and NFκB activation were not affected in IRAK4 kinase inactive knock-in macrophages (**Fig. 24**). Taken together, these data suggest that although IRAK4 kinase activity was required for recruiting IRAK1 to mediate TAK1-dependent NFκB activation, IRAKM-dependent MEKK3-mediated NFκB activation does not require IRAK4 kinase activity.

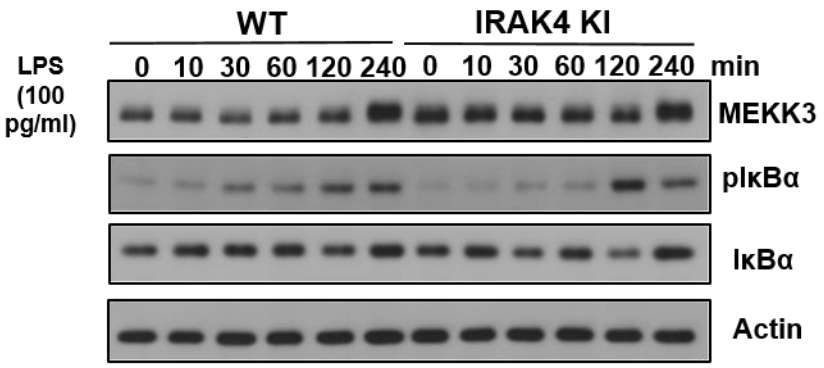

Figure 24. IRAK4 kinase activity is not required for low dose LPS-mediated NFκB activation. Cell lysates from wild-type (WT) and IRAK4 kinase activity dead knock in (IRAK4 KI) bone marrow-derived macrophages (BMDMs) untreated or treated with high dose LPS (100 pg/ml) for the indicated times were analyzed by Western blot analysis with antibodies against, MEKK3, p-IκBα, IκBα, and actin.

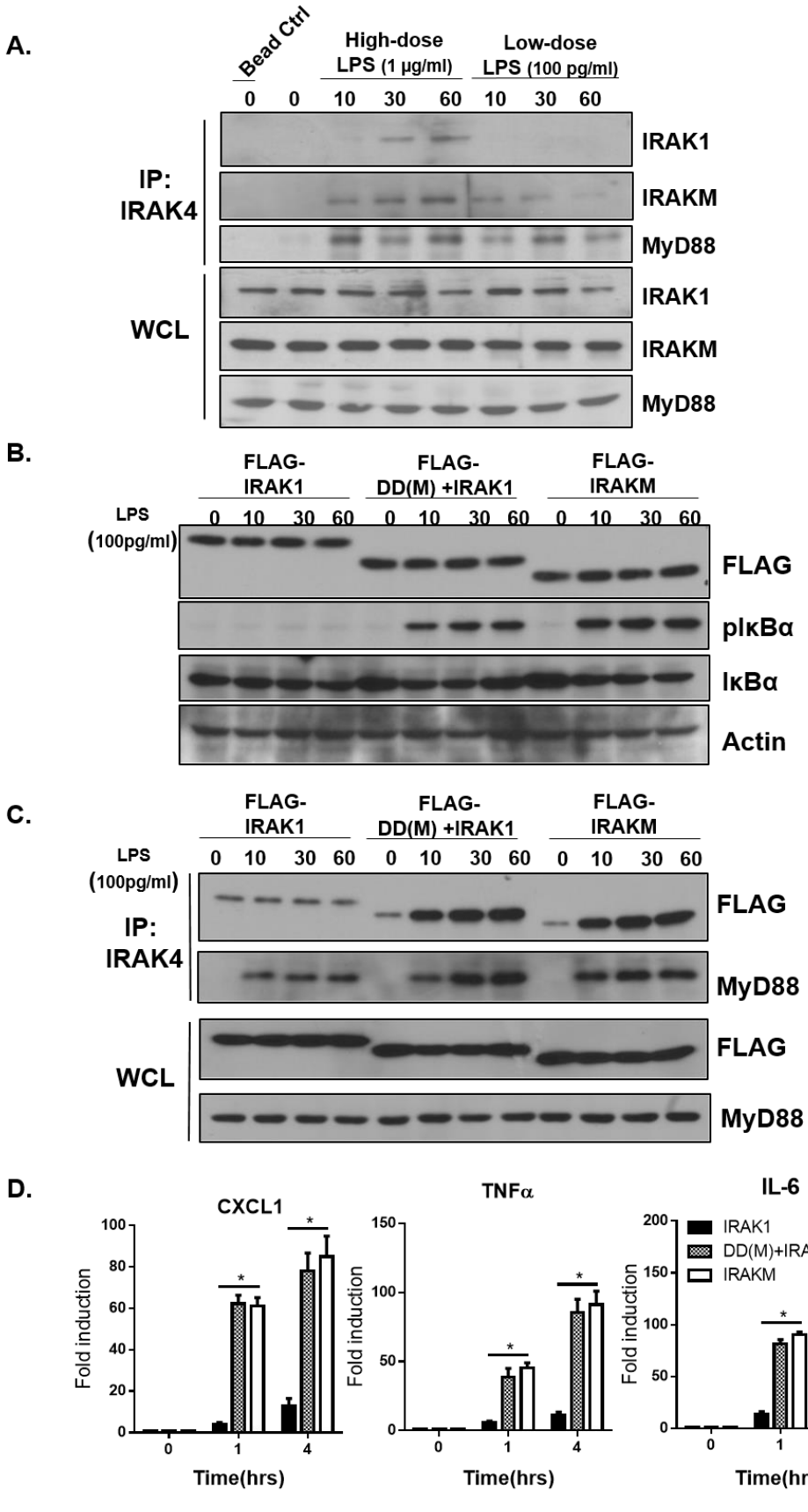
A.
Bead Ctrl
High-dose LPS (1 μg/ml)
Low-dose LPS (100 pg/ml)
0 0 10 30 60 10 30 60
IP: IRAK4
IRAK1
IRAKM
MyD88
WCL
IRAK1
IRAKM
MyD88
B.
FLAG-IRAK1
FLAG-DD(M) +IRAK1
FLAG-IRAKM
LPS (100pg/ml)
0 10 30 60 0 10 30 60 0 10 30 60
FLAG
pIκBα
IκBα
Actin
C.
FLAG-IRAK1
FLAG-DD(M) +IRAK1
FLAG-IRAKM
LPS (100pg/ml)
0 10 30 60 0 10 30 60 0 10 30 60
IP: IRAK4
FLAG
MyD88
WCL
FLAG
MyD88
D.
CXCL1
TNFα
IL-6
IRAK1
DD(M)+IRAK1
IRAKM
Fold induction
Time(hrs)
0 1 4
100 80 60 40 20 0
150 100 50 0
200 150 100 50 0
*

Figure 25. Low-dose LPS preferentially induces the formation of IRAKM Myddosome via the death domain of IRAKM. A. Wild-type BMDMs were treated with high dose LPS (1 μg/ml) and low dose LPS (100 pg/ml) for the indicated times, followed by immunoprecipitation (IP) with anti-IRAK-4 antibody and analyzed by Western blot analysis with antibody against IRAK1, IRAKM and MyD88. **B-D.** IRAK-1/2/M-triple deficient immortalized BMDMs infected with adenovirus expressing FLAG-tagged IRAK1, FLAG-tagged chimeric IRAKM death domain with IRAK1 kinase domain (DD(M)+IRAK1) and FLAG-tagged IRAKM were treated with low dose LPS (100 pg/ml) for indicated times. **B.** Cell lysates were analyzed by Western blot analysis with antibodies against FLAG, p-IκBα, IκBα, and actin. **C.** followeing by immunoprecipitation (IP) with anti-IRAK-4 antibody and analyzed by Western blot analysis with antibody against FLAG and MyD88. **D.** Total mRNAs were subjected to RT-PCR analyses for the levels of CXCL1, IL-6 and TNFα expression. Data represent mean ± SEM; *, $P<0.05$.

To further elucidate the mechanism for the specific activation of IRAKM-MEKK3-dependent pathway by low dose LPS, we compared IRAKM versus IRAK1 in their differential recruitment to the TLR-MyD88-IRAK4 complex. The crystal structure of Myddosome complex suggests the assembly of MyD88-IRAK4 with IRAK1, IRAK2 or IRAKM via the interaction of their death domains. We thus hypothesized that the specificity lies in the death domain of IRAKM versus IRAK1 in their formation of Myddosome in response to receptor activation by low versus high dose of ligands. To test this hypothesis, we generated a chimera protein by replacing the IRAK1 death domain with IRAKM death domain: DD(M)-IRAK1. Flag-tagged wild-type IRAK1, IRAKM, and DD(M)-IRAK1 in retroviral vectors were infected into IRAK1/2/M-TKO macrophages, followed by stimulation with low or high dose of LPS. We found that wild-type IRAKM and DD(M)-IRAK1 were able to interact with MyD88-IRAK4 and restore the low dose LPS-induced IκBα phosphorylation and gene expression, whereas wild-type IRAK1 failed to rescue the low dose LPS-mediated signaling (**Fig. 25B-D**). Taken together, our results suggest that the death domain of IRAKM is responsible for the specific recruitment to the

TLR-MyD88-IRAK4 complex in response to low dose LPS, leading to MEKK3-dependent NFκB activation.

IRAKM-dependent pathway is required for the development of alcohol-induced liver disease

Alcohol intake increases gut permeability, which allows accumulation of low levels of TLR ligands in the circulation and liver. The activation of hepatic macrophages (Kupffer cells) to portal endotoxin/LPS plays a key role in the early pathogenesis of ALD [115, 116, 148, 154, 155]. Thus, we propose that engagement of IRAKM-dependent signaling might be the dominant TLR-activated pathway during the development of ALD. To test this hypothesis, we subjected female IRAKM-deficient and littermate control wild-type mice to chronic ethanol feeding via the Lieber-DeCarli liquid diet to model steatosis and mild inflammation**.** Briefly, the ethanol-fed group was allowed free access to an ethanol-containing diet with increasing concentrations of ethanol as part of a complete liquid diet for 25 days. Control mice were pair-fed a diet that isocalorically substituted maltose dextrin for ethanol. Compared to pair-fed control mice, the alcohol-fed WT mice had significant increase in hepatocyte injury [assessed by serum aspartate aminotransferase (AST) and alanine aminotransferase (ALT) levels, **Fig. 26A**], steatosis [lipid droplets in hepatocytes (H&E and oil red staining), **Fig. 26B and D**] and hepatic triglyceride levels (**Fig. 26C**). Compared to WT mice, IRAKM-deficient mice had attenuated alcohol-induced hepatocelullar injury as evident by reduced serum AST and ALT levels (**Fig. 26A**). Notably, hepatic steatosis and triglyceride levels in alcohol-fed IRAKM-deficient mice were also significantly decreased compared with those in WT mice (**Fig. 26B-D**). Moreover, IRAKM

deficiency prevented the alcohol-induced upregulation of TNF-α, IL-6, and MCP-1 mRNA in the liver of alcohol-fed mice (**Fig. 26E**). Taken together, these data support the crucial role of IRAKM in the pathogenesis of alcohol-induced inflammatory responses in the liver.

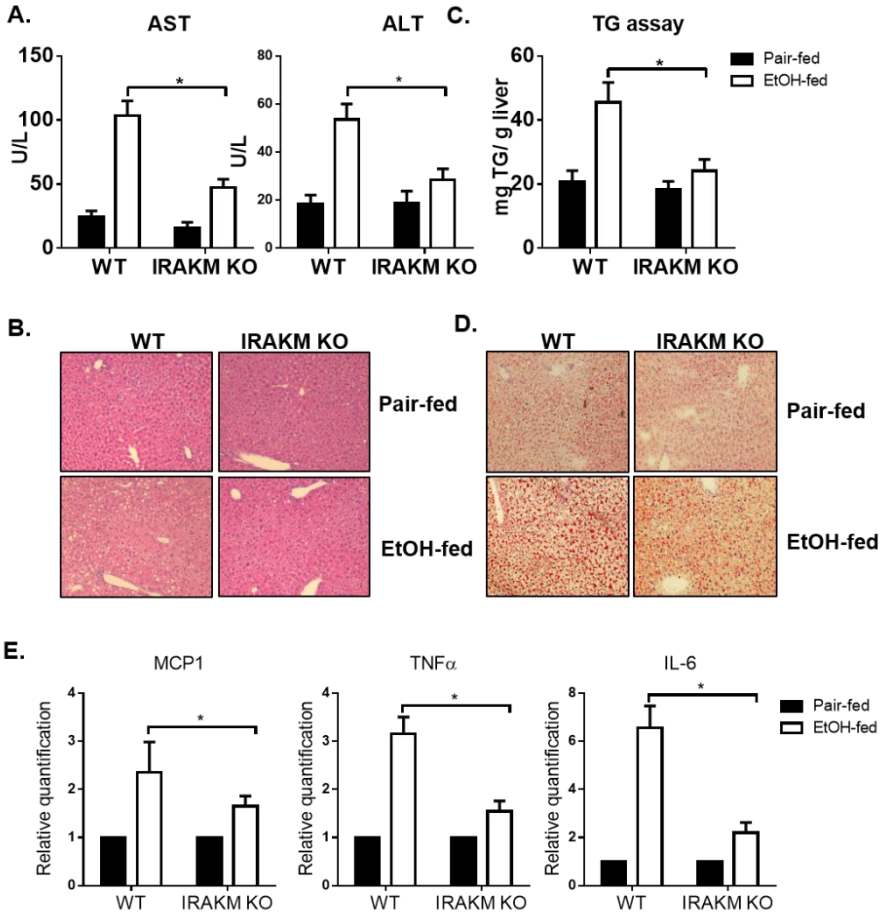

Figure 26. IRAKM-dependent pathway is required for the development of alcohol-induced liver disease. Wild-type and IRAKM KO mice were allowed free access to ethanol (EtOH) or pair-fed control diets. **A.** AST and ALT activity was determined in plasma. **B.** Paraffin-embedded liver sections were stained with hematoxylin and eosin. **C.** Hepatic triglyceride content was measured in whole liver homogenates. **D.** Frozen liver sections were subjected to Oil Red O staining. All images were acquired using a 10X objective. **E.** Total mRNAs from livers of WT and IRAKM KO mice (pair-fed and EtOH-fed) were subjected to RT-PCR analysis for the levels of MCP1, TNFα and IL-6 and normalized to 18sRNA. Data represent mean ± SEM; *, P<0.05.

IRAKM is required for TLR-mediated Mincle expression

The next question was how IRAKM-mediated pathway contributes to pathogenesis of ALD. Since low dose of LPS only induced minute amount of inflammatory cytokines and chemokines in wild-type BMDMs (**Fig. III-6**), we suspected that the impact of IRAKM on ALD might not due to its direct role in TLR-mediated inflammatory gene expression. Through a search for novel IRAKM-dependent genes, we found that Mincle, a sensor for cell death, is strongly induced by low does LPS, which was greatly reduced in IRAKM-deficient cells (**Fig. 28A**). It is important to note that the induction of Mincle mRNA was not affected in IRAK1/2 double deficient macrophages (data not shown). Similarly, low LPS-induced Mincle protein levels were not reduced in IRAK1/2-deficient cells, but greatly reduced in IRAKM-deficient macrophages**,** indicating that Mincle expression is mostly dependent on IRAKM (**Fig. 28B** and data not shown). We then examined the expression of Mincle in the liver tissue in pair-fed and alcohol-fed WT and IRAKM-deficient mice. Interestingly, by immune fluorescent staining, we found that Mincle expression was increased in the liver of alcohol-fed wild-type mice, which was co-localized with liver resident macrophage marker F4/80 (**Fig. 28C**). Importantly, ethanol-induced expression of Mincle was attenuated in IRAKM-deficient mice, implicating the potential importance of Mincle in IRAKM-mediated impact on ALD.

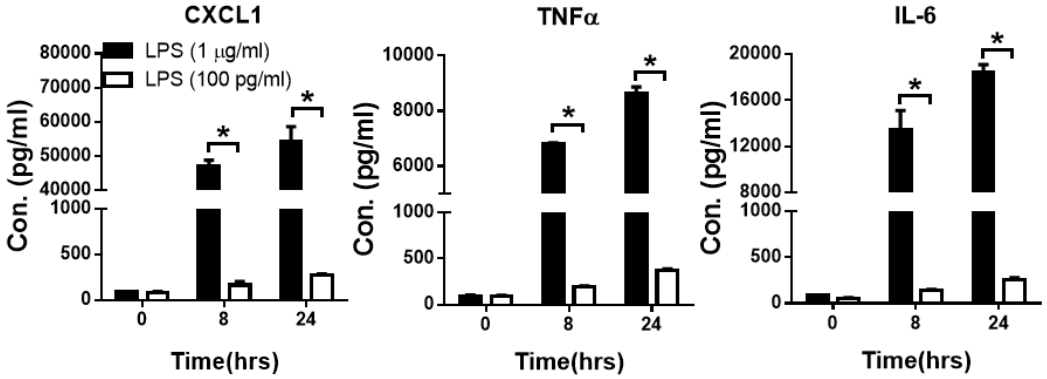

Figure 27. Low dose of LPS induced minute amount of inflammatory cytokines and chemokines production. Bone marrow-derived macrophages (BMDMs) were treated with high dose LPS (1 μg/ml) or low dose LPS (100 pg/ml) for 24 hours. Cell-free supernatants were collected and CXCL1, TNFα and IL-6 concentrations were measured by ELISA assay. Data represent mean ± SEM; *, $P<0.05$.

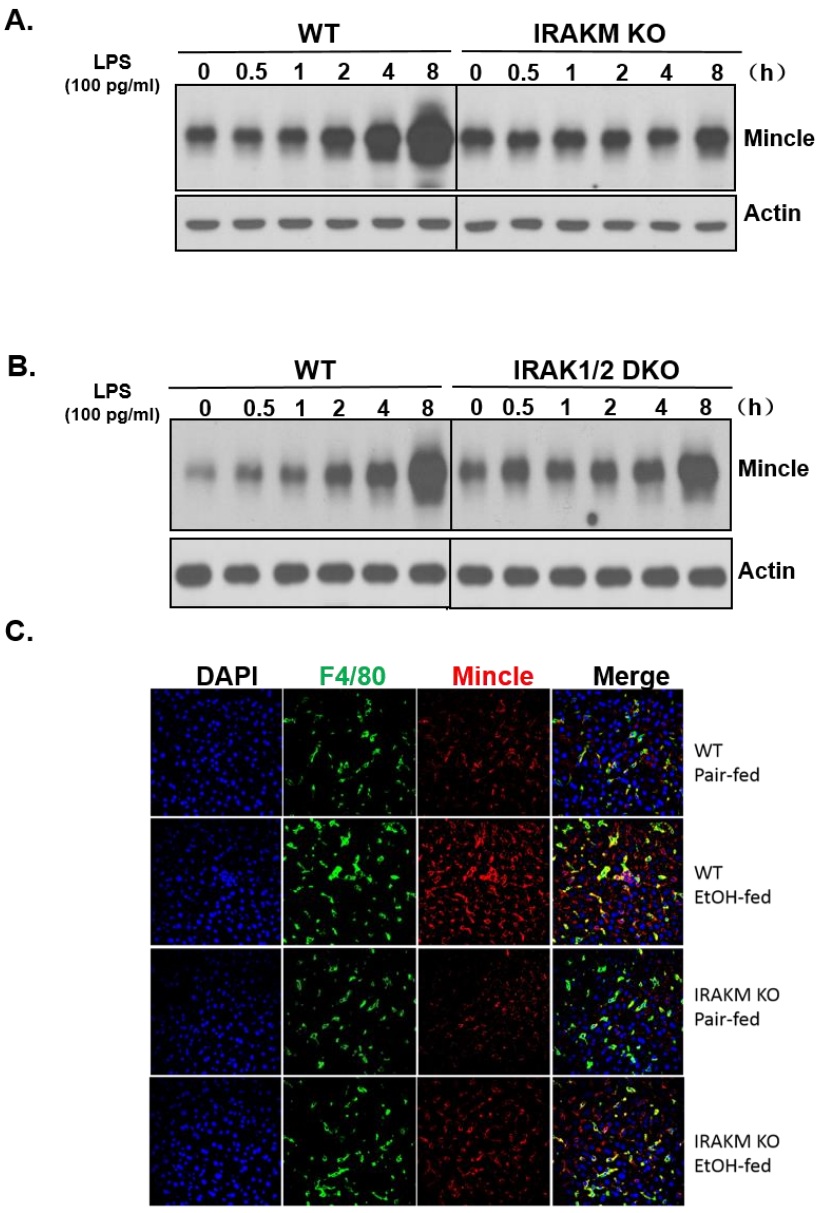

Figure 28. IRAKM is required for TLR and alcohol-induced Mincle upregulation. **A.** Cell lysates from wild-type (WT) and IRAKM KO bone marrow-derived macrophages (BMDMs) untreated or treated with low dose LPS (100 pg/ml) for the indicated times were analyzed by Western blot analysis with antibodies against Mincle and actin. **B.** Cell lysates from wild-type (WT) and IRAK1/2 double knock out (IRAK1/2 DKO) bone marrow-derived macrophages (BMDMs) untreated or treated with low dose LPS (100 pg/ml) for the indicated times were analyzed by Western blot analysis with antibodies against Mincle and actin. **C.** Immunostaining of F4/80 (green) and Mincle (red) was performed on frozen sections of liver from of WT and IRAKM KO mice (pair-fed and EtOH-fed). Confocal images are representative of five mice per group.

Mincle-mediated pathway is required for the development of alcohol-induced liver disease

Mincle was originally discovered based on its strong induction in macrophages by inflammatory stimuli, including TLR ligands [156]. One of the identified ligands for Mincle is spliceosome-associated protein (SAP) 130, a component of small nuclear ribonucloprotein, that diffuses out of dying cells, leading to onset of inflammation [52]. It is well documented that alcohol exposure induces endoplasmic reticulum (ER) stress and mitochondrial dysfunction in hepatocytes, which results in hepatocyte apoptosis and necrosis. Interestingly, upon challenge with ethanol and low dose LPS, hepatocytes released SAP130 to the culture media (**Fig. 29A**), implicating SAP130 as an endogenous ligand in the ALD model. Since Mincle expression was induced in myeloid cells in the liver of ethanol-fed mice in an IRAKM-dependent manner, we hypothesized TLR-induced IRAKM-dependent Mincle upregulation in liver resident macrophages provides a critical link between alcohol-induced cell death and onset of inflammation, contributing to the pathogenesis of ALD. To test this hypothesis, female Mincle-deficient and C57BL/6 mice were exposed to chronic ethanol feeding via the Lieber-DeCarli liquid diet, as described above**.** In contrast to wild-type control mice, Mincle-deficient mice had reduced alcohol-induced hepatocyte injury and steatosis, demonstrated by the levels of ALT/AST in the plasma, lipid drops in the hepatocytes (H & E and oil red staining), and TG levels in the liver (**Fig. 29B-E**). Moreover, Mincle deficiency attenuated the upregulation of TNF-α, IL-6, and MCP-1 in the liver of alcohol-fed mice, supporting the crucial role of Mincle in the pathogenesis of alcohol-induced inflammatory responses in the liver (**Fig. 29F**).

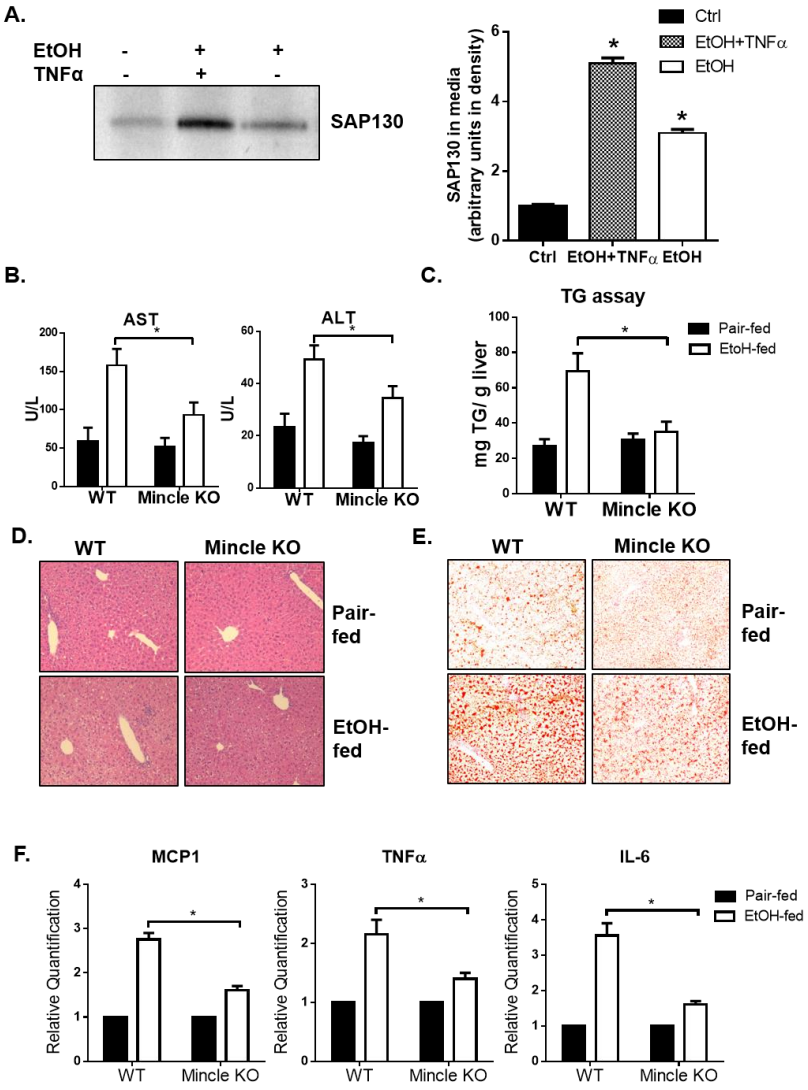

Figure 29. Mincle-dependent pathway is required for the development of alcohol-induced liver disease. A. Primary hepatocytes from WT mice were treated with EtOH (50 mM) with/without TNFα (30 ng/ml) for 24 hours. Cell-free supernatants were collected and SAP130 was measured by Western blot analysis with anti-SAP130 antibody. Band densities from three independent experiments were measured by ImageJ software and normalized to actin. Data represent mean ± SEM; *, P<0.05. Wild-type and Mincle KO mice were allowed free access to ethanol (EtOH) or pair-fed control diets. **B.** AST and ALT activity was determined in plasma. **C.** Paraffin-embedded liver sections were stained with hematoxylin and eosin. **D.** Hepatic triglyceride content was measured in whole liver homogenates. **E.** Frozen liver sections were subjected to Oil Red O staining. All images were acquired using a 10X objective. **F.** Total mRNAs from livers of WT and IRAKM KO mice (pair-fed and EtOH-fed) were subjected to RT-PCR analysis for the levels of MCP1, TNFα and IL-6 and normalized to 18sRNA. Data represent mean ± SEM; *, P<0.05.

SAP130-mediated Mincle activation is required for low concentration LPS induced inflammation through inflammasome activation

Since Mincle plays a critical in the pathogenesis of ALD, we then aimed to investigate how Mincle exerts its impact on the disease process. In addition to necrotic cell ligands, fungal and mycobacterial ligands for Mincle have been identified. Mincle is essential for recognition of the mycobacterial cord factor and its synthetic analog Trehalose-Dibehenate (TDB) [157]. Interestingly, while TDB has been shown to activate NLRP3 inflammasome [158, 159], Dectin-1, another member of C-type lectin receptors, activates processing of IL-1β via a noncanonical caspase-8 inflammasome [160]. Since we detected SAP130 in the culture media of hepatocytes treated with alcohol (**Fig. 29A**), it suggests that SAP130 might be an endogenous ligand in the ALD model. Thus, we examined whether SAP130 can also engage Mincle for inflammasome activation. Importantly, recombinant SAP130 indeed induced caspase-1 cleavage and IL-1β production in macrophages primed with low dose LPS (to up-regulate Mincle), which were abolished in Mincle-, ASC- and NLRP3-deficient macrophages (**Fig. 30A-B**). These results suggest that Mincle activation in macrophages results in activation of ASC-dependent inflammasomes.

Importantly, recent studies have shown that mice deficient in inflammasome components (adaptor ASC and caspase 1) or IL-1R are protected from ALD [117]. However, it remains unclear how inflammasome is activated in the liver of alcohol-fed mice. Based on the ability of SAP130 in activation of inflammasome, we hypothesized that Mincle senses necrotic cells induced by alcohol and subsequently activates ASC-dependent inflammasome(s), leading to caspase1 activation and IL-1β production. Importantly, we

indeed detected increased caspase-1 activity (shown as cleaved caspase 1 and processed IL-1β) in the liver of ethanol-fed mice, which was much reduced in IRAKM- and Mincle-deficient mice (**Fig. 30C-D**). Taken together, these results suggest that while low circulating LPS upregulates Mincle expression in macrophages/Kupffer cells in an IRAKM-dependent manner, SAP130 released from hepatocytes injured by ethanol triggers Mincle activation, leading to inflammasome activation and IL-1β production.

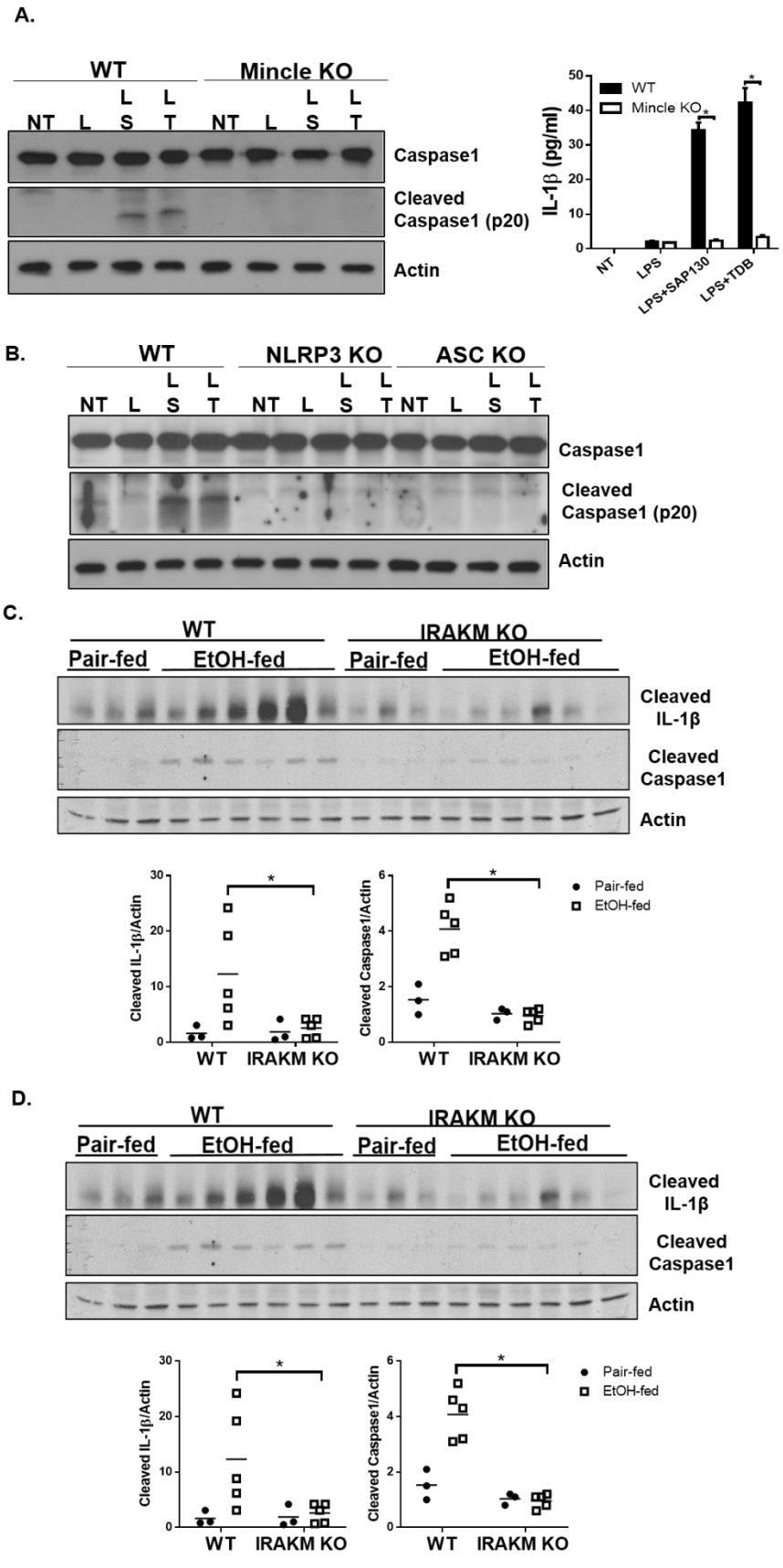
A.
WT
Mincle KO
NT L LS LT NT L LS LT
Caspase1
Cleaved Caspase1 (p20)
Actin
WT
Mincle KO
IL-1β (pg/ml)
NT
LPS
LPS+SAP130
LPS+TDB
B.
WT
NLRP3 KO
ASC KO
NT L LS LT NT L LS LT NT L LS LT
Caspase1
Cleaved Caspase1 (p20)
Actin
C.
WT
IRAKM KO
Pair-fed
EtOH-fed
Pair-fed
EtOH-fed
Cleaved IL-1β
Cleaved Caspase1
Actin
Cleaved IL-1β/Actin
Cleaved Caspase1/Actin
Pair-fed
EtOH-fed
WT
IRAKM KO
D.
WT
IRAKM KO
Pair-fed
EtOH-fed
Pair-fed
EtOH-fed
Cleaved IL-1β
Cleaved Caspase1
Actin
Cleaved IL-1β/Actin
Cleaved Caspase1/Actin
Pair-fed
EtOH-fed
WT
IRAKM KO

Figure 30. SAP130-mediated mincle activation is required for low concentration LPS induced inflammation through inflammasome activation. A. BMDMs from WT and Mincle KO mice **B.** BMDMs from WT, NLRP3 KO and ASC KO mice were treated with PBS (NT), LPS (100 pg/ml) for 24 hours (L), LPS (100 pg/ml, 24 hours) + SAP130 (5 μg/ml, 6 hours) (LS) or LPS (100 pg/ml, 24 hours) + TDB (100 μg/ml, 6 hours). Cell lysates and supernatants were collected together and were immunoblotted with the antibodies against caspase1, cleaved caspase1 (p20) and actin. Cell-free supernatants were collected and IL-1β was measured by ELISA. Data represent mean ± SEM; *, $P<0.05$. **C.** Tissue lysates from the whole liver of WT and IRAKM KO mice (pair-fed and EtOH-fed) were analyzed by Western blot analysis with antibodies against cleaved IL-1β, cleaved caspase1 (p20) and actin. Band densities were measured by ImageJ software and normalized to actin. Data represent mean ± SEM; *, $P<0.05$. **D.** Tissue lysates from the whole liver of WT and Mincle KO mice (pair-fed and EtOH-fed) were analyzed by Western blot analysis with antibodies against cleaved IL-1β, cleaved caspase1 (p20) and actin. Band densities were measured by ImageJ software and normalized to actin. Data represent mean ± SEM; *, $P<0.05$.

D. Discussion

Emerging evidence indicates that activation of innate immunity in response to alcohol exposure plays a key role in the development and progression of ALD [110-115, 117, 154, 161-166]. Here we report a novel TLR4-IRAKM-dependent signaling pathway that contributes to the pathogenesis of ALD. While alcohol intake increases gut permeability and accumulation of low levels of LPS in the circulation and liver, we found that low dose of LPS preferentially induces the formation of IRAKM Myddosome, leading to MEKK3-dependent NFκB activation in macrophages. Importantly, this novel IRAKM-dependent signaling pathway leads to inflammsome activation during ALD through the upregulation of Mincle, a sensor for cell death. While SAP130, the endogenous ligand of Mincle, was released from hepatocytes after exposing to alcohol, recombinant SAP130 activated ASC-dependent inflammasomes and IL-1 production in macrophages (**Fig. 31**). Induction of Mincle was ablated in liver of IRAKM-deficient mice and Mincle deficiency protected mice from ethanol-induced liver injury, accompanied by reduced inflammasome activation and IL-1β production. These results suggest that IRAKM-Mincle axis might provide a critical link for the cross-talks between alcohol-induced cell damage and innate immune activation during the development and pathogenesis of ALD.

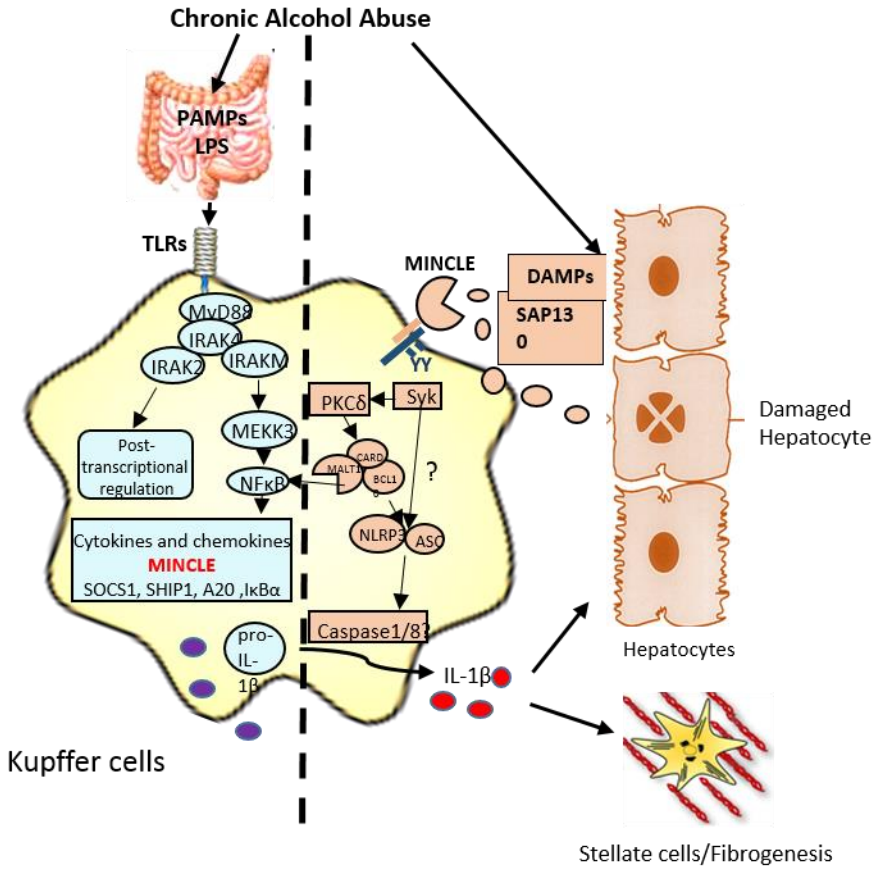

Figure 31. IRAKM-Mincle axis contributes to the pathogenesis and development of ALD. Chronic alcohol exposure results in increased intestinal permeability and changes in bacterial microflora increase levels of bacterial products in alcoholic patients and animal models of ALD. Further, alcohol exposure can induce endoplasmic reticulum (ER) stress and mitochondrial dysfunction in hepatocytes, contributing to hepatocellular injury and death. TLR4- induced IRAKM-mediated MEKK3-dependent NFκB activation is required for the up-regulation of Minlce in hepatic macrophages. Mincle sense the necroptotic hepatocytes-released nuclear protein, SAP130, which in turn activates the inflammasome activation in macrophages. Secreted IL-1β may further act on hepatocytes inducing pyroptosis or on Stellate cells which leads to fibrosis.

While low levels of LPS were detected in alcoholic patients and alcohol-treated experimental animals, mice deficient in TLR4 showed reduced alcohol-induced liver diseases [111, 112, 115, 116, 161, 162, 166]. TLR4 has ability to activate two distinct pathways: MyD88-dependent and MyD88-independent. MyD88-dependent pathway is activated by the adaptors TIRAP and MyD88, which leads to activation of NF-kB and to the induction of inflammatory cytokines. The second pathway (MyD88-independent) is activated by adaptors TRIF and TRAM, which activates IRF3 to induce Type I interferons (IFNs), as well as NF-kB activation [26, 122]. The TLR4-induced MyD88-independent TRIF/IRF3-dependent cascade has been directly implicated in steatosis and inflammation in ALD [166]. However, it remains unclear how MyD88-dependent pathway participates and contributes to the development and pathogenesis of ALD. This is the first study to show that MyD88 downstream component IRAKM is required for development and pathogenesis of ALD. Although the IRAK4 kinase activity was not required for IRAKM-dependent pathway, IRAK4 was recruited to MyD88 upon low dose LPS stimulation, which in turn recruits IRAKM for the formation of IRAKM Myddosome. Thus, IRAK4 probably functions as a structural protein in the IRAKM pathway. One important question is how the IRAKM Myddosome activates MEKK3. Since IRAKM does not have kinase activity, it is possible that MEKK3 is recruited to the IRAKM Myddosome for its activation, leading to the phosphorylation of IRAKM and consequent release of IRAKM-MEKK3 from the receptor complex to activate the IκB kinase complex for NFκB activation. Future studies are required to elucidate the IRAKM-MEKK3 NFκB activation mechanism.

IRAKM is well known as a negative regulator of inflammatory response during acute inflammation. Our previous study shows that IRAKM is capable to form Myddosome complex with MyD88 and IRAK4 in response to TLR ligands stimulation as IRAK1/2. IRAKM Myddosome is required for late phase NFκB activation through MEKK3 dependent pathway. This IRAKM-dependent pathway only induces expression of genes that are not regulated at the posttranscriptional levels (including inhibitory molecules SOCS-1, SHIP-1, A20 and IκBα), exerting an overall inhibitory effect on inflammatory response. Further, IRAKM specifically interacts with IRAK2, but not IRAK1, to suppress TLR-induced IRAK2 mediated translation of cytokines and chemokines [153]. Overall, IRAKM functions as suppressor of inflammation during infectious diseases and is required for the homeostasis. However, the role of IRAKM in low level chronic diseases has not been reported. In this paper, our data suggests that TLR4-induced IRAKM Myddosome dependent pathway plays as pathogenic role in ALD. Further biochemical analysis suggests that IRAKM-dependent MEKK3-mediated NFκB activation does not require IRAK4 kinase activity. The death domain of IRAKM is responsible for the specific recruitment to the TLR-MyD88-IRAK4 complex in response to low dose LPS, leading to MEKK3-dependent NFκB activation.

Since IRAK1 is not activated upon low dose LPS stimulation, we do not anticipate IRAK1 to be part of the receptor complex for the IRAKM pathway. We expect the death domain determines the specific recruitment of IRAKM the receptor complex induced by low dose ligands. Thus, we predict DD(M)-IRAK1, but not DD(1)-IRAKM, will restore TLR signaling in response to low dose TLR ligands.

Next important question we asked is that how IRAKM-dependent pathway mediates the pathogenesis of ALD. Since low dose of LPS only induced minute amount of inflammatory cytokines and chemokines in wild-type BMDMs, we suspect that the impact of IRAKM on ALD might not due to its direct role in TLR-mediated inflammatory gene expression. Through a search for novel IRAKM-dependent genes, we found that Mincle, a sensor for cell death, is strongly induced by low does LPS, which was greatly reduced in IRAKM-deficient cells. Mincle, a member of C-type lectin receptor, was discovered because it is strongly induced in macrophages by inflammatory stimuli, including TLR ligands [156]. Mincle-mediated pathway is critical for anti-fungal and anti-mycobacterial immune response [46, 51, 167, 168]. Recent study found that Mincle functions as a sensor non-homeostatic cell death which leads to sterile inflammation. Spliceosome-associated protein (SAP)130 was identified as the endogenous ligand that was recognized by Mincle following necrotic cell death [52]. In this study, we found that TLR-induced Mincle expression is dependent on IRAKM in BMDMs. Also, the upregulation of Mincle is also found in the liver of wild-type alcohol-fed mice and ablated in IRAKM deficient mice. Consistently, the alcohol-fed Mincle deficient mice also had significant decrease in hepatocyte injury, steatosis and liver inflammation levels.

Fungal, mycobacterial and necrotic cell ligands for Mincle have been identified, implicating this receptor in anti-microbial immunity and homeostasis. Mincle is essential for recognition of the mycobacterial cord factor and its synthetic analog Trehalose-Dibehenate (TDB) [157, 168, 169]. Interestingly, TDB has been shown to be able to activate NLRP3 inflammasome [158]. Further, Dectin-1, another member of C-type lectin receptors, is also able to activate processing of IL-1β via a noncanonical caspase-8

inflammasome [160]. Recent studies have shown that mice deficient in inflammasome components or IL-1R are protected from ALD [117]. However, how inflammasome gets activated in the alcohol-fed liver is still unclear. In this study, we found SAP130 is also capable to activate caspase-1 inflammasome in BMDMs. Alcohol-feeding induced caspase-1 and IL-1β activation was also decreased in the liver of IRAKM and Mincle deficient mice. However, how Mincle-mediated pathway activates inflammasome in cooperating with low dose LPS is still not unclear. This will be the future direction of this study.

Overall, here we first report that IRAKM-dependent pathway induced by low concentration of TLR ligands contributes to the pathogenesis of ALD by upregulating Mincle expression in hepatic macrophages. Activation of Minlce-mediated pathway by sensing SAP130 which released from necrotic hepatocytes leads to further liver inflammation through inflammasome activation. It provides a novel mechanistic insight of ALD and may be crucial for future pharmaceutical target design.

E. Materials and Methods

Biological reagents and cell culture—LPS (Escherichia coli 055:B5) and ATP (A2383) were purchased from Sigma-Aldrich. TDB was purchased from Invivogen. Antibodies against phosphorylated IκBα(Ser32/S36), JNK, IKKα/β(Ser176/180), and total IκBα were purchased from Cell signaling. Antibody to IRAK-4 was purchased from Enzo Life Science. Antibody to FLAG (anti-FLAG) and hemagglutinin (anti-HA) were purchased from Sigma-Aldrich. Antibody to MEKK3 was purchased from BD Bio-

sciences Pharmingen. Antibodies against IRAK1, TAK1 and Actin were from Santa Cruz Biotechnologies. Anti-IL-1β antibody (3ZD) was obtained from the Biological Resources Branch of the NIH. Anti-caspase-1 (p20) antibody was generated as previously described by L. Franchi and G. Nunez [170]. Anti-Mincle antibodies were generated as previously describes [52, 167].V5-tagged recombinant SAP130 was overexpressed in HEK-293 cells and purified as previously described [52]. Bone-marrow derived macrophages were obtained from the bone marrow of tibia and femur by flushing with DMEM. The cells were cultured in DMEM supplemented with 20% fetal bovine serum (FBS), penicillin G (100 μg/ml), and streptomycin (100 μg/ml), and 30% L929 supernatant for 5 days.

Plasmids and retroviruses—Mouse IRAKM and IRAK1 cDNA were purchased from Open Biosystems. IRAK1/IRAKM chimeric constructs were generated by overlapping PCR. The wild-type IRAK1, IRAKM and IRAK1/IRAKM chimeric mutant were cloned into pMX retroviral expression vector and transfected into phoenix cell for viral packaging. Immortalized IRAK1/2/3 triple deficient BMDMs were infected by the packaged retrovirus for 3 days and selected by puromycin (2μg/ml) for 2days for stable viral integration. For all PCR reactions high fidelity Pfu Turbo polymerase was used (Stratagene).

Immunoblotting—Cell were harvested and lysed in a Triton-containing lysis buffer (0.5% Triton X-100, 20 mM HEPES (pH 7.4), 150 mM NaCl, 12.5 mM β-glycerophosphate, 1.5 mM $MgCl_2$, 10 mM NaF, 2 mM dithiothreitol, 1 mM sodium orthovanadate, 2mM EGTA, 1 mM phenylmethylsulfonyl fluoride and complete protease inhibitor cocktail from Roche). Cell lysates were then separated by 10% SDS-PAGE, transferred to Immobilon-P membranes (Millipore), and subjected to immunoblotting.

Quantitative real-time PCR—Total RNA was isolated using TRIzol reagent (Invitrogen). 3μg of total RNA was then used for reverse transcription reaction using SuperScript-reverse transcriptase (Invitrogen). Q-PCR was performed in AB 7300 RealTime PCR System, and the gene expression of mouse CXCL1 (KC), TNFα, IL-6, MCP-1 Mincle, 18s RNA and β-actin was examined by SYBR® GREEN PCR Master Mix (Applied Biosystems). PCR amplification was performed in triplicate, and water was used to replace cDNA in each run as a negative control. The reaction protocol included pre-incubation at 95 ℃ to activate FastStart DNA polymerase for 10 min, amplification of 40 cycles that was set for 15 s at 95 ℃, and annealing for 60 s at 60 ℃. The results were normalized with the housekeeping gene β-actin or 18s RNA. Primer sequences were designed using AlleleID 6.0. The following primers were used: mouse TNFα forward, CAAAGGGAGAGTGGTCAGGT; mouse TNFα reverse, ATTGCACCTCAGGGAAGAGT; mouse actin forward, GGTCATCACTATTGGCAACG; mouse actin reverse, ACGGATGTCAACGTCACACT; mouse CXCL1 forward, TAGGGTGAGGACATGTGTGG; mouse CXCL1 reverse, AAATGTCCAAGGGAAGCGT; mouse IL-6 forward, GGACCAAGACCATCCAATTC; mouse IL-6 reverse, ACCACAGTGAGGAATGTCCA.

ELISA assay—Supernatants from cell cultures were collected and measured for the level of mouse cytokines IL-1β, CXCL1, IL-6 and TNFα using Duoset ELISA kits (R&D system) according to manufacturer's instructions.

Mouse models and samples collection— IRAKM KO and Mincle deficient mice were previously described [52, 128]. All procedures using animals were approved by the Cleveland Clinic Institutional Animal Care and Use Committee. Female mice were housed in shoe-box cages (2 animals/cage) with microisolator lids. Standard microisolator handling procedures were used throughout the study. Mice were age-matched, randomized into ethanol-fed and pair-fed groups and then adapted to a control liquid diet for 2 days. The ethanol-fed groups were allowed free access to an ethanol containing diet. Control mice were pair-fed a control diet which iso-calorically substituted maltose dextrins for ethanol over the entire feeding period**.** Chronic ethanol-induced liver injury: 1% (vol/vol) ethanol for 2 days followed by 2% ethanol (11% of total calories) for 2 days, 4% ethanol for 1 week, 5% ethanol for 1 week followed by 6% ethanol for the final week . Sample collection: At the end of the feeding protocols, mice were anesthetized, blood samples taken into non-heparinized syringes from the posterior vena cava and livers excised. Portions of each liver were then either fixed in formalin or frozen in optimal cutting temperature (OCT) compound (Sakura Finetek U.S.A. Inc.) for histology, frozen in RNAlater (Qiagen) or flash frozen in liquid nitrogen and stored at -80 ℃ until further analysis. Blood was transferred to EDTA-containing tubes for the isolation of plasma. Plasma was then stored at -80 ℃. Histopathology and immunohistochemistry of mouse liver: Formalin-fixed tissues were paraffin-embedded, sectioned, coded and stained with hematoxylin and eosin. Frozen liver sections were used for staining F4/80 and Mincle. All images presented in the results are representative of at least 3 images per liver and 4 mice per experimental condition

ALT/AST and triglyceride measurement—Plasma samples were assayed for alanine aminotransferase (ALT) and aspartate aminotransferase (AST) using commercially available enzymatic assay kits (Diagnostic Chemicals) following the manufacturer's instructions. Total hepatic triglycerides were assayed using the Triglyceride Reagent Kit from Pointe Scientific Inc. (Lincoln Park, MI).

Inflammasome activation—BMDMs were plated in 6-well plates at a concentration of 2.0 X 10^6 cells per well the day before the experiment. The day of the experiment, cells were primed with low concentration of LPS (100 pg/ml), SAP130 (10 μg/ml) or TDB (10 μg/ml) for the indicated time. Medium was then supplemented with ATP (5 mM) for indicated time points. For all experiments, cell-free supernatant was then either collected for ELISA analysis, or cell lysates and supernatants were collected together for immunoblotting by the addition of 1% Nonidet-P40 supplemented with complete protease inhibitor 'cocktail' (Roche) and 2 mM dithiothreitol directly to the well. Cells were scraped and lysed on ice for 30 minutes, then spun at 13,000 rpm. Protein concentration was measured. 4X Laemlli buffer was then added, samples were boiled and approximately 20 μg of sample was run on a 12% or 15% SDS-PAGE gel.

CHAPTER IV

GENERAL DISCUSSION AND FUTURE DIRECTIONS

With these studies, we have uncovered dual roles for IRAKM in TLR signaling pathways. First, during acute inflammation, IRAKM functions as an important negative regulator of inflammation. It forms an IRAKM Myddosome complex with MyD88-IRAK4 complex similar to IRAK1/2 myddosome. IRAKM Myddosome is required for the late phase TLR-induced NFκB activation. This IRAKM Myddosome mediated TLR-induced NFκB activation through TAK1-independent MEKK3-dependent pathway only induces expression of genes that are not regulated at the posttranscriptional levels (including inhibitory molecules SOCS-1, SHIP-1, A20 and IκBα), exerting an overall inhibitory effect on inflammatory response. Further, IRAKM specifically interacts with IRAK2, but not IRAK1, and suppresses TLR-induced IRAK2-mediated translation of cytokines and chemokines.

Second, in low grade inflammation scenario, we found that IRAKM-dependent pathway is required for low dose TLR4 ligand-induced NFκB activation. Biochemical studies suggested low dose LPS-induced IRAKM-dependent NFκB activation is independent of IRAK4 kinase activity and the death domain of IRAKM is responsible for the specific recruitment to the TLR-MyD88-IRAK4 complex in response to low dose LPS. Ex-vivo experiments showed low dose of LPS only induced minute amounts of inflammatory cytokines and chemokines in wild-type BMDMs. IRAKM-deficient mice were protected from alcohol-induced liver injury. Through our analysis of low dose LPS-induced IRAKM-dependent gene expression, we found a novel IRAKM dependent gene known as Mincle. As a sensor of cell death, Mincle is highly up-regulated upon low dose LPS stimulation which is dependent on IRAKM. Mincle deficient mice were also protected from alcohol-induced liver injury. Spliceosome-associated protein (SAP) 130 was identified as the endogenous ligand that was recognized by Mincle following necrotic cell death. Ex vivo studies showed that both IRAKM and Mincle are required for alcohol-feeding-induced inflammasome activation in the liver. Taken together, this study identifies an IRAKM-Mincle axis is critical for the pathogenesis of alcohol induced liver disease through the activation of inflammasome.

A. The Role of IRAKM in Acute Inflammation

IRAKM, also named as IRAK3, was identified in 1999, as an indispensable element of LPS-mediated signaling transduction [123]. It was found mainly expressed in cells of monomyeloic origin and was, therefore, designated IRAKM. Following studies with IRAKM deficient mice and cells suggest that IRAKM functions as a negative regulator of TLR signaling. Since IRAKM expression is induced by TLR ligands stimulation, it was thought to be a key component of a feedback regulatory system of innate immunity [128]. IRAKM deficient mice showed increased inflammatory cytokines and chemokines production or bacterial clearance, compared to wild-type control mice. IRAKM was shown to be required for endotoxin tolerance. On the molecular level, previous studies suggest that IRAKM prevents the dissociation of IRAKs from the adaptor MyD88, therefore, suppresses downstream signaling transduction. However, there has not been sufficient experimental evidences to support this. In our study, we provide two novel mechanisms for the regulatory role of IRAKM in TLR signaling.

IRAKM Myddosome

Myd88, an intracellular TIR domain containing protein, is utilized by IL-1R and all TLRs as an adaptor molecule except for TLR3. It contains an N-terminal death domain (DD) and a short intermediate domain (ID) [26, 122, 125, 171]. Through the DD, MyD88 interacts with IRAKs, a group of receptor proximal Ser/Ther kinases including IRAK1, IRAK2, IRAKM and IRAK4. All of the IRAKs, except IRAK4, contain a TRAF binding site at C-terminal motif which is required for binding to TRAF6 and subsequent NFκB activation through the TAK1-IKK complex. Recent crystal structure study reveals that 6 MyD88 DDs, 4 IRAK4 DDs and 4 IRAK2 DDs form a left-handed helical complex [127].

This helical signaling complex is referred as Myddosome complex and its assembly is sequential, in which MyD88 recruits IRAK-4 and the MyD88-IRAK4 complex recruits IRAK2 or the related IRAK1.

Our data suggested that IRAKM is also able to form a Myddosome complex with MyD88 and IRAK4, as IRAK1 and IRAK2. The DD of IRAKM shares a considerable sequence homology with IRAK2. By computational modeling, IRAKM DD has the capacity to dock to MyD88-IRAK4 complex to form a relatively stable complex. Detailed analysis suggested that IRAK4 binding residues with IRAK2 are highly conserved in IRAKM DD. E71, W74 and Q78 in IRAKM DD were suggested to be critical for binding with IRAK4 DD. By site-specific mutagenesis, we confirmed this TLR-induced binding interface between IRAK4 and IRAKM DD. Following functional tests, we confirmed the formation of IRAKM Myddosome complex is required for IRAKM-mediated signaling transduction.

A recent study from Dr. Hao Wu's group (the same group which resolved Myddosome crystal structure complex) indicates that formation of IRAK4 kinase domain (KD) dimers in Myddsosome complex is required for proximity-driven dimerization and activation of IRAK4 kinase activity. Our study indicated that IRAK1/2-mediated pathway is dependent on IRAK4 kinase activity, while IRAKM-mediated pathway is independent of IRAK4 kinase activity. Therefore, it is possible that IRAKM Myddosome complex may have a different structure with IRAK2 Myddosome. Future structural study on IRAKM Myddosome will be required to test this possibility.

TLR-induced IRAKM-mediated MEKK3-dependent NFκB activation

The previous work from our lab uncovered two parallel TLR/IL-1R-mediated NFκB activation pathways: TAK1-dependent and MEKK3-dependent, respectively. IRAK4 kinase activity and IRAK1 are required for TAK1-dependent pathway which leads to IKKα/β phosphorylation and IKKγ activation, resulting in NFκB activation through IκBα phosphorylation and degradation. The MEKK3-dependent pathway involves IKKα activation and IKKγ phosphorylation, which only leads to IκBα phosphorylation without degradation [65, 73, 129, 150, 151].

In this study, we found that IRAKM is required for TAK1-independent MEKK3-pathway. In response to TLR ligand simulation, IRAKM specifically interacts with MEKK3, not TAK1, through TRAF6, resulting in the phosphorylation of IKKγ and activation of IKKα. Furthermore, IRAK4 kinase activity is not required for IRAKM-mediated MEKK3 dependent pathway. One important question here is how the IRAKM Myddosome activates MEKK3. In regards to this question, testing whether IRAKM has kinase activity certainly warrants future study.

IRAKM has been considered to be a member of the pseudokinase family. Overexpression of IRAKM in HEK 293 cells did not lead to robust autophosphorylation as IRAK1 in *in vitro* kinase assay, rather an extremely weak autophosphorylation was observed [123]. Structurally, IRAKM lacks an aspartic acid residue in HRD motif in the catalytic loop which is crucial for the kinase activity. Interestingly, it was reported that murine IRAKM does has a weak but detectable autophosphorylation in *in vitro* kinase assay [172]. However, there was not enough experimental evidence to support this. Further

detailed biochemical study is required to define whether IRAKM has kinase activity or not and the potential role in IL-1R/TLR signaling.

Since IRAKM interacts with MEKK3, another possible scenario is that MEKK3 may directly phosphorylate IRAKM, leading to the activation of IRAKM and consequent release of IRAKM-MEKK3 from the receptor complex. This will be the future direction to study IRAKM-mediated MEKK3-dependent signaling pathway.

Post-translational modification of IRAKM

Among the four members of IRAK family, IRAK1 is the most characterized. Upon IL-1 or TLR ligands stimulation, IRAK1 is phosphorylated, ubiquitinated and degraded. Also it has been reported that IRAK1 may also undergo sumoylation besides phosphorylation and ubiquitination in TLR signaling. IRAK1, through Lysine 48 and Lysine K63-mediated ubiquination, is mediated by the E3 ligase β-TRCP and Pellino2, respectively [150, 151]. Recent study suggests that IRAK2 also undergoes phosphorylation and ubiquitination upon TLR ligand stimulation [173]. However, there is no report has been published on IRAKM modification. An ongoing project in our lab aims to find the phosphorylation sites of IRAKM in response to LPS treatment by mass spectroscopy analysis.

IRAKM-dependent second wave of NFκB activation and gene expression

In the absence of IRAK1 and IRAK2 (in IRAK 1/2 double-deficient cells), IRAKM is able to mediate prompt TLR-induced NFκB activation. This only indicates IRAKM Myddosome has the capability to activate NFκB. To further determine its physiological significance, we re-investigated TLR-induced NFκB activation in IRAKM single deficient

cells. Surprisingly, the late phase of TLR7-induced late phase NFκB activation was decreased in IRAKM deficient cells.

By analyzing pro-inflammatory genes expression and protein production, we found that, although TLR-induced IRAKM-mediated signaling in IRAK1/2 double deficient cells can mediate the induction of mRNAs expression of pro-inflammatory genes in early time points, the protein production was total abolished. It suggests that IRAKM-mediated pathway alone is not sufficient to induce the production of cytokines and chemokines. This phenomenon indicates the critical role of TLR-induced IRAK1/2-dependent post-transcriptional regulation in innate immune response.

Our previous study about the role of IRAK4 kinase activity in TLR-induced gene expression identified a group of genes which are not regulated on post-transcriptional levels [73]. Consistently, the expression of these genes was also substantially reduced in IRAKM deficient cells compared to that in wild-type cells. Several of the genes are important for the activation and homeostasis of the macrophages (including ETS2, SOD2, Bcl-2A1D and GPR84) Interestingly, we found another group of IRAK-M-dependent genes including A20, SOCS1, SHIP1 and IκBα. These molecules are all well-known inhibitory molecules of inflammation. They not only negatively regulate TLR-mediated signaling pathway, but also control other critical inflammation-related signaling pathways, such as JAK-STAT pathways, TNFα-activated pathway, PI3K-Akt pathway [174-177]. This study provided a novel mechanism which IRAKM exerts an overall inhibitory effect in acute inflammatory response through producing inhibitory molecules as feedback regulation system. The advantage for such an inhibitory mechanism could be that IRAKM

may exert broader inhibitory effects not just on TLR/IL-1R but also on other cytokine signaling cascades, so that the inflammatory response can be effectively controlled.

The gene expression data were consistent with the role of IRAK-M in TLR7-induced second wave NFκB activation, since most of the IRAK-M-dependent genes were late genes (induced after 1 hour). However, it is still mysterious why IRAKM-MEKK3 pathway is important for the late phase NFκB activation and gene expression. One possible answer is that IRAK1 is phosphorylated, ubiquinated and degraded upon TLR ligand stimulation, while IRAKM expression is induced upon treatment. Only IRAKM is left at late time points at which mediates second wave NKκB activation. Future detailed studies on the dynamic and kinetic change of IRAK family members and their roles in TLR signaling need to done to solve this question.

IRAKM suppresses IRAK2-mediated translational regulation

Previous studies from our lab found that IRAK-2 plays an important role in the regulation of TLR-mediated protein translation of cytokines and chemokines, including IL-6, CXCL1 (KC) and TNFα. Although the mRNAs of these pro-inflammatory genes were induced at similar or reduced levels in IRAKM deficient BMDMs, their protein production were actually increased in the IRAKM deficient cells. Based on these observations we investigated the role of IRAK-M in the regulation of cytokine and chemokine translation. By poly-ribosome fractionation experiments, we determined that the translational efficiency of these genes were increased in the absence of IRAKM. Through co-immunoprecipitation experiments, we found that IRAKM specifically interacts with IRAK2, not IRAK1. Therefore, we proposed that IRAKM suppress the pro-inflammatory cytokines and chemokines production through the interaction with IRAK2. However, it is

still unclear how IRAKM interacts with IRAK2 and inhibit its ability to mediate protein translation. Future studies are needed to detail the molecular mechanism of IRAK2-mediated post-transcriptional control of pro-inflammatory genes and how IRAKM binds to and regulates IRAK2.

B. The Role of IRAKM in Low Grade Inflammation

It has been reported that IRAKM deficient macrophages/dendritic cells produce more cytokines and chemokines compared to wild-type control cells in response to high dose TLR agonists. Furthermore IRAKM expression in myeloid lineage cells is known to impair host defense during infection. Infection or sepsis can induce IRAKM expression which functions as negative feedback regulation of immune response. This is an important mechanism which prevent sepsis-induced septic shock. However, the role of IRAKM in low-grade inflammatory diseases has not been reported before, to the best of our knowledge.

High-grade inflammation versus low-grade inflammation

High-level endotoxemia in human or experimental animals induces a robust, but transient immune response. Both pro- and anti-inflammatory mediators are activated, providing a compensatory mechanism to resolve inflammation and prevent further damages. This is an important and strict regulatory mechanism to maintain host homeostasis. Emerging evidence suggests that low-level endotoxemia-induced low-grade inflammation plays a crucial role during the pathogenesis and development of in several different chronic diseases. High-level endotoxemia-induced robust acute inflammation, low-level endotoxemia-mediated mild but persist chronic inflammation. However, the

molecular mechanisms of this persistent low-grade inflammation are still poorly understood.

With our studies, we provide new mechanistic insight of low-grade chronic inflammation. IRAKM-mediated pathway is crucial for low-dose TLR ligand-induced pro-inflammatory gene expression. Inflammation can be further amplified by IRAKM-dependent Mincle expression on macrophages which can sense cell death. Mincle expression is very low in resting cells. It is highly induced in response to different cell stresses or danger signals, including TLR ligands. Recent study identified dead cell-released SAP130, a nuclear protein, as the endogenous ligand for Mincle. Activation of Mincle signaling leads to cytokine and chemokine production and neutrophils infiltration. A recent study suggests that low-dose LPS treatment can lead to mitochondria dysfunction and cell necroptosis. Here we provide a direct evidence linking un-regulated cell death to inflammation. Also it provides a new angle to study chronic inflammatory disease.

Alcohol induced liver disease and inflammasome activation

The pathogenesis of ALD is multifactorial and current studies suggest that the damage is the end result of the interplay among ethanol metabolism, inflammation and innate immunity. TLR4 mediated TLR signaling activation has been shown to be critical during the initiation and development of ALD. TLR4 has ability to activate two distinct pathways: MyD88-dependent and MyD88-independent. MyD88-dependent pathway is activated by the adaptors TIRAP and MyD88, which leads to activation of NFκB and to the induction of inflammatory cytokines. The second pathway (MyD88-independent) is activated by adaptors TRIF and TRAM, which activates IRF3 to induce Type I interferons (IFNs), as well as NFκB activation. The TLR4-induced MyD88-independent TRIF/IRF3-

dependent cascade has been directly implicated in steatosis and inflammation in ALD. It is important to note that IL-1R, which exclusively signals through the MyD88 pathway, is required for ALD pathogenesis. However, it remains unclear how the MyD88-dependent pathway participates and contributes to the development and pathogenesis of ALD. Here our preliminary studies identify that downstream signaling components of MyD88, the IRAKM proteins, play a critical role in the development and pathogenesis of ALD. It has also been reported that inflammasome activation was observed in the liver from alcohol-fed mice. Mice deficient in inflammasome components or IL-1R are protected from ALD. However, how inflammasome gets activated in the alcohol-fed liver is still unclear. In this study, we found SAP130 is also capable to activate caspase-1 inflammasome in BMDMs. Alcohol-feeding induced caspase-1 and IL-1β activation was also decreased in the liver of IRAKM and Mincle deficient mice. However, how Mincle-mediated pathway activates inflammasome in cooperating with low dose LPS is still not unclear. This will be the future direction of this study.

C. IRAKM as a Target for Drug Development

Dysregulated immune responses are involved in many chronic diseases, such as inflammatory bowel disease, atherosclerosis, rheumatoid arthritis and autism. TLR-mediated inflammatory responses are suggested to be involved in the pathogenesis of some of these diseases. Therefore, suppression of the inflammatory response mediated by TLRs would be a direct and efficient treatment for these diseases. However, considering the critical function of TLR-mediated signaling in innate immune response, the side effects of such treatment might be detrimental and lead to susceptible to infection. The observation

that IRAKM deficiency leads to increased pro-inflammatory cytokine and chemokine production during acute inflammation. While our study indicates that IRAKM-mediated MEKK3-dependent pathway is crucial in low-grade inflammation. IRAKM may be a better drug targets than other IRAKs in preventing chronic inflammation.

REFERENCE

1. Litman, G.W., J.P. Cannon, and L.J. Dishaw, *Reconstructing immune phylogeny: new perspectives.* Nat Rev Immunol, 2005. **5**(11): p. 866-79.
2. Aderem, A. and D.M. Underhill, *Mechanisms of phagocytosis in macrophages.* Annu Rev Immunol, 1999. **17**: p. 593-623.
3. Agerberth, B. and G.H. Gudmundsson, *Host antimicrobial defence peptides in human disease.* Curr Top Microbiol Immunol, 2006. **306**: p. 67-90.
4. Medzhitov, R., *Recognition of microorganisms and activation of the immune response.* Nature, 2007. **449**(7164): p. 819-26.
5. Matzinger, P., *The danger model: a renewed sense of self.* Science, 2002. **296**(5566): p. 301-5.
6. Himms-Hagen, J., *Brown adipose tissue thermogenesis: interdisciplinary studies.* FASEB J, 1990. **4**(11): p. 2890-8.
7. Foti, M., et al., *Dendritic cells in pathogen recognition and induction of immune responses: a functional genomics approach.* J Leukoc Biol, 2006. **79**(5): p. 913-6.
8. Mogensen, T.H., *Pathogen recognition and inflammatory signaling in innate immune defenses.* Clin Microbiol Rev, 2009. **22**(2): p. 240-73, Table of Contents.
9. Pober, J.S. and W.C. Sessa, *Evolving functions of endothelial cells in inflammation.* Nat Rev Immunol, 2007. **7**(10): p. 803-15.
10. Ogawa, Y. and W.J. Calhoun, *The role of leukotrienes in airway inflammation.* J Allergy Clin Immunol, 2006. **118**(4): p. 789-98; quiz 799-800.

11. Hochreiter-Hufford, A. and K.S. Ravichandran, *Clearing the dead: apoptotic cell sensing, recognition, engulfment, and digestion.* Cold Spring Harb Perspect Biol, 2013. **5**(1): p. a008748.

12. Pancer, Z. and M.D. Cooper, *The evolution of adaptive immunity.* Annu Rev Immunol, 2006. **24**: p. 497-518.

13. Alder, M.N., et al., *Diversity and function of adaptive immune receptors in a jawless vertebrate.* Science, 2005. **310**(5756): p. 1970-3.

14. International Human Genome Sequencing, C., *Finishing the euchromatic sequence of the human genome.* Nature, 2004. **431**(7011): p. 931-45.

15. Song, W.Y., et al., *A receptor kinase-like protein encoded by the rice disease resistance gene, Xa21.* Science, 1995. **270**(5243): p. 1804-6.

16. Janeway, C.A., Jr., *Approaching the asymptote? Evolution and revolution in immunology.* Cold Spring Harb Symp Quant Biol, 1989. **54 Pt 1**: p. 1-13.

17. Lemaitre, B., et al., *The dorsoventral regulatory gene cassette spatzle/Toll/cactus controls the potent antifungal response in Drosophila adults.* Cell, 1996. **86**(6): p. 973-83.

18. Medzhitov, R., P. Preston-Hurlburt, and C.A. Janeway, Jr., *A human homologue of the Drosophila Toll protein signals activation of adaptive immunity.* Nature, 1997. **388**(6640): p. 394-7.

19. Poltorak, A., et al., *Defective LPS signaling in C3H/HeJ and C57BL/10ScCr mice: mutations in Tlr4 gene.* Science, 1998. **282**(5396): p. 2085-8.

20. Hoshino, K., et al., *Cutting edge: Toll-like receptor 4 (TLR4)-deficient mice are hyporesponsive to lipopolysaccharide: evidence for TLR4 as the Lps gene product.* J Immunol, 1999. **162**(7): p. 3749-52.

21. Doyle, S.L. and L.A. O'Neill, *Toll-like receptors: from the discovery of NFkappaB to new insights into transcriptional regulations in innate immunity.* Biochem Pharmacol, 2006. **72**(9): p. 1102-13.

22. Bowie, A. and L.A. O'Neill, *The interleukin-1 receptor/Toll-like receptor superfamily: signal generators for pro-inflammatory interleukins and microbial products.* J Leukoc Biol, 2000. **67**(4): p. 508-14.

23. Khan, J.A., et al., *Crystal structure of the Toll/interleukin-1 receptor domain of human IL-1RAPL.* J Biol Chem, 2004. **279**(30): p. 31664-70.

24. Diebold, S.S., et al., *Innate antiviral responses by means of TLR7-mediated recognition of single-stranded RNA.* Science, 2004. **303**(5663): p. 1529-31.

25. Gay, N.J., et al., *Assembly and localization of Toll-like receptor signalling complexes.* Nat Rev Immunol, 2014. **14**(8): p. 546-58.

26. Yamamoto, M., et al., *Role of adaptor TRIF in the MyD88-independent toll-like receptor signaling pathway.* Science, 2003. **301**(5633): p. 640-3.

27. Yamamoto, M., et al., *Essential role for TIRAP in activation of the signalling cascade shared by TLR2 and TLR4.* Nature, 2002. **420**(6913): p. 324-9.

28. Shigeoka, A.A., et al., *TLR2 is constitutively expressed within the kidney and participates in ischemic renal injury through both MyD88-dependent and -independent pathways.* J Immunol, 2007. **178**(10): p. 6252-8.

29. Kawai, T. and S. Akira, *The role of pattern-recognition receptors in innate immunity: update on Toll-like receptors.* Nat Immunol, 2010. **11**(5): p. 373-84.

30. Erridge, C., *Endogenous ligands of TLR2 and TLR4: agonists or assistants?* J Leukoc Biol, 2010. **87**(6): p. 989-99.

31. Ozinsky, A., et al., *The repertoire for pattern recognition of pathogens by the innate immune system is defined by cooperation between toll-like receptors.* Proc Natl Acad Sci U S A, 2000. **97**(25): p. 13766-71.

32. Hayashi, F., et al., *The innate immune response to bacterial flagellin is mediated by Toll-like receptor 5.* Nature, 2001. **410**(6832): p. 1099-103.

33. Heil, F., et al., *Species-specific recognition of single-stranded RNA via toll-like receptor 7 and 8.* Science, 2004. **303**(5663): p. 1526-9.

34. Alexopoulou, L., et al., *Recognition of double-stranded RNA and activation of NF-kappaB by Toll-like receptor 3.* Nature, 2001. **413**(6857): p. 732-8.

35. Latz, E., et al., *TLR9 signals after translocating from the ER to CpG DNA in the lysosome.* Nat Immunol, 2004. **5**(2): p. 190-8.

36. Cambi, A. and C.G. Figdor, *Dual function of C-type lectin-like receptors in the immune system.* Curr Opin Cell Biol, 2003. **15**(5): p. 539-46.

37. Zelensky, A.N. and J.E. Gready, *The C-type lectin-like domain superfamily.* FEBS J, 2005. **272**(24): p. 6179-217.

38. Drickamer, K., *C-type lectin-like domains.* Curr Opin Struct Biol, 1999. **9**(5): p. 585-90.

39. Drickamer, K. and A.J. Fadden, *Genomic analysis of C-type lectins.* Biochem Soc Symp, 2002(69): p. 59-72.

40. Geijtenbeek, T.B. and S.I. Gringhuis, *Signalling through C-type lectin receptors: shaping immune responses.* Nat Rev Immunol, 2009. **9**(7): p. 465-79.

41. Kingeter, L.M. and X. Lin, *C-type lectin receptor-induced NF-kappaB activation in innate immune and inflammatory responses.* Cell Mol Immunol, 2012. **9**(2): p. 105-12.

42. Gorjestani, S., et al., *Phospholipase Cgamma2 (PLCgamma2) is key component in Dectin-2 signaling pathway, mediating anti-fungal innate immune responses.* J Biol Chem, 2011. **286**(51): p. 43651-9.

43. Wevers, B.A., et al., *Fungal engagement of the C-type lectin mincle suppresses dectin-1-induced antifungal immunity.* Cell Host Microbe, 2014. **15**(4): p. 494-505.

44. Batbayar, S., D.H. Lee, and H.W. Kim, *Immunomodulation of Fungal beta-Glucan in Host Defense Signaling by Dectin-1.* Biomol Ther (Seoul), 2012. **20**(5): p. 433-45.

45. Graham, L.M. and G.D. Brown, *The Dectin-2 family of C-type lectins in immunity and homeostasis.* Cytokine, 2009. **48**(1-2): p. 148-55.

46. Ishikawa, T., et al., *Identification of distinct ligands for the C-type lectin receptors Mincle and Dectin-2 in the pathogenic fungus Malassezia.* Cell Host Microbe, 2013. **13**(4): p. 477-88.

47. Matsunaga, I. and D.B. Moody, *Mincle is a long sought receptor for mycobacterial cord factor.* J Exp Med, 2009. **206**(13): p. 2865-8.

48. Richardson, M.B. and S.J. Williams, *MCL and Mincle: C-Type Lectin Receptors That Sense Damaged Self and Pathogen-Associated Molecular Patterns.* Front Immunol, 2014. **5**: p. 288.

49. Miyake, Y., et al., *Self and nonself recognition through C-type lectin receptor, Mincle.* Self Nonself, 2010. **1**(4): p. 310-313.

50. Marakalala, M.J., L.M. Graham, and G.D. Brown, *The role of Syk/CARD9-coupled C-type lectin receptors in immunity to Mycobacterium tuberculosis infections.* Clin Dev Immunol, 2010. **2010**: p. 567571.

51. Yamasaki, S., et al., *C-type lectin Mincle is an activating receptor for pathogenic fungus, Malassezia.* Proc Natl Acad Sci U S A, 2009. **106**(6): p. 1897-902.

52. Yamasaki, S., et al., *Mincle is an ITAM-coupled activating receptor that senses damaged cells.* Nat Immunol, 2008. **9**(10): p. 1179-88.

53. Suzuki, Y., et al., *Involvement of Mincle and Syk in the changes to innate immunity after ischemic stroke.* Sci Rep, 2013. **3**: p. 3177.

54. Schoenen, H., et al., *Cutting edge: Mincle is essential for recognition and adjuvanticity of the mycobacterial cord factor and its synthetic analog trehalose-dibehenate.* J Immunol, 2010. **184**(6): p. 2756-60.

55. Harton, J.A., et al., *Cutting edge: CATERPILLER: a large family of mammalian genes containing CARD, pyrin, nucleotide-binding, and leucine-rich repeat domains.* J Immunol, 2002. **169**(8): p. 4088-93.

56. Chamaillard, M., et al., *An essential role for NOD1 in host recognition of bacterial peptidoglycan containing diaminopimelic acid.* Nat Immunol, 2003. **4**(7): p. 702-7.

57. Girardin, S.E., et al., *Nod1 detects a unique muropeptide from gram-negative bacterial peptidoglycan.* Science, 2003. **300**(5625): p. 1584-7.

58. Shaw, M.H., et al., *The ever-expanding function of NOD2: autophagy, viral recognition, and T cell activation.* Trends Immunol, 2011. **32**(2): p. 73-9.

59. Abbott, D.W., et al., *The Crohn's disease protein, NOD2, requires RIP2 in order to induce ubiquitinylation of a novel site on NEMO.* Curr Biol, 2004. **14**(24): p. 2217-27.

60. Yoneyama, M., et al., *The RNA helicase RIG-I has an essential function in double-stranded RNA-induced innate antiviral responses.* Nat Immunol, 2004. **5**(7): p. 730-7.

61. Andrejeva, J., et al., *The V proteins of paramyxoviruses bind the IFN-inducible RNA helicase, mda-5, and inhibit its activation of the IFN-beta promoter.* Proc Natl Acad Sci U S A, 2004. **101**(49): p. 17264-9.

62. Kang, D.C., et al., *mda-5: An interferon-inducible putative RNA helicase with double-stranded RNA-dependent ATPase activity and melanoma growth-suppressive properties.* Proc Natl Acad Sci U S A, 2002. **99**(2): p. 637-42.

63. Satoh, T., et al., *LGP2 is a positive regulator of RIG-I- and MDA5-mediated antiviral responses.* Proc Natl Acad Sci U S A. **107**(4): p. 1512-7.

64. Akira, S., S. Uematsu, and O. Takeuchi, *Pathogen recognition and innate immunity.* Cell, 2006. **124**(4): p. 783-801.

65. Kim, T.W., et al., *A critical role for IRAK4 kinase activity in Toll-like receptor-mediated innate immunity.* J Exp Med, 2007. **204**(5): p. 1025-36.

66. Brown, J., et al., *TLR-signaling networks: an integration of adaptor molecules, kinases, and cross-talk.* J Dent Res, 2011. **90**(4): p. 417-27.

67. Rajan, J.V., et al., *Activation of the NLRP3 inflammasome by intracellular poly I:C.* FEBS letters, 2010. **584**(22): p. 4627-32.

68. Kawagoe, T., et al., *Sequential control of Toll-like receptor-dependent responses by IRAK1 and IRAK2.* Nat Immunol, 2008. **9**(6): p. 684-91.

69. Deng, L., et al., *Activation of the IkappaB kinase complex by TRAF6 requires a dimeric ubiquitin-conjugating enzyme complex and a unique polyubiquitin chain.* Cell, 2000. **103**(2): p. 351-61.

70. Wang, C., et al., *TAK1 is a ubiquitin-dependent kinase of MKK and IKK.* Nature, 2001. **412**(6844): p. 346-51.

71. Krappmann, D. and C. Scheidereit, *A pervasive role of ubiquitin conjugation in activation and termination of IkappaB kinase pathways.* EMBO Rep, 2005. **6**(4): p. 321-6.

72. Zhou, H., et al., *IRAK-M mediates Toll-like receptor/IL-1R-induced NFkappaB activation and cytokine production.* EMBO J, 2013. **32**(4): p. 583-96.

73. Fraczek, J., et al., *The kinase activity of IL-1 receptor-associated kinase 4 is required for interleukin-1 receptor/toll-like receptor-induced TAK1-dependent NFkappaB activation.* J Biol Chem, 2008. **283**(46): p. 31697-705.

74. Meylan, E., et al., *RIP1 is an essential mediator of Toll-like receptor 3-induced NF-kappa B activation.* Nat Immunol, 2004. **5**(5): p. 503-7.

75. Choi, Y.J., et al., *TRIF mediates Toll-like receptor 5-induced signaling in intestinal epithelial cells.* J Biol Chem, 2010. **285**(48): p. 37570-8.

76. Anderson, P., *Post-transcriptional control of cytokine production.* Nat Immunol, 2008. **9**(4): p. 353-9.

77. Caput, D., et al., *Identification of a common nucleotide sequence in the 3'-untranslated region of mRNA molecules specifying inflammatory mediators.* Proc Natl Acad Sci U S A, 1986. **83**(6): p. 1670-4.

78. Shaw, G. and R. Kamen, *A conserved AU sequence from the 3' untranslated region of GM-CSF mRNA mediates selective mRNA degradation.* Cell, 1986. **46**(5): p. 659-67.

79. Carballo, E., W.S. Lai, and P.J. Blackshear, *Feedback inhibition of macrophage tumor necrosis factor-alpha production by tristetraprolin.* Science, 1998. **281**(5379): p. 1001-5.

80. Ronkina, N., et al., *The mitogen-activated protein kinase (MAPK)-activated protein kinases MK2 and MK3 cooperate in stimulation of tumor necrosis factor biosynthesis and stabilization of p38 MAPK.* Mol Cell Biol, 2007. **27**(1): p. 170-81.

81. Carpenter, S., et al., *Post-transcriptional regulation of gene expression in innate immunity.* Nat Rev Immunol, 2014. **14**(6): p. 361-76.

82. Matsushita, K., et al., *Zc3h12a is an RNase essential for controlling immune responses by regulating mRNA decay.* Nature, 2009. **458**(7242): p. 1185-90.

83. Uehata, T. and S. Akira, *mRNA degradation by the endoribonuclease Regnase-1/ZC3H12a/MCPIP-1.* Biochim Biophys Acta, 2013. **1829**(6-7): p. 708-13.

84. Asano, K., et al., *A multifactor complex of eukaryotic initiation factors, eIF1, eIF2, eIF3, eIF5, and initiator tRNA(Met) is an important translation initiation intermediate in vivo.* Genes Dev, 2000. **14**(19): p. 2534-46.

85. Fukunaga, R. and T. Hunter, *MNK1, a new MAP kinase-activated protein kinase, isolated by a novel expression screening method for identifying protein kinase substrates.* EMBO J, 1997. **16**(8): p. 1921-33.

86. Ueda, T., et al., *Mnk2 and Mnk1 are essential for constitutive and inducible phosphorylation of eukaryotic initiation factor 4E but not for cell growth or development.* Mol Cell Biol, 2004. **24**(15): p. 6539-49.

87. Rowlett, R.M., et al., *MNK kinases regulate multiple TLR pathways and innate proinflammatory cytokines in macrophages.* Am J Physiol Gastrointest Liver Physiol, 2008. **294**(2): p. G452-9.

88. Thornberry, N.A., et al., *A novel heterodimeric cysteine protease is required for interleukin-1 beta processing in monocytes.* Nature, 1992. **356**(6372): p. 768-74.

89. Cerretti, D.P., et al., *Molecular cloning of the interleukin-1 beta converting enzyme.* Science, 1992. **256**(5053): p. 97-100.

90. Antonopoulos, C., et al., *IL-18 is a key proximal mediator of contact hypersensitivity and allergen-induced Langerhans cell migration in murine epidermis.* Journal of Leukocyte Biology, 2008. **83**(2): p. 361-7.

91. Fernandes-Alnemri, T., et al., *The pyroptosome: a supramolecular assembly of ASC dimers mediating inflammatory cell death via caspase-1 activation.* Cell death and differentiation, 2007. **14**(9): p. 1590-604.

92. Schroder, K., R. Zhou, and J. Tschopp, *The NLRP3 inflammasome: a sensor for metabolic danger?* Science, 2010. **327**(5963): p. 296-300.

93. Shaw, P.J., M.F. McDermott, and T.D. Kanneganti, *Inflammasomes and autoimmunity.* Trends in molecular medicine, 2011. **17**(2): p. 57-64.

94. Franchi, L., et al., *The inflammasome: a caspase-1-activation platform that regulates immune responses and disease pathogenesis.* Nature Immunology, 2009. **10**(3): p. 241-7.

95. Franchi, L., et al., *Inflammasomes as microbial sensors.* European Journal of Immunology, 2010. **40**(3): p. 611-5.

96. Muruve, D.A., et al., *The inflammasome recognizes cytosolic microbial and host DNA and triggers an innate immune response.* Nature, 2008. **452**(7183): p. 103-7.

97. Ghiringhelli, F., et al., *Activation of the NLRP3 inflammasome in dendritic cells induces IL-1beta-dependent adaptive immunity against tumors.* Nature Medicine, 2009. **15**(10): p. 1170-8.

98. Kahlenberg, J.M. and G.R. Dubyak, *Mechanisms of caspase-1 activation by P2X7 receptor-mediated K+ release.* Am J Physiol Cell Physiol, 2004. **286**: p. 1100-1108.

99. Kahlenberg, J.M., et al., *Potentiation of Caspase-1 Activation by the P2X7 Receptor Is Dependent on TLR Signals and Requires NF-kB-Driven Protein Synthesis1*. The Journal of Immunology, 2005. **175**: p. 7611-7622.

100. Mariathasan, S., et al., *Cryopyrin activates the inflammasome in response to toxins and ATP*. Nature, 2006. **440**(7081): p. 228-32.

101. Matsushima, H., et al., *Intravital imaging of IL-1beta production in skin.* The Journal of investigative dermatology, 2010. **130**(6): p. 1571-80.

102. Solle, M., *Altered Cytokine Production in Mice Lacking P2X7 Receptors.* Journal of Biological Chemistry, 2000. **276**(1): p. 125-132.

103. Solle, M., et al., *Altered cytokine production in mice lacking P2X(7) receptors.* The Journal of biological chemistry, 2001. **276**(1): p. 125-32.

104. Zhou, R., et al., *A role for mitochondria in NLRP3 inflammasome activation.* Nature, 2011. **469**(7329): p. 221-5.

105. Rehm, J., et al., *Alcohol as a risk factor for global burden of disease.* Eur Addict Res, 2003. **9**(4): p. 157-64.

106. Mandayam, S., M.M. Jamal, and T.R. Morgan, *Epidemiology of alcoholic liver disease.* Semin Liver Dis, 2004. **24**(3): p. 217-32.

107. Rajendram, R., G. Lewison, and V.R. Preedy, *Worldwide alcohol-related research and the disease burden.* Alcohol Alcohol, 2006. **41**(1): p. 99-106.

108. Mills, S.J. and S.A. Harrison, *Comparison of the natural history of alcoholic and nonalcoholic fatty liver disease.* Curr Gastroenterol Rep, 2005. **7**(1): p. 32-6.

109. Purohit, V., B. Gao, and B.J. Song, *Molecular mechanisms of alcoholic fatty liver.* Alcohol Clin Exp Res, 2009. **33**(2): p. 191-205.

110. Enomoto, N., et al., *Role of Kupffer cells and gut-derived endotoxins in alcoholic liver injury.* J Gastroenterol Hepatol, 2000. **15 Suppl**: p. D20-5.

111. Fujimoto, M., et al., *Plasma endotoxin and serum cytokine levels in patients with alcoholic hepatitis: relation to severity of liver disturbance.* Alcohol Clin Exp Res, 2000. **24**(4 Suppl): p. 48S-54S.

112. Uesugi, T., et al., *Toll-like receptor 4 is involved in the mechanism of early alcohol-induced liver injury in mice.* Hepatology, 2001. **34**(1): p. 101-8.

113. Szabo, G. and S. Bala, *Alcoholic liver disease and the gut-liver axis.* World J Gastroenterol, 2010. **16**(11): p. 1321-9.

114. Pijls, K.E., et al., *Intestinal epithelial barrier function in liver cirrhosis: an extensive review of the literature.* Liver Int, 2013. **33**(10): p. 1457-69.

115. Seki, E., et al., *TLR4 enhances TGF-beta signaling and hepatic fibrosis.* Nat Med, 2007. **13**(11): p. 1324-32.

116. Seki, E. and D.A. Brenner, *Toll-like receptors and adaptor molecules in liver disease: update.* Hepatology, 2008. **48**(1): p. 322-35.

117. Petrasek, J., et al., *IL-1 receptor antagonist ameliorates inflammasome-dependent alcoholic steatohepatitis in mice.* J Clin Invest, 2012. **122**(10): p. 3476-89.

118. Luedde, T., N. Kaplowitz, and R.F. Schwabe, *Cell Death and Cell Death Responses in Liver Disease: Mechanisms and Clinical Relevance.* Gastroenterology, 2014.

119. Rock, F.L., et al., *A family of human receptors structurally related to Drosophila Toll.* Proceedings of the National Academy of Sciences of the United States of America, 1998. **95**(2): p. 588-93.

120. Hemmi, H., et al., *A Toll-like receptor recognizes bacterial DNA.* Nature, 2000. **408**(6813): p. 740-5.

121. Zhang, D., et al., *A toll-like receptor that prevents infection by uropathogenic bacteria.* Science, 2004. **303**(5663): p. 1522-6.

122. Wesche, H., et al., *MyD88: an adapter that recruits IRAK to the IL-1 receptor complex.* Immunity, 1997. **7**(6): p. 837-47.

123. Wesche, H., et al., *IRAK-M is a novel member of the Pelle/interleukin-1 receptor-associated kinase (IRAK) family.* The Journal of biological chemistry, 1999. **274**(27): p. 19403-10.

124. Cao, Z., W.J. Henzel, and X. Gao, *IRAK: a kinase associated with the interleukin-1 receptor.* Science, 1996. **271**(5252): p. 1128-31.

125. Muzio, M., et al., *IRAK (Pelle) family member IRAK-2 and MyD88 as proximal mediators of IL-1 signaling.* Science, 1997. **278**(5343): p. 1612-5.

126. Li, S., et al., *IRAK-4: a novel member of the IRAK family with the properties of an IRAK-kinase.* Proceedings of the National Academy of Sciences of the United States of America, 2002. **99**(8): p. 5567-72.

127. Lin, S.C., Y.C. Lo, and H. Wu, *Helical assembly in the MyD88-IRAK4-IRAK2 complex in TLR/IL-1R signalling.* Nature, 2010. **465**(7300): p. 885-90.

128. Kobayashi, K., et al., *IRAK-M is a negative regulator of Toll-like receptor signaling.* Cell, 2002. **110**(2): p. 191-202.

129. Yao, J., et al., *Interleukin-1 (IL-1)-induced TAK1-dependent Versus MEKK3-dependent NFkappaB activation pathways bifurcate at IL-1 receptor-associated kinase modification.* The Journal of biological chemistry, 2007. **282**(9): p. 6075-89.

130. Anderson, P., *Post-transcriptional control of cytokine production.* Nature immunology, 2008. **9**(4): p. 353-9.

131. Fraczek, J., et al., *The kinase activity of IL-1 receptor-associated kinase 4 is required for interleukin-1 receptor/toll-like receptor-induced TAK1-dependent NFkappaB activation.* The Journal of biological chemistry, 2008. **283**(46): p. 31697-705.

132. Kim, T.W., et al., *A critical role for IRAK4 kinase activity in Toll-like receptor-mediated innate immunity.* The Journal of experimental medicine, 2007. **204**(5): p. 1025-36.

133. Fukunaga, R. and T. Hunter, *MNK1, a new MAP kinase-activated protein kinase, isolated by a novel expression screening method for identifying protein kinase substrates.* The EMBO journal, 1997. **16**(8): p. 1921-33.

134. Ueda, T., et al., *Mnk2 and Mnk1 are essential for constitutive and inducible phosphorylation of eukaryotic initiation factor 4E but not for cell growth or development.* Molecular and cellular biology, 2004. **24**(15): p. 6539-49.

135. Wan, Y., et al., *Interleukin-1 receptor-associated kinase 2 is critical for lipopolysaccharide-mediated post-transcriptional control.* The Journal of biological chemistry, 2009. **284**(16): p. 10367-75.

136. Weber, C.H. and C. Vincenz, *The death domain superfamily: a tale of two interfaces?* Trends in biochemical sciences, 2001. **26**(8): p. 475-81.

137. Xiao, H., et al., *Pellino 3b negatively regulates interleukin-1-induced TAK1-dependent NF kappaB activation.* The Journal of biological chemistry, 2008. **283**(21): p. 14654-64.

138. Kawagoe, T., et al., *Sequential control of Toll-like receptor-dependent responses by IRAK1 and IRAK2.* Nature immunology, 2008. **9**(6): p. 684-91.

139. Lye, E., et al., *The role of interleukin 1 receptor-associated kinase-4 (IRAK-4) kinase activity in IRAK-4-mediated signaling.* The Journal of biological chemistry, 2004. **279**(39): p. 40653-8.

140. Arnold, K., et al., *The SWISS-MODEL workspace: a web-based environment for protein structure homology modelling.* Bioinformatics, 2006. **22**(2): p. 195-201.

141. Krissinel, E. and K. Henrick, *Secondary-structure matching (SSM), a new tool for fast protein structure alignment in three dimensions.* Acta crystallographica. Section D, Biological crystallography, 2004. **60**(Pt 12 Pt 1): p. 2256-68.

142. Emsley, P. and K. Cowtan, *Coot: model-building tools for molecular graphics.* Acta crystallographica. Section D, Biological crystallography, 2004. **60**(Pt 12 Pt 1): p. 2126-32.

143. Krissinel, E. and K. Henrick, *Inference of macromolecular assemblies from crystalline state.* Journal of molecular biology, 2007. **372**(3): p. 774-97.

144. Qin, J., et al., *TLR8-mediated NF-kappaB and JNK activation are TAK1-independent and MEKK3-dependent.* The Journal of biological chemistry, 2006. **281**(30): p. 21013-21.

145. Yoshida, H., *ER stress and diseases.* FEBS J, 2007. **274**(3): p. 630-58.

146. Dara, L., C. Ji, and N. Kaplowitz, *The contribution of endoplasmic reticulum stress to liver diseases.* Hepatology, 2011. **53**(5): p. 1752-63.

147. Shinohara, M., C. Ji, and N. Kaplowitz, *Differences in betaine-homocysteine methyltransferase expression, endoplasmic reticulum stress response, and liver injury between alcohol-fed mice and rats.* Hepatology, 2010. **51**(3): p. 796-805.

148. Mandrekar, P. and G. Szabo, *Signalling pathways in alcohol-induced liver inflammation.* J Hepatol, 2009. **50**(6): p. 1258-66.

149. Takeda, K. and S. Akira, *TLR signaling pathways.* Semin Immunol, 2004. **16**(1): p. 3-9.

150. Cui, W., et al., *beta-TrCP-mediated IRAK1 degradation releases TAK1-TRAF6 from the membrane to the cytosol for TAK1-dependent NF-kappaB activation.* Molecular and cellular biology, 2012. **32**(19): p. 3990-4000.

151. Kim, T.W., et al., *Pellino 2 is critical for Toll-like receptor/interleukin-1 receptor (TLR/IL-1R)-mediated post-transcriptional control.* The Journal of biological chemistry, 2012. **287**(30): p. 25686-95.

152. Yin, W., et al., *The kinase activity of interleukin-1 receptor-associated kinase 2 is essential for lipopolysaccharide-mediated cytokine and chemokine mRNA stability and translation.* J Interferon Cytokine Res, 2011. **31**(5): p. 415-22.

153. Zhou, H., et al., *IRAK-M mediates Toll-like receptor/IL-1R-induced NFkappaB activation and cytokine production.* The EMBO journal, 2013. **32**(4): p. 583-96.

154. Szabo, G., A. Dolganiuc, and P. Mandrekar, *Pattern recognition receptors: a contemporary view on liver diseases.* Hepatology, 2006. **44**(2): p. 287-98.

155. Jagavelu, K., et al., *Endothelial cell toll-like receptor 4 regulates fibrosis-associated angiogenesis in the liver.* Hepatology, 2010. **52**(2): p. 590-601.

156. Matsumoto, M., et al., *A novel LPS-inducible C-type lectin is a transcriptional target of NF-IL6 in macrophages.* J Immunol, 1999. **163**(9): p. 5039-48.

157. Ishikawa, E., et al., *Direct recognition of the mycobacterial glycolipid, trehalose dimycolate, by C-type lectin Mincle.* J Exp Med, 2009. **206**(13): p. 2879-88.

158. Schweneker, K., et al., *The mycobacterial cord factor adjuvant analogue trehalose-6,6'-dibehenate (TDB) activates the Nlrp3 inflammasome.* Immunobiology, 2013. **218**(4): p. 664-73.

159. Shenderov, K., et al., *Cord factor and peptidoglycan recapitulate the Th17-promoting adjuvant activity of mycobacteria through mincle/CARD9 signaling and the inflammasome.* J Immunol, 2013. **190**(11): p. 5722-30.

160. Gringhuis, S.I., et al., *Dectin-1 is an extracellular pathogen sensor for the induction and processing of IL-1beta via a noncanonical caspase-8 inflammasome.* Nat Immunol, 2012. **13**(3): p. 246-54.

161. Paik, Y.H., et al., *Toll-like receptor 4 mediates inflammatory signaling by bacterial lipopolysaccharide in human hepatic stellate cells.* Hepatology, 2003. **37**(5): p. 1043-55.

162. Hritz, I., et al., *The critical role of toll-like receptor (TLR) 4 in alcoholic liver disease is independent of the common TLR adapter MyD88.* Hepatology, 2008. **48**(4): p. 1224-31.

163. Cohen, J.I., et al., *Complement and alcoholic liver disease: role of C1q in the pathogenesis of ethanol-induced liver injury in mice.* Gastroenterology, 2010. **139**(2): p. 664-74, 674 e1.

164. Pradere, J.P., et al., *Toll-like receptor 4 and hepatic fibrogenesis.* Semin Liver Dis, 2010. **30**(3): p. 232-44.

165. Lee, U.E. and S.L. Friedman, *Mechanisms of hepatic fibrogenesis.* Best Pract Res Clin Gastroenterol, 2011. **25**(2): p. 195-206.

166. Petrasek, J., et al., *Interferon regulatory factor 3 and type I interferons are protective in alcoholic liver injury in mice by way of crosstalk of parenchymal and myeloid cells.* Hepatology, 2011. **53**(2): p. 649-60.

167. Wells, C.A., et al., *The macrophage-inducible C-type lectin, mincle, is an essential component of the innate immune response to Candida albicans.* J Immunol, 2008. **180**(11): p. 7404-13.

168. Feinberg, H., et al., *Mechanism for recognition of an unusual mycobacterial glycolipid by the macrophage receptor mincle.* J Biol Chem, 2013. **288**(40): p. 28457-65.

169. Behler, F., et al., *Role of Mincle in alveolar macrophage-dependent innate immunity against mycobacterial infections in mice.* J Immunol, 2012. **189**(6): p. 3121-9.

170. Franchi, L. and G. Nunez, *The Nlrp3 inflammasome is critical for aluminium hydroxide-mediated IL-1beta secretion but dispensable for adjuvant activity.* Eur J Immunol, 2008. **38**(8): p. 2085-9.

171. Takeuchi, O. and S. Akira, *MyD88 as a bottle neck in Toll/IL-1 signaling.* Current topics in microbiology and immunology, 2002. **270**: p. 155-67.

172. Rosati, O. and M.U. Martin, *Identification and characterization of murine IRAK-2.* Biochem Biophys Res Commun, 2002. **297**(1): p. 52-8.

173. Pauls, E., et al., *Two phases of inflammatory mediator production defined by the study of IRAK2 and IRAK1 knock-in mice.* J Immunol, 2013. **191**(5): p. 2717-30.

174. Liang, Y., et al., *SOCS signaling in autoimmune diseases: molecular mechanisms and therapeutic implications.* Eur J Immunol, 2014. **44**(5): p. 1265-75.

175. Catrysse, L., et al., *A20 in inflammation and autoimmunity.* Trends Immunol, 2014. **35**(1): p. 22-31.

176. Pujari, R., et al., *A20-mediated negative regulation of canonical NF-kappaB signaling pathway.* Immunol Res, 2013. **57**(1-3): p. 166-71.

177. Conde, C., G. Gloire, and J. Piette, *Enzymatic and non-enzymatic activities of SHIP-1 in signal transduction and cancer.* Biochem Pharmacol, 2011. **82**(10): p. 1320-34.

178. McCullough, A.J., *Epidemiology of the metabolic syndrome in the USA.* Journal of digestive diseases, 2011. **12**(5): p. 333-40.

179. Hirosumi, J., et al., *A central role for JNK in obesity and insulin resistance.* Nature, 2002. **420**(6913): p. 333-6.

180. Hotamisligil, G.S., *Inflammation and metabolic disorders.* Nature, 2006. **444**(7121): p. 860-7.

181. Warnberg, J., et al., *Inflammatory proteins are related to total and abdominal adiposity in a healthy adolescent population: the AVENA Study.* The American journal of clinical nutrition, 2006. **84**(3): p. 505-12.

182. Zieske, A.W., et al., *Elevated serum C-reactive protein levels and advanced atherosclerosis in youth.* Arteriosclerosis, thrombosis, and vascular biology, 2005. **25**(6): p. 1237-43.

183. Erridge, C., *Diet, commensals and the intestine as sources of pathogen-associated molecular patterns in atherosclerosis, type 2 diabetes and non-alcoholic fatty liver disease.* Atherosclerosis, 2011. **216**(1): p. 1-6.

184. Creely, S.J., et al., *Lipopolysaccharide activates an innate immune system response in human adipose tissue in obesity and type 2 diabetes.* American journal of physiology. Endocrinology and metabolism, 2007. **292**(3): p. E740-7.

185. Dasu, M.R., S. Ramirez, and R.R. Isseroff, *Toll-like receptors and diabetes: a therapeutic perspective.* Clinical science, 2012. **122**(5): p. 203-14.

186. Cani, P.D., et al., *Changes in gut microbiota control metabolic endotoxemia-induced inflammation in high-fat diet-induced obesity and diabetes in mice.* Diabetes, 2008. **57**(6): p. 1470-81.

187. Cani, P.D., et al., *Metabolic endotoxemia initiates obesity and insulin resistance.* Diabetes, 2007. **56**(7): p. 1761-72.

188. Holvoet, P., et al., *Association between circulating oxidized low-density lipoprotein and incidence of the metabolic syndrome.* JAMA : the journal of the American Medical Association, 2008. **299**(19): p. 2287-93.

189. Shi, H., et al., *TLR4 links innate immunity and fatty acid-induced insulin resistance.* The Journal of clinical investigation, 2006. **116**(11): p. 3015-25.

190. Himes, R.W. and C.W. Smith, *Tlr2 is critical for diet-induced metabolic syndrome in a murine model.* FASEB journal : official publication of the Federation of American Societies for Experimental Biology, 2010. **24**(3): p. 731-9.

191. Kiechl, S., et al., *Toll-like receptor 4 polymorphisms and atherogenesis.* The New England journal of medicine, 2002. **347**(3): p. 185-92.

192. Kirii, H., et al., *Lack of interleukin-1beta decreases the severity of atherosclerosis in ApoE-deficient mice.* Arteriosclerosis, thrombosis, and vascular biology, 2003. **23**(4): p. 656-60.

193. Bjorkbacka, H., et al., *Reduced atherosclerosis in MyD88-null mice links elevated serum cholesterol levels to activation of innate immunity signaling pathways.* Nature medicine, 2004. **10**(4): p. 416-21.

194. Chi, H., et al., *Interleukin-1 receptor signaling mediates atherosclerosis associated with bacterial exposure and/or a high-fat diet in a murine apolipoprotein E heterozygote model: pharmacotherapeutic implications.* Circulation, 2004. **110**(12): p. 1678-85.

195. Michelsen, K.S., et al., *Lack of Toll-like receptor 4 or myeloid differentiation factor 88 reduces atherosclerosis and alters plaque phenotype in mice deficient in apolipoprotein E.* Proceedings of the National Academy of Sciences of the United States of America, 2004. **101**(29): p. 10679-84.

196. Fresno, M., R. Alvarez, and N. Cuesta, *Toll-like receptors, inflammation, metabolism and obesity.* Archives of physiology and biochemistry, 2011. **117**(3): p. 151-64.

197. Konner, A.C. and J.C. Bruning, *Toll-like receptors: linking inflammation to metabolism.* Trends in endocrinology and metabolism: TEM, 2011. **22**(1): p. 16-23.

198. Kenny, E.F. and L.A. O'Neill, *Signalling adaptors used by Toll-like receptors: an update.* Cytokine, 2008. **43**(3): p. 342-9.

199. Gay, N.J., M. Gangloff, and L.A. O'Neill, *What the Myddosome structure tells us about the initiation of innate immunity.* Trends in immunology, 2011. **32**(3): p. 104-9.

200. Brown, J., et al., *TLR-signaling networks: an integration of adaptor molecules, kinases, and cross-talk.* Journal of dental research, 2011. **90**(4): p. 417-27.

201. Subramanian, M., et al., *Treg-mediated suppression of atherosclerosis requires MYD88 signaling in DCs.* J Clin Invest, 2013. **123**(1): p. 179-88.

202. Hosoi, T., et al., *Myeloid differentiation factor 88 (MyD88)-deficiency increases risk of diabetes in mice.* PloS one, 2010. **5**(9).

203. Kano, A., et al., *Endothelial cells require STAT3 for protection against endotoxin-induced inflammation.* The Journal of experimental medicine, 2003. **198**(10): p. 1517-25.

204. Kang, Z., et al., *Astrocyte-restricted ablation of interleukin-17-induced Act1-mediated signaling ameliorates autoimmune encephalomyelitis.* Immunity, 2010. **32**(3): p. 414-25.

205. Boillee, S., et al., *Onset and progression in inherited ALS determined by motor neurons and microglia.* Science, 2006. **312**(5778): p. 1389-92.

206. Kang, Z., et al., *Epithelial cell-specific Act1 adaptor mediates interleukin-25-dependent helminth expulsion through expansion of Lin(-)c-Kit(+) innate cell population.* Immunity, 2012. **36**(5): p. 821-33.

207. Caligiuri, G., et al., *Effects of sex and age on atherosclerosis and autoimmunity in apoE-deficient mice.* Atherosclerosis, 1999. **145**(2): p. 301-8.

208. Smith, D.D., et al., *Increased aortic atherosclerotic plaque development in female apolipoprotein E-null mice is associated with elevated thromboxane A2 and decreased prostacyclin production.* J Physiol Pharmacol, 2010. **61**(3): p. 309-16.

209. Monteiro, R. and I. Azevedo, *Chronic inflammation in obesity and the metabolic syndrome.* Mediators of inflammation, 2010. **2010**.

210. Emanuela, F., et al., *Inflammation as a Link between Obesity and Metabolic Syndrome.* Journal of nutrition and metabolism, 2012. **2012**: p. 476380.

211. Klover, P.J., et al., *Chronic exposure to interleukin-6 causes hepatic insulin resistance in mice.* Diabetes, 2003. **52**(11): p. 2784-9.

212. De Taeye, B.M., et al., *Macrophage TNF-alpha contributes to insulin resistance and hepatic steatosis in diet-induced obesity.* American journal of physiology. Endocrinology and metabolism, 2007. **293**(3): p. E713-25.

213. Cheung, A.T., et al., *Tumor necrosis factor-alpha induces hepatic insulin resistance in obese Zucker (fa/fa) rats via interaction of leukocyte antigen-related tyrosine phosphatase with focal adhesion kinase.* Diabetes, 2000. **49**(5): p. 810-9.

214. Ehses, J.A., et al., *IL-1 antagonism reduces hyperglycemia and tissue inflammation in the type 2 diabetic GK rat.* Proceedings of the National Academy of Sciences of the United States of America, 2009. **106**(33): p. 13998-4003.

215. Plomgaard, P., et al., *Tumor necrosis factor-alpha induces skeletal muscle insulin resistance in healthy human subjects via inhibition of Akt substrate 160 phosphorylation.* Diabetes, 2005. **54**(10): p. 2939-45.

216. Huber, S.A., et al., *Interleukin-6 exacerbates early atherosclerosis in mice.* Arteriosclerosis, thrombosis, and vascular biology, 1999. **19**(10): p. 2364-7.

217. Elhage, R., et al., *Differential effects of interleukin-1 receptor antagonist and tumor necrosis factor binding protein on fatty-streak formation in apolipoprotein E-deficient mice.* Circulation, 1998. **97**(3): p. 242-4.

218. Avouac, J. and Y. Allanore, *Cardiovascular risk in rheumatoid arthritis: effects of anti-TNF drugs.* Expert opinion on pharmacotherapy, 2008. **9**(7): p. 1121-8.

219. Dixon, W.G. and D.P. Symmons, *What effects might anti-TNFalpha treatment be expected to have on cardiovascular morbidity and mortality in rheumatoid arthritis?*

A review of the role of TNFalpha in cardiovascular pathophysiology. Annals of the rheumatic diseases, 2007. **66**(9): p. 1132-6.

220. Ferrante, A., et al., *Long-term anti-tumour necrosis factor therapy reverses the progression of carotid intima-media thickness in female patients with active rheumatoid arthritis.* Rheumatology international, 2009. **30**(2): p. 193-8.

221. Kleemann, R., S. Zadelaar, and T. Kooistra, *Cytokines and atherosclerosis: a comprehensive review of studies in mice.* Cardiovascular research, 2008. **79**(3): p. 360-76.

222. Aird, W.C., *Phenotypic heterogeneity of the endothelium: I. Structure, function, and mechanisms.* Circulation research, 2007. **100**(2): p. 158-73.

223. Hotamisligil, G.S., N.S. Shargill, and B.M. Spiegelman, *Adipose expression of tumor necrosis factor-alpha: direct role in obesity-linked insulin resistance.* Science, 1993. **259**(5091): p. 87-91.

224. Xu, H., et al., *Chronic inflammation in fat plays a crucial role in the development of obesity-related insulin resistance.* The Journal of clinical investigation, 2003. **112**(12): p. 1821-30.

225. Neels, J.G. and J.M. Olefsky, *Inflamed fat: what starts the fire?* The Journal of clinical investigation, 2006. **116**(1): p. 33-5.

226. Nishimura, S., I. Manabe, and R. Nagai, *Adipose tissue inflammation in obesity and metabolic syndrome.* Discovery medicine, 2009. **8**(41): p. 55-60.

227. Wajchenberg, B.L., et al., *Adipose tissue at the crossroads in the development of the metabolic syndrome, inflammation and atherosclerosis.* Arquivos brasileiros de endocrinologia e metabologia, 2009. **53**(2): p. 145-50.

228. Weisberg, S.P., et al., *Obesity is associated with macrophage accumulation in adipose tissue.* The Journal of clinical investigation, 2003. **112**(12): p. 1796-808.

229. Lumeng, C.N., J.L. Bodzin, and A.R. Saltiel, *Obesity induces a phenotypic switch in adipose tissue macrophage polarization.* The Journal of clinical investigation, 2007. **117**(1): p. 175-84.

230. Fujisaka, S., et al., *Regulatory mechanisms for adipose tissue M1 and M2 macrophages in diet-induced obese mice.* Diabetes, 2009. **58**(11): p. 2574-82.

231. Prieur, X., et al., *Differential lipid partitioning between adipocytes and tissue macrophages modulates macrophage lipotoxicity and M2/M1 polarization in obese mice.* Diabetes, 2011. **60**(3): p. 797-809.

232. Zeyda, M. and T.M. Stulnig, *Adipose tissue macrophages.* Immunology letters, 2007. **112**(2): p. 61-7.

233. Shaul, M.E., et al., *Dynamic, M2-like remodeling phenotypes of CD11c+ adipose tissue macrophages during high-fat diet--induced obesity in mice.* Diabetes, 2010. **59**(5): p. 1171-81.

234. Zeyda, M., et al., *Newly identified adipose tissue macrophage populations in obesity with distinct chemokine and chemokine receptor expression.* International journal of obesity, 2010. **34**(12): p. 1684-94.

235. Morris, D.L., et al., *CX3CR1 deficiency does not influence trafficking of adipose tissue macrophages in mice with diet-induced obesity.* Obesity, 2012. **20**(6): p. 1189-99.

236. Ohashi, K., et al., *Adiponectin promotes macrophage polarization toward an anti-inflammatory phenotype.* The Journal of biological chemistry, 2010. **285**(9): p. 6153-60.

237. Nguyen, M.T., et al., *A subpopulation of macrophages infiltrates hypertrophic adipose tissue and is activated by free fatty acids via Toll-like receptors 2 and 4 and JNK-dependent pathways.* The Journal of biological chemistry, 2007. **282**(48): p. 35279-92.

238. Sun, K., C.M. Kusminski, and P.E. Scherer, *Adipose tissue remodeling and obesity.* The Journal of clinical investigation, 2011. **121**(6): p. 2094-101.

239. Lafontan, M. and D. Langin, *Lipolysis and lipid mobilization in human adipose tissue.* Progress in lipid research, 2009. **48**(5): p. 275-97.

240. Landin, K., et al., *Increased Insulin Resistance and Fat-Cell Lipolysis in Obese but Not Lean Women with a High Waist Hip Ratio.* European journal of clinical investigation, 1990. **20**(5): p. 530-535.

241. Tsujita, T., C. Morimoto, and H. Okuda, *Mechanism of increase in basal lipolysis of enlarged adipocytes in obese animals.* Obesity research, 1995. **3**: p. S633-S636.

242. Kosteli, A., et al., *Weight loss and lipolysis promote a dynamic immune response in murine adipose tissue.* The Journal of clinical investigation, 2010. **120**(10): p. 3466-79.

243. Lacey, D.C., et al., *Defining GM-CSF- and macrophage-CSF-dependent macrophage responses by in vitro models.* Journal of immunology, 2012. **188**(11): p. 5752-65.

244. Fleetwood, A.J., et al., *Granulocyte-macrophage colony-stimulating factor (CSF) and macrophage CSF-dependent macrophage phenotypes display differences in cytokine profiles and transcription factor activities: implications for CSF blockade in inflammation.* Journal of immunology, 2007. **178**(8): p. 5245-52.

245. Verreck, F.A., et al., *Human IL-23-producing type 1 macrophages promote but IL-10-producing type 2 macrophages subvert immunity to (myco)bacteria.* Proceedings of the National Academy of Sciences of the United States of America, 2004. **101**(13): p. 4560-5.

246. Brocheriou, I., et al., *Antagonistic regulation of macrophage phenotype by M-CSF and GM-CSF: implication in atherosclerosis.* Atherosclerosis, 2011. **214**(2): p. 316-24.

247. Chitu, V. and E.R. Stanley, *Colony-stimulating factor-1 in immunity and inflammation.* Current opinion in immunology, 2006. **18**(1): p. 39-48.

248. Hamilton, J.A., *Colony-stimulating factors in inflammation and autoimmunity.* Nature reviews. Immunology, 2008. **8**(7): p. 533-44.

249. Waldo, S.W., et al., *Heterogeneity of human macrophages in culture and in atherosclerotic plaques.* The American journal of pathology, 2008. **172**(4): p. 1112-26.

250. Wolfs, I.M., M.M. Donners, and M.P. de Winther, *Differentiation factors and cytokines in the atherosclerotic plaque micro-environment as a trigger for macrophage polarisation.* Thrombosis and haemostasis, 2011. **106**(5): p. 763-71.

251. Chinetti-Gbaguidi, G. and B. Staels, *Macrophage polarization in metabolic disorders: functions and regulation.* Current opinion in lipidology, 2011. **22**(5): p. 365-72.

252. Seimon, T.A., et al., *Atherogenic lipids and lipoproteins trigger CD36-TLR2-dependent apoptosis in macrophages undergoing endoplasmic reticulum stress.* Cell metabolism, 2010. **12**(5): p. 467-82.

253. Gallardo-Soler, A., et al., *Arginase I induction by modified lipoproteins in macrophages: a peroxisome proliferator-activated receptor-gamma/delta-mediated effect that links lipid metabolism and immunity.* Mol Endocrinol, 2008. **22**(6): p. 1394-402.

254. van Tits, L.J., et al., *Oxidized LDL enhances pro-inflammatory responses of alternatively activated M2 macrophages: a crucial role for Kruppel-like factor 2.* Atherosclerosis, 2011. **214**(2): p. 345-9.

255. Hamilton, J.A., et al., *Oxidized LDL can induce macrophage survival, DNA synthesis, and enhanced proliferative response to CSF-1 and GM-CSF.* Arterioscler Thromb Vasc Biol, 1999. **19**(1): p. 98-105.

256. Podrez, E.A., et al., *Macrophage scavenger receptor CD36 is the major receptor for LDL modified by monocyte-generated reactive nitrogen species.* J Clin Invest, 2000. **105**(8): p. 1095-108.

257. Hazen, S.L., et al., *Molecular chlorine generated by the myeloperoxidase-hydrogen peroxide-chloride system of phagocytes converts low density lipoprotein cholesterol into a family of chlorinated sterols.* J Biol Chem, 1996. **271**(38): p. 23080-8.

258. Hazen, S.L., et al., *Formation of nitric oxide-derived oxidants by myeloperoxidase in monocytes: pathways for monocyte-mediated protein nitration and lipid peroxidation In vivo.* Circ Res, 1999. **85**(10): p. 950-8.

259. Vita, J.A., et al., *Serum myeloperoxidase levels independently predict endothelial dysfunction in humans.* Circulation, 2004. **110**(9): p. 1134-9.

260. Zhang, R., et al., *Association between myeloperoxidase levels and risk of coronary artery disease.* JAMA, 2001. **286**(17): p. 2136-42.

261. Baldus, S., et al., *Myeloperoxidase serum levels predict risk in patients with acute coronary syndromes.* Circulation, 2003. **108**(12): p. 1440-5.

262. Hazen, S.L. and J.W. Heinecke, *3-Chlorotyrosine, a specific marker of myeloperoxidase-catalyzed oxidation, is markedly elevated in low density lipoprotein isolated from human atherosclerotic intima.* J Clin Invest, 1997. **99**(9): p. 2075-81.

263. Fischer, B., A. von Knethen, and B. Brune, *Dualism of oxidized lipoproteins in provoking and attenuating the oxidative burst in macrophages: role of peroxisome proliferator-activated receptor-gamma.* Journal of immunology, 2002. **168**(6): p. 2828-34.

264. Itabe, H., T. Obama, and R. Kato, *The Dynamics of Oxidized LDL during Atherogenesis.* Journal of lipids, 2011. **2011**: p. 418313.

265. Nagy, L., et al., *Oxidized LDL regulates macrophage gene expression through ligand activation of PPARgamma.* Cell, 1998. **93**(2): p. 229-40.

266. Rios, F.J., et al., *Co-stimulation of PAFR and CD36 is required for oxLDL-induced human macrophages activation.* PloS one, 2012. **7**(5): p. e36632.

267. Staels, B., *Cardiovascular biology: a cholesterol tether.* Nature, 2002. **417**(6890): p. 699-701.

268. Haghighat, A., et al., *Granulocyte colony-stimulating factor and granulocyte macrophage colony-stimulating factor exacerbate atherosclerosis in apolipoprotein E-deficient mice.* Circulation, 2007. **115**(15): p. 2049-54.

269. Shaposhnik, Z., et al., *Granulocyte macrophage colony-stimulating factor regulates dendritic cell content of atherosclerotic lesions.* Arteriosclerosis, thrombosis, and vascular biology, 2007. **27**(3): p. 621-7.

270. Zhu, S.N., et al., *GM-CSF regulates intimal cell proliferation in nascent atherosclerotic lesions.* The Journal of experimental medicine, 2009. **206**(10): p. 2141-9.

271. Suganami, T., J. Nishida, and Y. Ogawa, *A paracrine loop between adipocytes and macrophages aggravates inflammatory changes: role of free fatty acids and tumor necrosis factor alpha.* Arteriosclerosis, thrombosis, and vascular biology, 2005. **25**(10): p. 2062-8.

272. Miyazaki, T., J. Kurokawa, and S. Arai, *AIMing at metabolic syndrome. -Towards the development of novel therapies for metabolic diseases via apoptosis inhibitor of macrophage (AIM).* Circulation journal : official journal of the Japanese Circulation Society, 2011. **75**(11): p. 2522-31.

273. Suganami, T., et al., *Role of the Toll-like receptor 4/NF-kappaB pathway in saturated fatty acid-induced inflammatory changes in the interaction between adipocytes and macrophages.* Arteriosclerosis, thrombosis, and vascular biology, 2007. **27**(1): p. 84-91.

274. Rotter, V., I. Nagaev, and U. Smith, *Interleukin-6 (IL-6) induces insulin resistance in 3T3-L1 adipocytes and is, like IL-8 and tumor necrosis factor-alpha, overexpressed in human fat cells from insulin-resistant subjects.* The Journal of biological chemistry, 2003. **278**(46): p. 45777-84.

275. Trujillo, M.E., et al., *Interleukin-6 regulates human adipose tissue lipid metabolism and leptin production in vitro.* The Journal of clinical endocrinology and metabolism, 2004. **89**(11): p. 5577-82.

276. Jager, J., et al., *Interleukin-1beta-induced insulin resistance in adipocytes through down-regulation of insulin receptor substrate-1 expression.* Endocrinology, 2007. **148**(1): p. 241-51.

277. Lagathu, C., et al., *Long-term treatment with interleukin-1beta induces insulin resistance in murine and human adipocytes.* Diabetologia, 2006. **49**(9): p. 2162-73.

278. Stienstra, R., et al., *The inflammasome-mediated caspase-1 activation controls adipocyte differentiation and insulin sensitivity.* Cell metabolism, 2010. **12**(6): p. 593-605.

279. Lundberg, A.M., et al., *Toll-like receptor 3 and 4 signalling through the TRIF and TRAM adaptors in haematopoietic cells promotes atherosclerosis.* Cardiovascular research, 2013. **99**(2): p. 364-73.

280. Richards, M.R., et al., *The LPS2 mutation in TRIF is atheroprotective in hyperlipidemic low density lipoprotein receptor knockout mice.* Innate immunity, 2013. **19**(1): p. 20-9.

281. Harari, O.A., et al., *Absence of TRAM restricts Toll-like receptor 4 signaling in vascular endothelial cells to the MyD88 pathway*. Circulation research, 2006. **98**(9): p. 1134-40.

282. Hou, B., B. Reizis, and A.L. DeFranco, *Toll-like receptors activate innate and adaptive immunity by using dendritic cell-intrinsic and -extrinsic mechanisms.* Immunity, 2008. **29**(2): p. 272-82.

283. Fernandez-Real, J.M., et al., *CD14 modulates inflammation-driven insulin resistance.* Diabetes, 2011. **60**(8): p. 2179-86.

284. Alkhouri, N., et al., *Adipocyte apoptosis, a link between obesity, insulin resistance, and hepatic steatosis.* The Journal of biological chemistry, 2010. **285**(5): p. 3428-38.

285. Tordjman, K., et al., *PPARalpha deficiency reduces insulin resistance and atherosclerosis in apoE-null mice.* The Journal of clinical investigation, 2001. **107**(8): p. 1025-34.

286. Chen, N., et al., *Whole-body insulin resistance in the absence of obesity in FVB mice with overexpression of Dgat1 in adipose tissue.* Diabetes, 2005. **54**(12): p. 3379-86.

287. Hatley, M.E., et al., *Increased production of 12/15 lipoxygenase eicosanoids accelerates monocyte/endothelial interactions in diabetic db/db mice.* J Biol Chem, 2003. **278**(28): p. 25369-75.

288. Shi, W., et al., *Endothelial responses to oxidized lipoproteins determine genetic susceptibility to atherosclerosis in mice.* Circulation, 2000. **102**(1): p. 75-81.

289. Abu-Soud, H.M. and S.L. Hazen, *Nitric oxide is a physiological substrate for mammalian peroxidases.* J Biol Chem, 2000. **275**(48): p. 37524-32.

290. Karaskov, E., et al., *Chronic palmitate but not oleate exposure induces endoplasmic reticulum stress, which may contribute to INS-1 pancreatic beta-cell apoptosis.* Endocrinology, 2006. **147**(7): p. 3398-407.

291. Febbraio, M., E. Guy, and R.L. Silverstein, *Stem cell transplantation reveals that absence of macrophage CD36 is protective against atherosclerosis.* Arteriosclerosis, thrombosis, and vascular biology, 2004. **24**(12): p. 2333-8.

292. Galkina, E., et al., *Lymphocyte recruitment into the aortic wall before and during development of atherosclerosis is partially L-selectin dependent.* The Journal of experimental medicine, 2006. **203**(5): p. 1273-82.

APPENDIX

APPENDIX I

MYD88-DEPENDENT INTERPLAY BETWEEN MYELOID AND ENDOTHELIAL CELLS IN THE INITIATION AND PROGRESSION OF OBESITY-ASSOCIATED INFLAMMATORY DISEASES

Minjia Yu[1,2,#], **Hao Zhou[1,3,#]**, Junjie Zhao[1], Nengming Xiao[1], Sanjoy Roychowdhury[5], David Schmitt[4], Bingqing Hu[1], Clifford V. Harding[8], Amy G. Hise[8,9], Stanley L. Hazen[4], Anthony L. DeFranco[7], Paul L. Fox[4], Richard E. Morton[4], Paul E. Dicorleto[4], Maria Febbraio[6], Laura E. Nagy[5], Jonathan D. Smith[4], Jian-an Wang[2], and Xiaoxia Li[1,*]

[1]Department of Immunology, Cleveland Clinic, Cleveland, OH 44195, USA

[2]Department of Cardiology, Second Affiliated Hospital, School of Medicine, Zhejiang University, Hangzhou, Zhejiang, 310009, China

[3]Department of Biological, Geological, and Environmental Sciences, Cleveland State University, Cleveland, OH 44115, USA

[4]Department of Cellular and Molecular Medicine, Cleveland Clinic, Cleveland, OH 44195, USA

[5]Department of Pathobiology, Cleveland Clinic, Cleveland, OH 44195, USA

[6]Department of Molecular Cardiology, Cleveland Clinic, Cleveland, OH 44195, USA

[7]Department of Microbiology and Immunology, University of California, San Francisco, CA, 94143, USA

[8]Department of Pathology, Case Western Reserve University/University Hospitals Case Medical Center, Cleveland, OH 44106, USA

[9]Center for Global Health and Diseases, Case Western Reserve University, School of Medicine, Cleveland, OH 44106, USA

[#]**These authors contribute equally to this work.**

This work was published in the *Journal of Experimental Medicine* (2014) 211:887-907

A. Abstract

Low grade systemic inflammation is often associated with metabolic syndrome which plays a critical role in the development of the obesity-associated inflammatory diseases including insulin resistance and atherosclerosis. Here we investigate how TLR-MyD88 signaling in myeloid and endothelial cells coordinately participates in the initiation and progression of high fat diet-induced systemic inflammation and metabolic inflammatory diseases. MyD88 deficiency in myeloid cells inhibits macrophage recruitment to adipose tissue and their switch to an M1-like phenotype. This is accompanied by substantially reduced diet-induced systemic inflammation, insulin resistance, and atherosclerosis. MyD88 deficiency in endothelial cells results in a moderate reduction in diet-induced adipose macrophage infiltration and M1 polarization, selective insulin sensitivity in adipose tissue, and amelioration of spontaneous atherosclerosis. Both in vivo and ex vivo studies suggest that MyD88-dependent GM-CSF production from the endothelial cells might play a critical role in the initiation of obesity-associated inflammation and development of atherosclerosis by priming the monocytes in the adipose and arterial tissues to differentiate into M1-like inflammatory macrophages. Taken together, these results implicate a critical MyD88-dependent interplay between myeloid and endothelial cells in the initiation and progression of obesity-associated inflammatory diseases.

B. Introduction

The metabolic syndrome is characterized by a cluster of physiological alterations including glucose intolerance/insulin resistance, abdominal obesity, atherogenic dyslipidemia (low concentration of plasma high-density lipoprotein cholesterol and high concentration of plasma triglycerides), and elevated blood pressure. Occurring together, these conditions increase the risk for atherosclerosis and type 2 diabetes mellitus (T2DM), which are typical obesity-associated diseases that are endemic in developed countries, currently affecting 25% of the population and growing [178]. Recent investigations have increasingly shown that low grade systemic inflammation is often associated with metabolic syndrome, which probably plays a critical role in the development of these metabolic diseases [179-182]. Previous studies have shown that a high fat diet (HFD) can increase the gut permeability, triggering the accumulation of systemic inflammatory stimuli [183], including pathogen-associated molecular patterns (PAMPs), such as ligands for Toll-like receptors (TLRs), endogenous TLR ligands such as fatty acids and inflammatory cytokines, including Interleukin-1 (IL-1) [184-189]. Although inflammation is generally considered to be a localized reaction, it is now understood that a "systemic inflammatory response" can occur when inflammatory stimuli gain access to the circulation [180].

Genetic studies and mouse disease models have shown the participation of TLR and IL-1R in the development of HFD-induced systemic inflammation and obesity-associated inflammatory diseases. TLR4 deficiency reduced diet-induced insulin resistance and systemic inflammation [189], while TLR2-deficient mice were partially protected from diet-induced obesity [190]. Human TLR4 null mutations are associated with reduced risk

of atherosclerosis [191]. ApoE$^{-/-}$ mice, a commonly used model, spontaneously develop atherosclerosis; deficiency in TLR4, IL-1 and IL-1R each reduced vascular inflammation and atherosclerosis in ApoE$^{-/-}$ mice [192-195]. These previous studies suggested that exogenous/endogenous TLR ligands and the pro-inflammatory cytokine IL-1 can activate IL-1R/TLRs in multiple tissues including adipose, liver, pancreas, aorta, heart and muscle. As a consequence, a chronic systemic inflammatory response is established which is strongly associated with the development of type II diabetes and atherosclerosis [183, 196, 197]. Much effort has been devoted towards the understanding of IL-1R/TLR-mediated signaling mechanisms, with the long-term objective to identify new therapeutic targets and develop more effective anti-inflammatory small molecule drugs. Upon ligand stimulation, IL-1R and TLRs form either homo- or hetero oligomers. The adapter molecule MyD88 is recruited to all IL-1R/TLR oligomers, except TLR3, followed by the recruitment of the serine/threonine interleukin-1 receptor kinases (IRAKs) [127, 171, 198-200]. Genetic and biochemical studies revealed that through activation of MyD88-IRAKs, downstream kinases are organized by multiple adapter molecules into parallel and sequential signaling cascades, leading to activation of the transcription factor nuclear factor κB (NFκB) and MAPKs[129, 131, 132], resulting in the production of inflammatory cytokines and chemokines.

Although TLR-MyD88 signaling has been implicated in obesity-associated inflammatory diseases, the molecular and cellular mechanisms are not completely understood. In this study, we investigated how TLR-MyD88 signaling in different cellular compartments coordinately participates in the initiation of HFD-induced systemic inflammation and metabolic inflammatory diseases. The cell-type specific MyD88$^{-/-}$ mice

are crucial, since complete MyD88$^{-/-}$ mice (1) are immune compromised and prone to infection; (2) do not adequately reflect specific role of MyD88 in different cell types [201]. Indeed, several previous studies using complete MyD88$^{-/-}$ mice produced conflicting results regarding the role of MyD88 in obesity-associated inflammatory diseases, which might be due to the immune deficiency of complete MyD88$^{-/-}$ mice and the housing environment in different institutions [193, 195, 202]. Therefore, studies using cell-type specific MyD88$^{-/-}$ mice are necessary and timely to elucidate the mechanistic role of TLR-MyD88 signaling in obesity-associated inflammatory diseases.

Using cell-type specific MyD88-deficient mice, our findings for the first time demonstrate the MyD88-dependent cooperative actions of myeloid and endothelial cells in the development and progression of metabolic inflammatory diseases. MyD88 deficiency in myeloid cells (MyD88^{MC-KO}) substantially reduced diet-induced systemic inflammation, insulin resistance, and atherosclerosis. Furthermore, deletion of MyD88 in myeloid cells prevented macrophage infiltration into adipose tissue and aborted a switch in ATM phenotype from M2-like to M1-like. Using an adipocyte-macrophage ex vivo co-culture system and adipocyte-derived endogenous TLR ligand FFA, we demonstrated the influence of adipocytes on MyD88-dependent induction of M1-associated genes in macrophages, indicating the cross-talk between adipocytes and macrophages. On the other hand, MyD88 deficiency in endothelial cells (MyD88^{EC-KO}) showed moderate reduction in diet-induced adipose M1-like macrophages with selective insulin sensitivity in adipose tissue, and amelioration of spontaneous atherosclerosis. Both in vivo and ex vivo studies suggest that MyD88-dependent GM-CSF production from the endothelial cells might play a critical role in the initiation of obesity-associated inflammation and development of

atherosclerosis by priming the monocytes in the adipose and arterial tissues to M1-like inflammatory macrophages. Taken together, these results implicate a critical MyD88-dependent interplay among adipocytes, macrophages and endothelial cells in the initiation of diet-induced systemic inflammatory state and metabolic diseases.

C. Results

Generation of myeloid- and endothelial-specific MyD88-deficient mice

Endothelial cell-specific MyD88-deficient mice created by cre-lox technology were validated by PCR (**Fig. 32A**). Tie2eCre transgenic mice (generated using the Tie2 5' promoter and first intron enhancer element) express Cre within endothelium of brain, heart, and liver, among others [203, 204]. It is important to note that Tie2eCre (distinct from Tie2Cre) is restricted to endothelium, and Cre expression is minimally leaky [203, 204]. MyD88 expression was abolished in CD31+ endothelial cells from the aortas of Tie2eCreMyD88$^{fl/fl}$ (MyD88$^{EC\text{-}KO}$) mice compared to control (Tie2eCreMyD88$^{fl/+}$, Con $^{EC\text{-}KO}$), but showed normal MyD88 expression in monocytes (**Fig. 32A**). To generate myeloid specific MyD88-deficient mice, we utilized CD11bCre transgenic mice (generated with the promoter for CD11b, an integrin expressed exclusively in the myeloid lineage) [204-206]. These mice express Cre in macrophages, microglia, as well as activated liver kupffer cells. CD11bCreMyD88$^{fl/+}$ mice were bred to MyD88$^{fl/fl}$ to generate control mice (CD11bCreMyD88$^{fl/+}$, Con$^{MC\text{-}KO}$) and myeloid-specific MyD88-deficient mice (CD11bCreMyD88$^{fl/fl}$, MyD88$^{MC\text{-}KO}$). PCR analysis showed that MyD88 expression was diminished in CD11b+ monocytes derived from CD11bCreMyD88$^{fl/fl}$ (MyD88$^{MC\text{-}KO}$) mice compared to that in Con$^{MC\text{-}KO}$ mice (**Fig. 32A**).

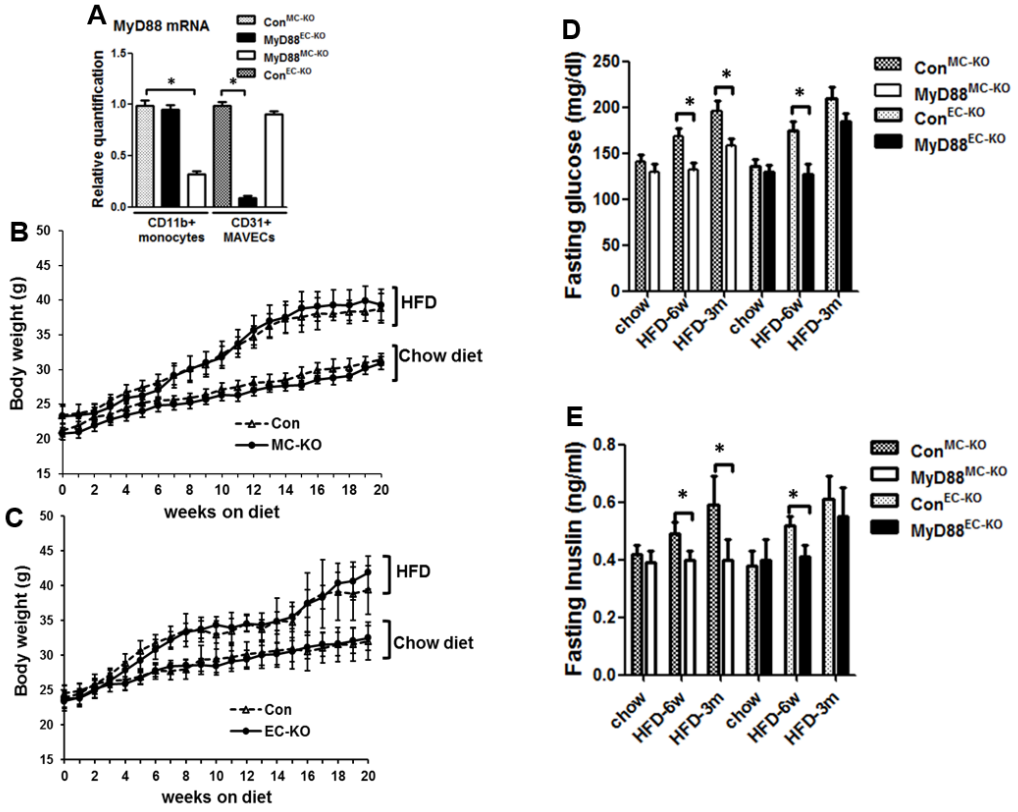

Figure 32. MyD88 deficiency in myeloid and endothelial cells improves diet-induced hyperglycemia and hyperinsulinemia. (A)PCR for MyD88 mRNA of mouse CD11b+ splenic monocytes (CD11b+ monocytes) and CD31+ primary aortic vascular endothelial cells (MAVECs) from MyD88^{EC-KO}, MyD88^{MC-KO} and their respective littermate controls (Con^{MC-KO} and Con^{EC-KO}). Data are presented as mean ± SD based on 5-7 for each group and are representative of three independent experiments. Body weights of **(B)** MyD88^{MC-KO} or **(C)** MyD88^{EC-KO} male mice and their littermate controls (maintained on a chow diet or HFD) were measured weekly from 6 to 26 weeks of age. **(D)** Serum fasting glucose and **(E)** fasting insulin levels were measured in MyD88^{MC-KO}, MyD88^{EC-KO} male mice and their respective littermate controls fed on chow diet (6 months of age) or HFD (for 6 weeks or 3 months starting from 6 weeks old). (n = 9-11 mice per genotype). Data are representative of two independent experiments.

MyD88 deficiency in myeloid and endothelial cells reduce diet-induced insulin resistance

We first analyzed metabolic parameters of MyD88^{MC-KO} and MyD88^{EC-KO} mice on chow diet or HFD. There were no substantial differences in weight gain over the course of 20 weeks (**Fig. 32B-C**) with similar levels of serum cholesterol, triglycerides and non-esterified fatty acids (**data not shown**) in MyD88^{MC-KO} and MyD88^{EC-KO} mice fed on chow or high-fat diet compared to their respective littermate controls. These results indicate that MyD88 deficiency in endothelial or myeloid cells did not affect diet-induced weight gain and lipid homeostasis. We then examined glucose metabolism in the MyD88^{MC-KO} and MyD88^{EC-KO} mice. Interestingly, after HFD (for 6 weeks and 3 months), fasting glucose and fasting insulin levels were substantially decreased in MyD88^{MC-KO} mice compared with the littermate controls (**Fig. 32D-E**). By performing GTT, we found that HFD fed MyD88^{MC-KO} mice had much improved glucose tolerance compared with the littermate controls (**Fig. 33A-B**). Endothelial MyD88 deficiency also improved insulin sensitivity, but the impact was more dramatic at early phase (6 weeks) compared to that after 3 months of HFD **(Fig. 33C-D)**. As controls, we noticed that the glucose tolerance and insulin sensitivity in chow diet fed MyD88^{MC-KO} and MyD88^{EC-KO} mice were comparable with their respective littermate controls (**Fig. 32D-E, data not shown**).

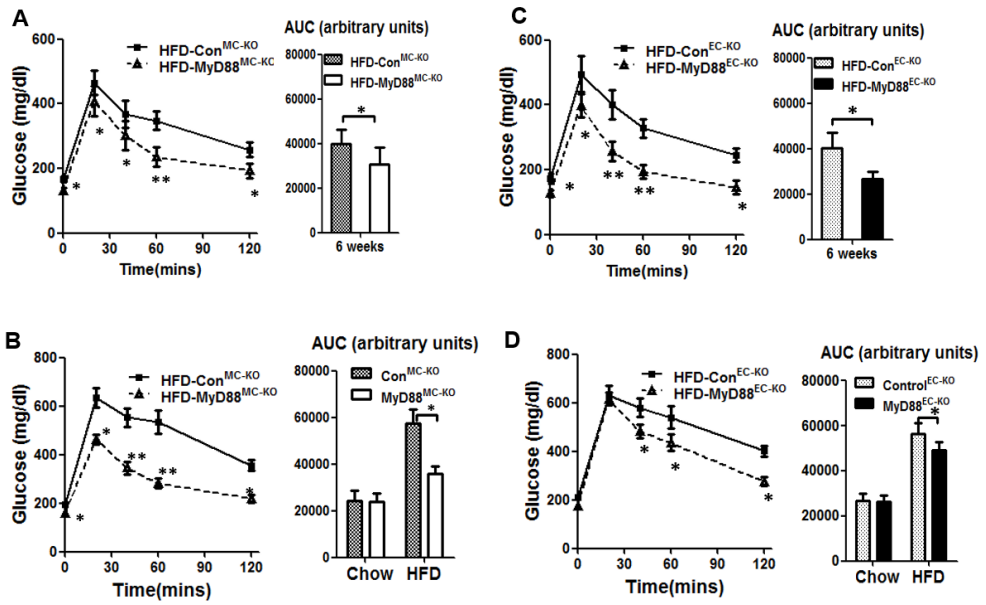

Figure 33. Deletion of MyD88 in myeloid cells and endothelial cells reduces diet-induced insulin resistance. GTTs (Glucose tolerance tests) in MyD88^{MC-KO} male mice and littermate controls on high fat diet (HFD) for **(A)** 6 weeks or **(B)** 3 months starting from 6-week old (6 months old mice on chow diet as controls， data not shown). Area under curve (AUC) was calculated. GTT in MyD88^{EC-KO} mice and their littermate controls on high fat diet (HFD) for **(C)** 6 weeks or **(D)** 3 months starting from 6-week old (6 months old mice on chow diet as controls， data not shown). AUC was calculated. Data are presented as mean ± S.E.M (n = 9-11 mice per genotype) and are representative of two independent experiments. (*P < 0.05, **P < 0.01)

Deletion of MyD88 in myeloid cells and endothelial cells preserves insulin signaling in different tissues

Since MyD88 deficiency in myeloid and endothelial cells attenuated diet-induced insulin resistance, we then examined insulin sensitivity in several tissues (including adipose tissue, muscle and liver) by IP injecting HFD-fed mice with insulin or saline after an overnight fast. As expected, compared with normal chow fed mice, insulin-induced AKT phosphorylation, tyrosine phosphorylation of IRS1 (insulin receptor substrate 1) and IRS1 interaction with PI3K (p85-phosphoinositide 3 kinase) were greatly reduced in adipose tissue, liver and muscle of HFD-fed wild-type control mice (**Fig. 34A-D**), demonstrating diet-induced insulin insensitivity of these tissues. Interestingly, while insulin-induced AKT phosphorylation was preserved in all three tissues of HFD-fed $MyD88^{MC\text{-}KO}$ mice, endothelial-specific MyD88 deficiency only rescued insulin signaling substantially in adipose tissue(**Fig. 34E-H**). Consistently, insulin-induced IRS-1 tyrosine phosphorylation and its association with PI3K (p85) were preserved in adipose tissue, liver and muscle of HFD-fed $MyD88^{MC\text{-}KO}$ mice, but only restored in adipose tissue of HFD-fed $MyD88^{EC\text{-}KO}$ mice, compared to that in their respective HFD-fed littermate controls(**Fig. 34E-H**). Thus, endothelial-derived MyD88 plays a more important role in HFD-induced insulin resistance in the adipose tissue than that in liver and muscle.

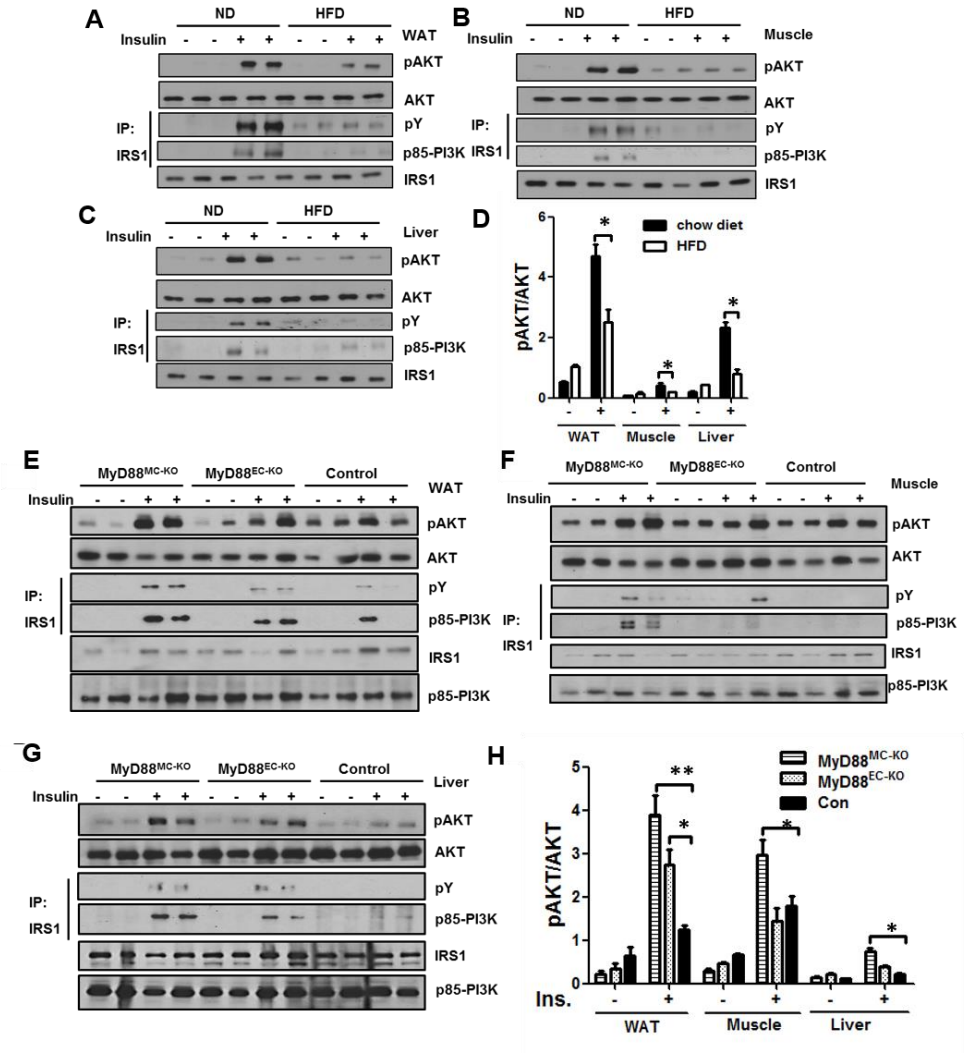

Figure 34. Deletion of MyD88 in myeloid cells and endothelial cells preserves insulin signaling. After overnight fast, 5-month-old of control group (CD11bCreMyD88$^{fl/+}$ and Tie2eCreMyD88$^{fl/+}$) male mice kept on chow diet or HFD were injected with either saline (-) or 25 mU/kg of insulin (+). **(A)** white Adipose tissues (WAT), **(B)** muscles and **(C)** livers were collected 5 minutes later. **(E)** white Adipose tissues (WAT), **(F)** muscles and **(G)** livers of MyD88^{MC-KO}, MyD88^{EC-KO} and control group male mice kept on HFD for 3 months were collected at 5 minutes after saline or insulin injection. Protein extracts were prepared, immunoprecipitated with anti-IRS-1, followed by western analysis with antibodies for phosphotyrosine (PY20, pY) or p85-PI3K. The levels of IRS1, activated AKT (pSer473, pAKT) and total AKT, were determined by immunoblotting of the original lysates. (**D** and **H**) The levels of pAKT and AKT were quantified by densitometry. The ratio of pAKT to AKT was expressed as a mean ± S.E.M. (*P < 0.05, **P < 0.01). (n = 4 mice per genotype). The results are representative of three independent experiments.

Myeloid- and endothelial-specific MyD88 deficiency protect mice from atherosclerosis in ApoE$^{-/-}$ mice

Atherosclerosis is a chronic inflammatory disease of the arteries, representing the underlining cause of the majority of cardiovascular disease. Obesity is an independent risk factor for the development of cardiovascular atherosclerosis. Obesity-induced insulin resistance and impaired glucose metabolism can exacerbate atherosclerosis. To study the impact of MyD88 deficiency in endothelial or myeloid cells on the pathogenesis of atherosclerosis, we employed the ApoE-deficient mice, which spontaneously develop hypercholesterolemia and atherosclerosis. Since female ApoE$^{-/-}$ mice were shown to develop more severe phenotype than male ApoE$^{-/-}$[207, 208]**,** we decided to use the female mice in this model. MyD88^{MC-KO}, MyD88^{EC-KO} mice and respective littermate controls were crossed to ApoE$^{-/-}$ mice to generate MyD88^{MC-KO}ApoE$^{-/-}$, MyD88^{EC-KO}ApoE$^{-/-}$ mice and control mice (Con^{MC-KO}ApoE$^{-/-}$ and Con^{EC-KO}ApoE$^{-/-}$ mice). Total plasma cholesterol levels and cholesterol distribution were similar among 18-week old female MyD88^{MC-KO} ApoE$^{-/-}$, MyD88^{EC-KO} ApoE$^{-/-}$ and their respective littermate controls either on chow diet or HFD (data not shown).

We first compared the severity of atherosclerosis in chow fed MyD88^{MC-KO}ApoE$^{-/-}$, MyD88^{EC-KO}ApoE$^{-/-}$ and their respective littermate controls at 18 weeks of age. En face and aortic root section analysis of atherosclerotic lesions showed about 60-70% reduction in both MyD88^{MC-KO} ApoE$^{-/-}$ and MyD88^{EC-KO} ApoE$^{-/-}$ mice compared to littermate controls (**Fig. 35A-D**). Thus, MyD88 deficiency in endothelial or myeloid cells inhibited vascular lesion formation in this model of spontaneous atherosclerosis. Consistently, under chow diet MyD88 deficiency in myeloid or endothelial cells had similar impact on insulin

sensitivity of aortas compared to that in their littermate controls **(Fig. 35E).** We then examined expression of inflammatory genes in arterial tissue of both MyD88^{MC-KO}ApoE$^{-/-}$ and MyD88^{EC-KO}ApoE$^{-/-}$mice. The expression levels of M-CSF, MCP-1, iNOS, VCAM-1, ICAM-1, and especially GM-CSF, were substantially reduced in the arterial tissue of MyD88 $^{EC-KO}$ApoE$^{-/-}$mice, whereas TNFα, IL-6 and IL-1 were similarly decreased in arterial tissue of MyD88^{EC-KO}ApoE$^{-/-}$ and MyD88^{MC-KO}ApoE$^{-/-}$ mice compared to that of littermate controls (**Fig. 36A-B**).

Since it is well known that the pathology of atherosclerosis in ApoE$^{-/-}$ mice is further aggravated upon HFD feeding, we then compared diet-induced atherosclerotic lesions of the endothelial- and myeloid-specific MyD88-deficient mice with their littermate controls. En face and aortic root section analysis of atherosclerotic lesions showed about 70% versus 40% reduction respectively in lesion areas of MyD88^{MC-KO} ApoE$^{-/-}$ mice and MyD88^{EC-KO} ApoE$^{-/-}$ mice compared to their littermate controls (**Fig. 35A-D**). It is important to note that HFD substantially induced insulin resistance in the aortas of wild-type control mice. Both MyD88^{MC-KO} ApoE$^{-/-}$ and MyD88^{EC-KO} ApoE$^{-/-}$ mice showed improved insulin sensitivity of aortas compared to their littermate controls **(Fig. 35E).** The expression of inflammatory genes (CXCL1, TNFα, IL-6, IL-1) was more dramatically decreased in arterial tissue of MyD88^{MC-KO} ApoE$^{-/-}$ than that in MyD88^{EC-KO}ApoE$^{-/-}$mice compared to their respective littermate controls **(Fig. 36C-D).** On the other hand, the expression of several inflammatory genes (M-CSF, MCP-1, iNOS, VCAM-1 and ICAM-1) were equally decreased in arterial tissue of MyD88 $^{MC-KO}$ ApoE$^{-/-}$ and MyD88 $^{EC-KO}$ApoE$^{-/-}$mice compared to littermate controls **(Fig. 36C-D).** It is important to note that the expression of GM-CSF was more dramatically decreased in arterial tissue of MyD88^{EC-}

^{KO} ApoE$^{-/-}$ than that in MyD88^{MC-KO}ApoE$^{-/-}$mice compared to that in littermate controls **(Fig. 36C-D).** Lastly, through the analysis of gene expression in aorta, we did notice that the expression of Arg1 and IL-10 were always enhanced in the arterial tissue of either chow or HFD fed MyD88^{EC-KO} ApoE$^{-/-}$ and MyD88^{MC-KO}ApoE$^{-/-}$ mice compared to that in their respective littermate controls (**Fig. 36A-D**), which will be further discussed below.

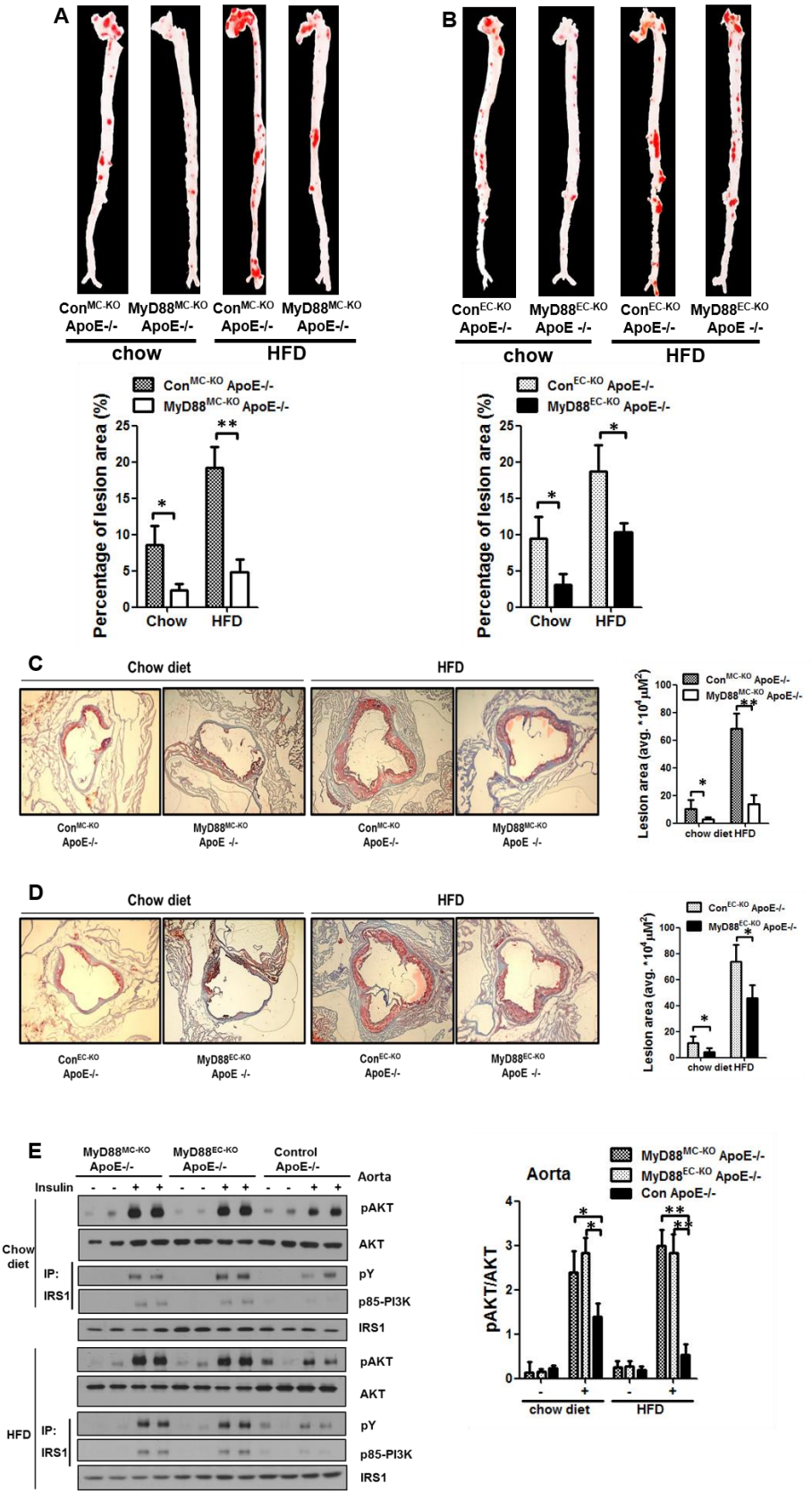
A
Con^MC-KO ApoE-/-
MyD88^MC-KO ApoE-/-
Con^MC-KO ApoE-/-
MyD88^MC-KO ApoE-/-
chow
HFD
Con^MC-KO ApoE-/-
MyD88^MC-KO ApoE-/-
Percentage of lesion area (%)
Chow
HFD
B
Con^EC-KO ApoE-/-
MyD88^EC-KO ApoE -/-
Con^EC-KO ApoE-/-
MyD88^EC-KO ApoE -/-
chow
HFD
Con^EC-KO ApoE-/-
MyD88^EC-KO ApoE-/-
Percentage of lesion area (%)
Chow
HFD
C
Chow diet
HFD
Con^MC-KO ApoE-/-
MyD88^MC-KO ApoE -/-
Con^MC-KO ApoE-/-
MyD88^MC-KO ApoE -/-
Con^MC-KO ApoE-/-
MyD88^MC-KO ApoE-/-
Lesion area (avg. *10^4 μM^2)
chow diet HFD
D
Chow diet
HFD
Con^EC-KO ApoE-/-
MyD88^EC-KO ApoE -/-
Con^EC-KO ApoE-/-
MyD88^EC-KO ApoE -/-
Con^EC-KO ApoE-/-
MyD88^EC-KO ApoE-/-
Lesion area (avg. *10^4 μM^2)
chow diet HFD
E
MyD88^MC-KO ApoE-/-
MyD88^EC-KO ApoE-/-
Control ApoE-/-
Aorta
Insulin
Chow diet
IP: IRS1
pAKT
AKT
pY
p85-PI3K
IRS1
HFD
IP: IRS1
pAKT
AKT
pY
p85-PI3K
IRS1
Aorta
MyD88^MC-KO ApoE-/-
MyD88^EC-KO ApoE-/-
Con ApoE-/-
pAKT/AKT
chow diet
HFD

Figure 35. Myeloid - and endothelial-specific MyD88 deficiency protect mice from atherosclerosis. (A) MyD88^{MC-KO} ApoE$^{-/-}$, **(B)** MyD88^{EC-KO} ApoE$^{-/-}$ female mice and their respective littermate controls (Con^{MC-KO} ApoE$^{-/-}$ and Con^{EC-KO} ApoE$^{-/-}$), were fed on chow diet or HFD for 12 weeks beginning at 6 weeks of age. Enface (oil-red O staining) analysis was done for the whole aorta tree from end of the curvature of the aortic arch to the iliac bifurcation from these mice. Total mean lesion area was quantified based on image-analysis by Photoshop software shown. Data are presented as mean ± S.E.M (n = 9-12 mice per genotype) and are representative of two independent experiments. (*P < 0.05, **P < 0.01). Cross-sections of aortic roots from **(C)** MyD88^{MC-KO} ApoE$^{-/-}$, **(D)** MyD88^{EC-KO} ApoE$^{-/-}$ female mice and their respective littermate controls fed on chow diet or HFD for 12 weeks were stained with oil red O (Scale bar=250μm). Total mean lesion area was quantified by Photoshop software and shown as mean ± S.E.M and are representative of three independent experiments.. (*P < 0.05, **P < 0.01). (n = 6-7 mice per genotype). **(E)** Aortas of MyD88^{MC-KO} ApoE$^{-/-}$, MyD88^{EC-KO} ApoE$^{-/-}$ and control group female mice kept on either chow diet or HFD for 3 months were collected at 5 minutes after saline or insulin injection. Protein extracts were analyzed as described in Fig. 2A-D. The levels of pAKT and AKT were quantified by densitometry. The ratio of pAKT to AKT was expressed as a mean ± S.E.M. (*P < 0.05, **P < 0.01). (n = 4 mice per genotype). The results are representative of three independent experiments.

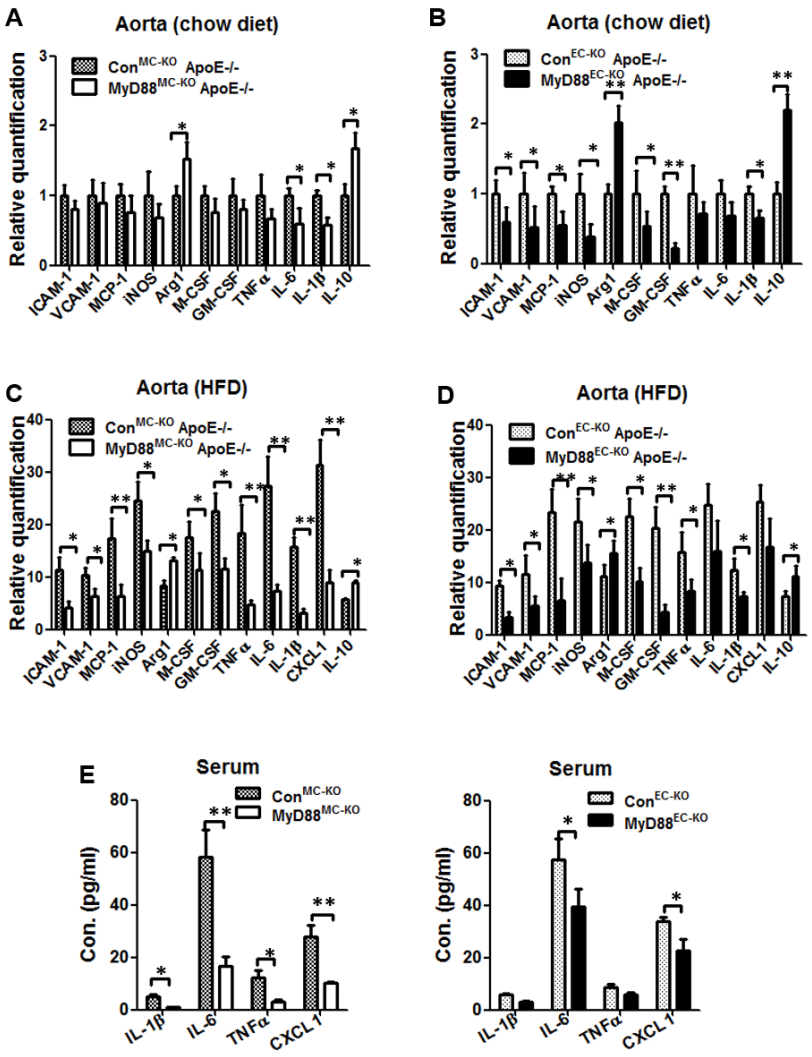

Figure 36. MyD88 deficiency in myeloid and endothelial cells ameliorates arterial tissues inflammation under hypercholesterolemia and diet-induced systemic inflammation. Total RNA of aortas was isolated from MyD88^{MC-KO} ApoE$^{-/-}$ female mice and littermate control mice on chow diet **(A)** or HFD **(B)**; MyD88^{EC-KO} ApoE$^{-/-}$ female mice and their respective littermate controls on chow diet **(C)** or HFD **(D)**; and followed by quantitative real-time PCR and normalized to β-actin for the indicated genes. The mean value of each gene in control groups on chow diet was set to 1. The mean value of each gene in mice on HFD was normalized to that in their respective controls on chow diet. Data are presented as mean ± S.E.M (n = 9-12mice per genotype) and are representative of two independent experiments. **(E)** Protein levels of IL-1β, IL-6, TNFα and CXCL1 in the serum from MyD88^{MC-KO} ApoE$^{-/-}$, MyD88^{EC-KO} ApoE$^{-/-}$ female mice and their respective littermate controls were analyzed by ELISA. (n = 7-9 mice per genotyping). Data are presented in as mean ± S.E.M. (*P < 0.05, **P < 0.01). The results are representative of two independent experiments.

Myeloid-derived MyD88 is required for HFD-induced systemic inflammation

Recent studies have shown a direct link between "chronic systemic inflammation" and diet-induced metabolic syndrome and consequent obesity-associated inflammatory diseases [180, 209-221]. Low-grade inflammation triggered by the HFD was indeed detected in the circulation of control mice, whereas diet-induced serum pro-inflammatory cytokines (IL-1, IL-6, TNF and CXCL1) were greatly reduced in MyD88^{MC-KO} mice (**Fig. 36E**). On the other hand, the deletion of MyD88 in endothelial cells only moderately reduced serum levels of these pro-inflammatory cytokines (**Fig. 36E**). As shown in **Fig. 35A-D**, myeloid MyD88 also plays a more critical role than endothelial MyD88 in HFD-induced atherosclerosis, suggesting that systemic inflammation might contribute to HFD-induced exacerbation on atherosclerosis. Under systemic inflammation, in addition to ox-LDL and IL-1, the endothelium is probably also activated by other circulating inflammatory stimuli through MyD88-independent pathways, including TNFα and IL-6[222]. Taken together, our results suggest that while both myeloid and endothelial MyD88 participate in the initiation of obesity-induced inflammatory diseases, myeloid MyD88 might play a more dominant role in disease progression through its impact on systemic inflammation.

Myeloid MyD88 participates in HFD-induced switching of adipose tissue macrophages (ATM) from M2-like to M1-like

Metabolic-triggered inflammation in white adipose tissue plays a key role in initiation of inflammatory diseases associated with metabolic syndrome, by directly impacting local and systemic insulin signaling and consequent long-term systemic

inflammation [223-227]. Obesity-induced adipose tissue inflammation is characterized by the presence of an increased number of adipose tissue infiltrating macrophages [228]. Compared to littermate controls, MyD88^{MC-KO} mice showed markedly reduced infiltration of macrophages and fewer so called “crown-like structures (CLS)”, which are associated with inflammation and apoptotic/necrotic adipocytes (**Fig. 37A-B and F4/80 levels in 37D**). In support of the histology, mRNA expression levels of inflammatory genes were greatly decreased in adipose tissue of MyD88^{MC-KO} mice compared to controls (**Fig. 37C**).

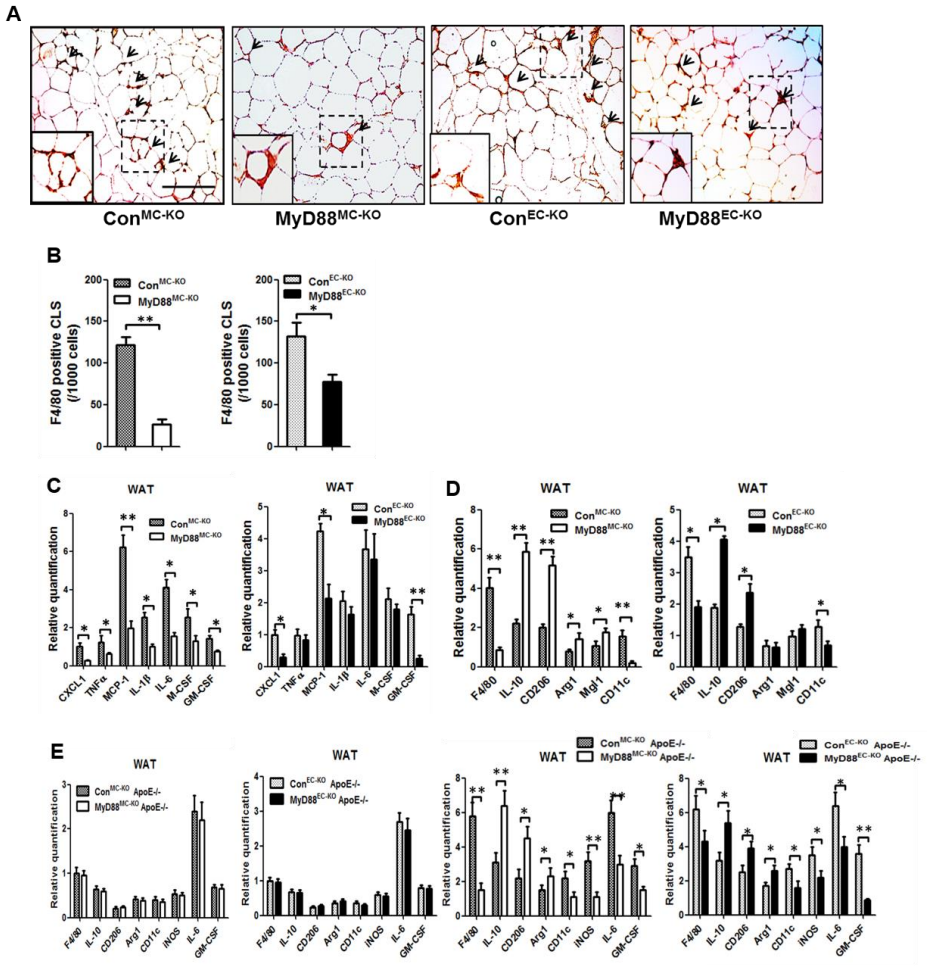

Figure 37. Deletion of MyD88 in myeloid cells and endothelial cells reduces diet-induced adipose tissue inflammation. $MyD88^{MC\text{-}KO}$, $MyD88^{EC\text{-}KO}$ male mice and their respective littermate controls on HFD for 14 weeks were sacrificed and epididymal fat pad was collected. **(A)** Paraffin sections of epididymal fat pad were stained with anti-F4/80 antibody (Scale bar=50μm). Arrowheads indicate F4/80 positive staining; representative CLSs were enlarged and shown in the insert. **(B)** The number of CLSs was counted. Results are shown as mean ± S.E.M of five different sections per mouse and are representative of five mice per genotype with similar results. The results are representative of two independent experiments. **(C-D)** Total adipose tissue RNA from $MyD88^{MC\text{-}KO}$, $MyD88^{EC\text{-}KO}$ and their respective littermate control mice were analyzed by quantitative real-time PCR and normalized to β-actin for the indicated genes. Data are presented as mean ± S.E.M (n = 9-11 per genotype) and are representative of two independent experiments. (*P<0.05, **P < 0.01). $MyD88^{MC\text{-}KO}$ $ApoE^{-/-}$, $MyD88^{EC\text{-}KO}$ $ApoE^{-/-}$ male mice and their respective littermate controls fed on either chow diet **(E)** or HFD **(F)** for 12 weeks were sacrificed and epididymal fat pad was collected. Total adipose tissue RNA were analyzed by quantitative real-time PCR and normalized to β-actin for the indicated genes. Data are presented as mean ± S.E.M (n = 5-6 per genotype) and are representative of two independent experiments. (*P<0.05, **P < 0.01).

ATMs consist of at least two different phenotypes, classically activated M1-like macrophages and alternatively activated, resident M2-like macrophages. In obesity, infiltrating M1-like macrophages lead to an overall switch in adipose tissue phenotype, associated with insulin resistance and chronic inflammation [224, 228-238]. Interestingly, we found that gene markers for M2-like macrophages, including IL-10, C-type mannose receptor 2(CD206), Arginase-1, and macrophage galactose N-acetyl-galactosamine–specific lectin 1 (Mgl-1) were increased in adipose tissue of $MyD88^{MC\text{-}KO}$, while M1-like marker CD11c was decreased (**Fig. 37D**), which is consistent with the improved adipose inflammatory status of these mice. When gated on CD11b+F4/80+ cells from adipose tissue of HFD-fed mice, the elimination of MyD88 in myeloid cells increased the number of M2-like macrophages (CD11c-CD206+) with decreased M1-like macrophages (CD11c+CD206-), confirming the critical role of MyD88-dependent signaling in HFD-induced ATM switching from M2- to M1-like macrophages **(Fig. 38A**). We then sorted for

M1-like (F4/80+CD11c+) and M2-like (F4/80+CD206+) macrophages from adipose tissues of HFD-fed MyD88^{MC-KO} and control mice, followed by gene expression analysis. Inflammatory gene expression (iNOS and IL-6) was much higher in M1-like than that in M2-like macrophages and substantially reduced in MyD88-deficient M1- and M2-like macrophages compared to their corresponding control macrophages, respectively (**Fig. 38B**). On the other hand, M2-associated gene expression (Mgl1 and IL-10) was much higher in M2-like than that in M1-like macrophages and significantly increased in MyD88-deficient M2- and M1-like macrophages compared to their corresponding control macrophages (**Fig. 38B**). These data indicate that deletion of MyD88 in myeloid cells aborted HFD-induced switch of ATMs from M2- to M1-like subtype at cellular and molecular levels.

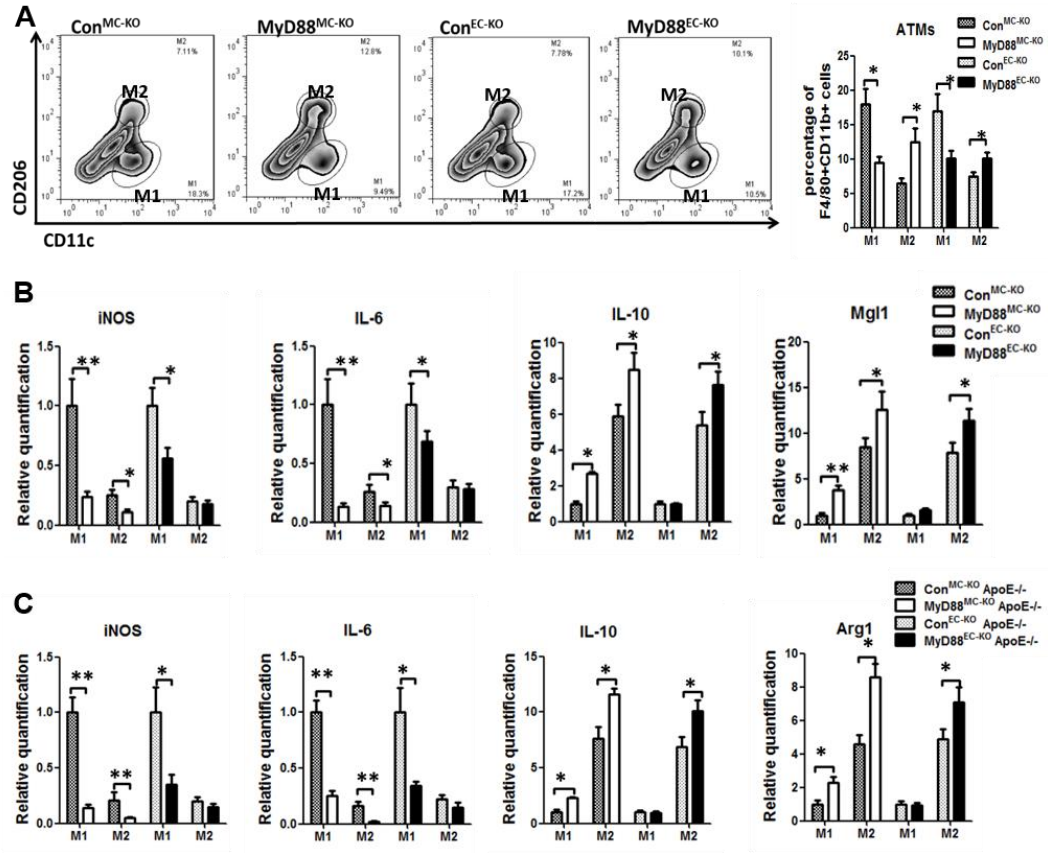

Figure 38. MyD88 participates in HFD-induced switching of adipose tissue macrophages (ATM) from M2 to M1. (A) Stromal vascular fraction (SVF) cells from epididymal fat pad of 6 month old MyD88^{MC-KO}, MyD88^{EC-KO} mice and their respective littermate controls on HFD were analyzed by flow cytometry. CD11b+F4/80+ (ATMs) were further analyzed with anti-CD11c and anti-CD206 antibodies. M1-like (F4/80+CD11c+) cells and M2-like (F4/80+CD206+) subsets were shown as mean ± S.E.M (n = 9-12 mice per genotype) and are representative of two independent experiments. (*P<0.05, **P < 0.01). **(B)**Total RNA isolated from M1- or M2-like macrophages was analyzed by quantitative real-time PCR and normalized to β-actin for the indicated genes. The mean value of each gene in M1-like cells from control groups was set to 1. Data are presented as mean ± S.E.M (n = 5-7 per genotype) and are representative of two independent experiments. (**C)**Total RNA was isolated from M1-like (F4/80+CD11c+) cells or M2-like (F4/80+ CD206+) cells in aortic lesions and analyzed by quantitative real-time PCR and normalized to β-actin for the indicated genes. The mean value of each gene in M1-like cells from control groups was set to 1. Data are presented as mean ± S.E.M (n = 5-6 mice per genotype and are representative of two independent experiments. (*P<0.05, **P < 0.01).

Similar M1- and M2-associated gene expression patterns were observed in adipose tissues of mice bred onto ApoE$^{-/-}$ background fed on HFD (**Fig. 37D and Fig. AI-37E-F**). It is interesting to note MyD88 deficiency in myeloid cells also led to a shift from M1-associated [iNOS; TNF, IL-1 and IL-6] to M2-like [Arg1 and IL-10] gene expression in arterial tissue of chow and HFD fed mice (**Fig. 36A and AI-5C**). This finding was confirmed by immunestaining of sections of aortic roots of MyD88^{MC-KO} mice and littermate control mice on both chow diet and HFD (**Fig. 39A-D**). MyD88 deficiency in myeloid cells indeed led to a shift from M1-like (F4/80+iNOS+) to M2-like (F4/80+Arginase1+) macrophages in the aortic lesions of mice on chow diet or HFD (**Fig. 39A-D**). This result was further corroborated by gene expression profile from sorted macrophages from aortic tissues of HFD-fed mice. Inflammatory gene expression (iNOS and IL-6) was substantially reduced in sorted MyD88-deficient M1- (F4/80+CD11c+) and M2-like (F4/80+CD206+) macrophages compared to their corresponding control

macrophages, respectively (**Fig. 38C**). Importantly, M2-associated gene expression (Arg1 and IL-10) was much higher in M2-like than that in M1-like macrophages and significantly increased in MyD88-deficient M2-like and M1-like macrophages compared to their wild-type control macrophages, respectively (**Fig. 38C**).

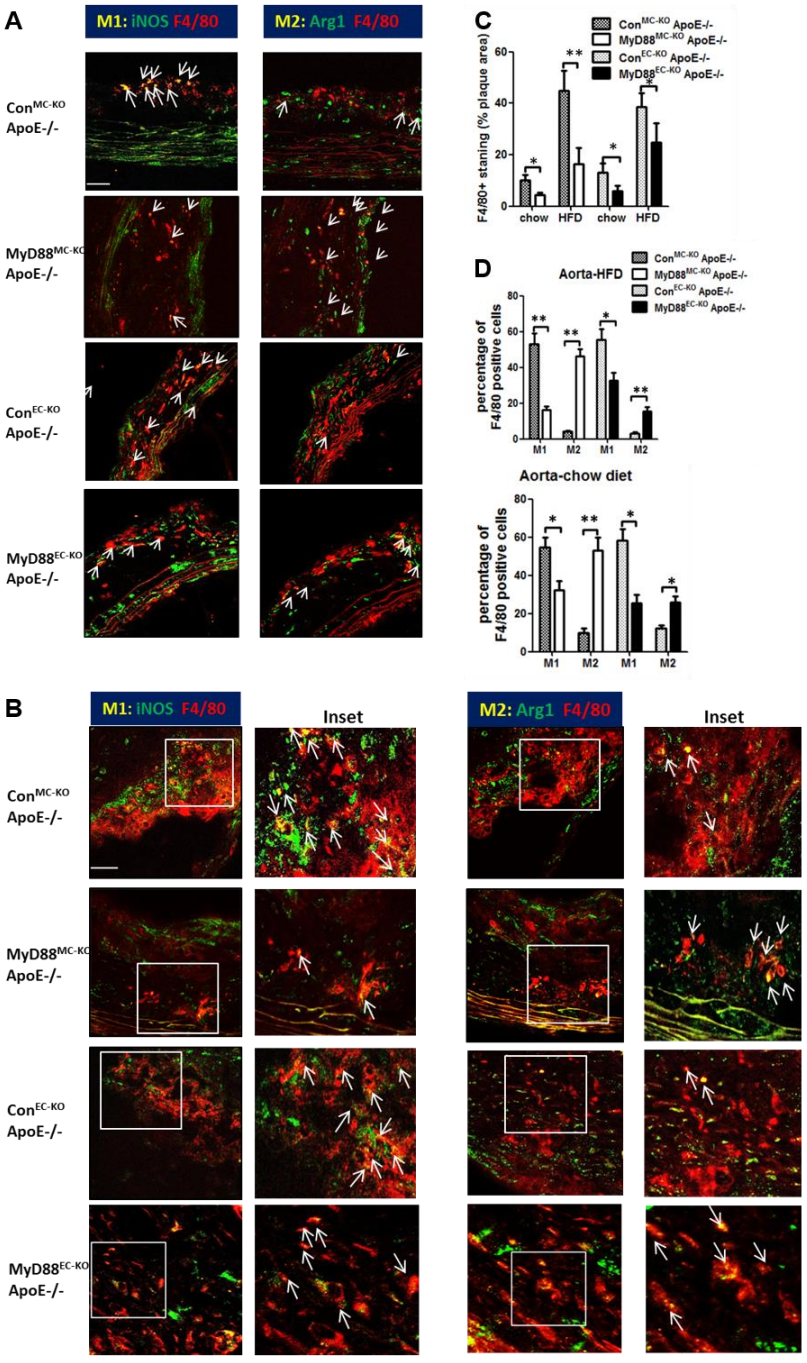

Figure 39. Deletion of MyD88 in myeloid cells and endothelial cells prevents M1 macrophages polarization in arterial tissue under hypercholesterolemia. Immunostaining of atherosclerotic lesions from $MyD88^{MC\text{-}KO}$ $ApoE^{-/-}$, $MyD88^{EC\text{-}KO}$ $ApoE^{-/-}$ female mice and their respective littermate controls on chow diet **(A)** or HFD **(B)** for 3 months. Macrophages were identified as F4/80+ (red) cells. Co-expression of F4/80 and iNOS (green) or Arg1 (green) was identified by image overlay. Inset: magnification of the zone delimited in the frame. Arrowheads indicate representative M1-like (F4/80+iNOS+) or M2-like (F4/80+Arg1+) cells (scale bar=20μm) (n = 4-5 mice per genotype). The results are representative of three independent experiments. **(C)** Lesional macrophage content as determined by percentage of F4/80 positive staining area (mean ± S.E.M). **(D)** Enumeration of M1-like or M2-like macrophages by immunofluorescence in aortic root sections as shown in G. Results are shown as average ± S.E.M of five different sections per mouse and are representative of 4-5 mice per genotype with similar results. (*P<0.05, **P < 0.01)

Since myeloid-derived MyD88 had a dramatic impact on the ATM phenotype, we set up an adipocyte-macrophage ex vivo co-culture system to explore the cross-talk between adipocytes and macrophges. BMDMs and 3T3L1 adipocytes were cultured in the bottom and inner wells of Boyden chambers, respectively, which permitted passage of humoral factors between the chamber wells. Pro-inflammatory cytokine/chemokine mRNAs and proteins in the supernatant were higher in macrophages co-cultured with adipocytes than those in macrophages cultured alone (**Fig. 40A**). The effects of co-culturing were augmented by the increase of ratios of adipocytes/macrophages (**Fig. 40A)**. Interestingly, we also found that Arginase-1 and CD206 (M2 markers) expression were reduced by co-culturing (**Fig. 40B**). Furthermore, the expression of M1-associated genes including IL-12a, IL-12b, IRF5 and NOS2 was concomitantly upregulated by the increase of ratios of adipocytes/macrophages (**Fig. 40C**)**.** All these effects were reduced in MyD88KO BMDMs (**Fig. 40A-C**), demonstrating that MyD88 participates in the cross-talk between adipocytes and macrophages, which might play a critical role in HFD-induced switching of ATMs from M2-like to M1-like phenotype. The next question is what the relevant ligands here. ATMs are exposed to high local concentrations of FFAs released

from enlarged adipocytes and augmented by increased lipolysis in obesity [239-242]. We indeed detected FFA in the conditioned media of the co-culture experiment of adipocytes and macrophages by ELISA (**Fig. 40D**). This finding suggests that FFA from adipocytes might serve as a TLR ligand to activate macrophages in our co-culture system. In support of this, we found that palmitate-induced inflammatory gene expression was substantially reduced in MyD88-deficient macrophages compared to that in control cells, while completely abolished in TLR4-/- and partially impaired in TLR2-/- macrophages, suggesting the possible role of saturated fatty acids (SFAs) in promoting TLR-MyD88-dependent switching of ATMs from M2-like to M1-like inflammatory macrophages (**data not shown**).

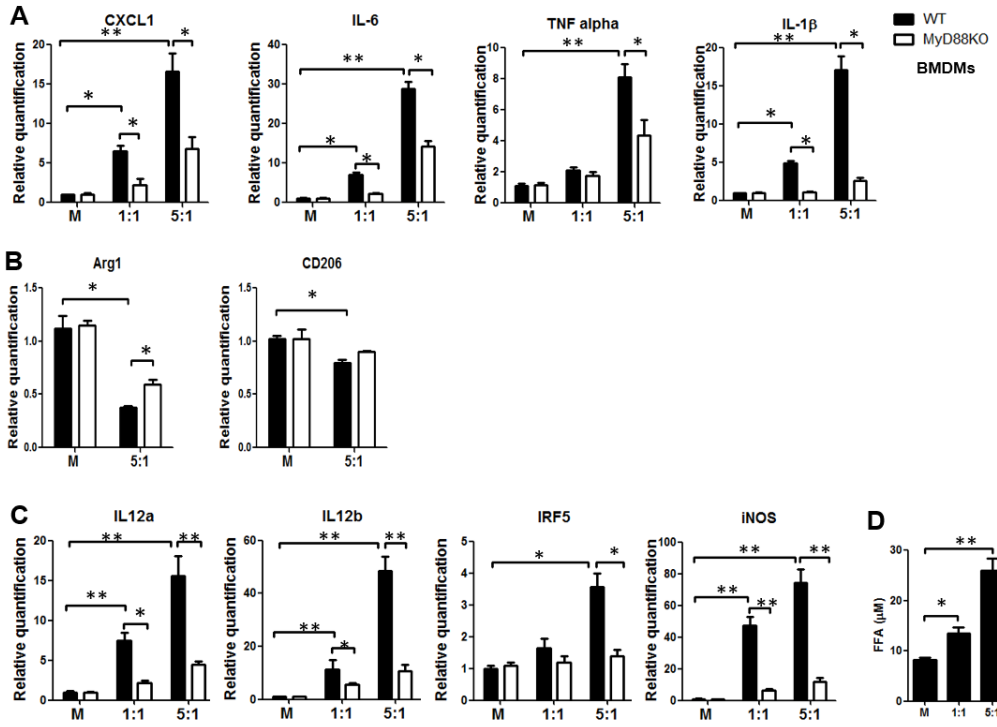

Figure 40. MyD88-dependent cross-talk between adipocytes and macrophages promotes M1 polarization. Bone marrow-derived macrophages (BMDMs) of WT and MyD88KO male mice were plated in the bottom wells of Boyden chambers, with or without (indicated as M) 3T3 adipocytes in the inserts at a ratio of 1:1 or 5:1 (adipocytes: BMDMs cell numbers). mRNA expression levels of **(A)** CXCL1, IL-6, TNF-α, IL-1β, **(B)** Arginase-1, CD206, **(C)** IL12a, IL12b, IRF5 and iNOS in the BMDMs were analyzed. The expression of mRNA normalized to β-actin expression. The data are presented as fold induction over the levels of mRNAs in WT macrophages cultured alone. (n = 5 wells in each group) Data represent the mean ± S.E.M. of the results from three independent experiments. **(D)** Concentration of FFA in the supernatant was measured by ELISA (n = 5 wells in each group). Data are expressed as mean ± S.E.M of the results from three independent experiments. (*P<0.05, **P < 0.01).

Endothelial MyD88 mediates GM-CSF production to prime M1-like inflammatory macrophages

Interestingly, MyD88$^{EC\text{-}KO}$ mice also showed moderate reduction in HFD-induced M1-like macrophages in adipose tissue (**Fig. 37C-D and Fig. 38A-B**). Consistently, endothelial-specific MyD88 deficiency rescued insulin signaling substantially in adipose tissue **(Fig. 34E & H).** Furthermore, MyD88 deficiency in endothelial cells (MyD88$^{EC\text{-}KO}$ApoE$^{-/-}$) showed substantial reduction in lesion areas, aortic wall inflammation (including a shift from M1- to M2-like macrophages) and improved insulin sensitivity of aortas in both chow and HFD-fed mice (**Fig. 35B, 35D, 35E, 36B, 36D, Fig. 38C and 39A-D**). Based on these results, we hypothesized that MyD88-signaling in endothelial cells mediates the cross-talk with macrophages to impact on the initiation of atherosclerosis and diet-induced exacerbation on atherosclerotic lesions. Interestingly, we noticed that the expression of GM-CSF was substantially decreased in the arterial tissue and adipose tissue of MyD88$^{EC\text{-}KO}$ mice compared to controls (**Fig. 36B & D, 37C and 41A**). Immunostaining showed that GM-CSF was indeed co-localized with CD31+ endothelial cells in the aortic root lesions of Con$^{EC\text{-}KO}$ApoE$^{-/-}$ mice, which was abated in that of the MyD88$^{EC\text{-}KO}$ApoE$^{-/-}$

mice, demonstrating MyD88-dependent GM-CSF expression in endothelial cells (**Fig. 41B**). GM-CSF is well-known for its function in promoting monocyte differentiation towards M1 pro-inflammatory macrophages [131, 243-251]. Based on our results and previous studies on GM-CSF, we proposed that MyD88-dependent signaling in endothelial cells induces the production of GM-CSF, which in turn primes the monocytes/macrophages to become M1-like inflammatory macrophages.

To test this hypothesis, we need to know the relevant ligands for the MyD88-dependent signaling in endothelial cells. Ox-LDL (oxidized and related modified forms of low density lipoproteins) is an endogenous TLR2/4 ligand, which accumulates in the vessel wall and is an emerging cardiovascular risk factor [238, 252]. Ox-LDL may trigger TLR signaling in macrophages and as well as directly on endothelial cells. In addition to ox-LDL, the endothelium, the interface between vascular structures and blood, can also be activated by a variety of circulating inflammatory stimuli [222], including TNF , IL-6 and IL-1. Therefore, the most relevant ligands for MyD88-dependent signaling in endothelial cells are ox-LDL and IL-1. Interestingly, we found that both ox-LDL and IL-1 can strongly induce GM-CSF expression in primary endothelial cells, which was completely abolished in MyD88-deficient endothelial cells (**Fig. 41C**). We wondered then whether GM-CSF produced by ox-LDL- and IL-1-treated endothelial cells is able to influence the macrophage function. We indeed found that the conditioned medium from ox-LDL-treated wild-type endothelial cells (but not MyD88-deficient endothelial cells) was able to induce GM-CSF-target gene PPBP (CXCL7,[246, 251]) in CD11b+ monocytes and enhanced the expression of M1-associated genes including IL-12a, IL-12b and iNOS (**Fig. 41D**). Similar results were observed with IL-1-treated endothelial cells (data not

shown). Neutralization with anti-GM-CSF greatly reduced the expression of PPBP and M1-associated genes in monocytes in response to the conditioned medium from ox-LDL-treated endothelial cells (**Fig. 41D**). Moreover, the conditioned medium from ox-LDL-treated wild-type endothelial cells (but not MyD88-deficient endothelial cells) was able to increase the ratio of CD11c (M1) to CD206 (M2), which was also blocked by anti-GM-CSF, supporting the role of GM-CSF in monocyte differentiation towards M1-like macrophages (**Fig. 41D**). It is important to note that ox-LDL used in this study was generated by using MPO/H2O2/Nitrite system (see methods). We found that the ox-LDL generated by this protocol can consistently activate TLR-induced inflammatory genes and synergize with GM-CSF for up-regulation of M1-associated genes [253-262].

Since ox-LDL has been shown to directly act on macrophages in vivo [263-266], we wondered whether it is possible that GM-CSF produced by ox-LDL activated endothelial cells synergizes with SFAs and ox-LDL to further promote M1-like proinflammatory macrophages. Palmitate and ox-LDL indeed enhanced the expression of M1-associated genes in GM-CSF-primed macrophages as compared to that in M-CSF-primed macrophages (**Fig. 41E**). Interestingly, the expression of M1-associated gene expression was more robustly enhanced in the adipocyte-macrophage ex vivo co-culture system when using GM-CSF-primed macrophages as compared to that of M-CSF-primed macrophages (**Fig. 41F**). Taken together, these results suggest a potential role of GM-CSF in priming ATMs to become M1-like macrophages during their cross-talk with adipocytes. It is important to note that endothelial-specific MyD88 deficiency substantially reduced HFD-induced GM-CSF expression in adipose tissue (**Fig. 37C**), which was correlated with selective rescue of insulin signaling in adipose tissue of HFD fed MyD88$^{EC\text{-}KO}$ mice (**Fig.**

34E and 34H). These findings implicate the MyD88-dependent involvement of endothelial cells in the cross-talk between adipocytes and macrophages, which might be important for the initiation of obesity-associated inflammatory diseases. In support of this, endothelial MyD88 deficiency improved insulin sensitivity more dramatic at early phase (6 weeks) compared to that after 3 months of HFD **(Fig. 33C-D); and** $MyD88^{EC\text{-}KO}ApoE^{-/-}$ mice showed greater reduction in atherosclerotic lesions developed under chow diet (70% reduction) than that in HFD (40% reduction).

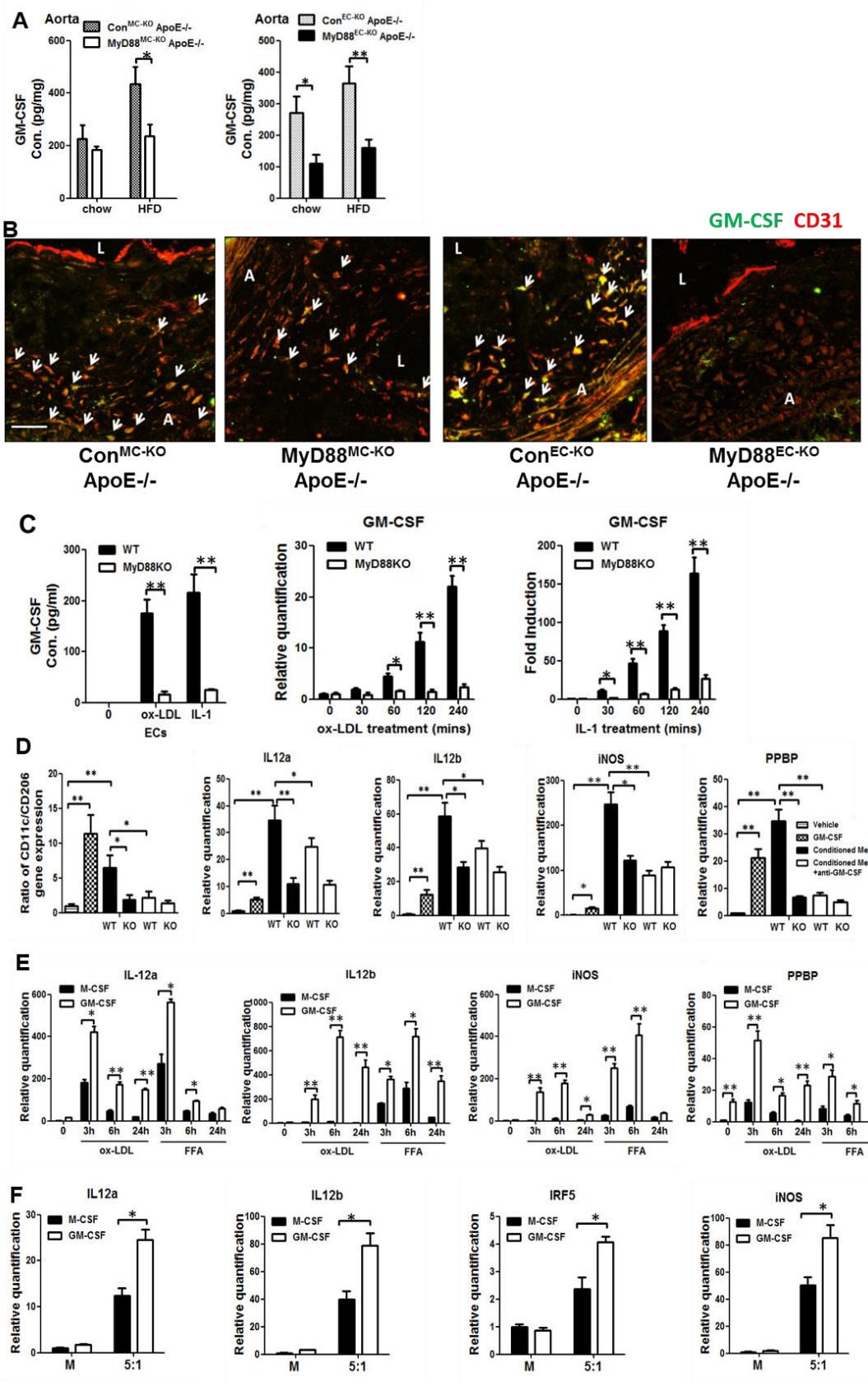
A
Aorta
Con^MC-KO ApoE-/-
MyD88^MC-KO ApoE-/-
GM-CSF Con. (pg/mg)
chow
HFD
Aorta
Con^EC-KO ApoE-/-
MyD88^EC-KO ApoE-/-
GM-CSF Con. (pg/mg)
chow
HFD
B
GM-CSF CD31
L
A
Con^MC-KO ApoE-/-
MyD88^MC-KO ApoE-/-
Con^EC-KO ApoE-/-
MyD88^EC-KO ApoE-/-
C
GM-CSF
WT
MyD88KO
GM-CSF Con. (pg/ml)
0
ox-LDL
IL-1
ECs
GM-CSF
Relative quantification
ox-LDL treatment (mins)
GM-CSF
Fold Induction
IL-1 treatment (mins)
D
Ratio of CD11c/CD206 gene expression
IL12a
IL12b
iNOS
PPBP
Relative quantification
WT KO WT KO
Vehicle
GM-CSF
Conditioned Medium
Conditioned Medium +anti-GM-CSF
E
IL-12a
IL12b
iNOS
PPBP
Relative quantification
M-CSF
GM-CSF
0
3h
6h
24h
ox-LDL
FFA
F
IL12a
IL12b
IRF5
iNOS
Relative quantification
M-CSF
GM-CSF
M
5:1

Figure 41. Endothelial MyD88 mediates GM-CSF production to prime M1 inflammatory macrophages. (A) Protein level of GM-CSF in whole aorta lysate taken from $MyD88^{MC\text{-}KO}$ $ApoE^{-/-}$, $MyD88^{EC\text{-}KO}$ $ApoE^{-/-}$ female mice and their respective littermate controls on chow diet or HFD for 12 weeks beginning at 6 weeks of age were analyzed by ELISA. Data are expressed as mean ± S.E.M (n=5-6 per genotype) of the results from three independent experiments. (*P<0.05, **P < 0.01). **(B)** Immunostaining of GM-CSF (green) in conjunction with CD31 (red) were performed for frozen sections of aortic roots from $MyD88^{MC\text{-}KO}$ $ApoE^{-/-}$, $MyD88^{EC\text{-}KO}$ $ApoE^{-/-}$ female mice and their respective littermate controls on chow diet (3 months of age). Then the tissues were examined by confocal microscopy. Arrowheads indicate representative CD31+ GM-CSF+ cells (scale bar=20μm, L: lumen, A: arterial wall). Shown as are representative of five mice per genotype with similar results **(C)** Wild-type (WT) and MyD88-deficient (MyD88KO) primary aortic endothelial cells (ECs) were treated with ox-LDL (100 μg/ml) or IL-1 (1 ng/ml) for the indicated times (time 0 were treated with native LDL). Protein levels of GM-CSF in supernatant from cells treated for 24 hours were analyzed by ELISA. The levels of GM-CSF mRNA were measured by real-time PCR and presented as fold induction over the expression of WT cells at time 0. **(D)** WT and MyD88 KO ECs were treated with ox-LDL for 24h, then changed into fresh medium. After 48h, the medium was collected and used to culture sorted CD11b positive splenic monocytes for 24h with or without anti-GM-CSF neutralizing antibody (conditioned medium, conditioned medium + anti-GM-CSF). Monocytes were cultured in normal medium as negative control (vehicle). Monocytes in normal medium were treated with 50 ng/ml recombinant GM-CSF alone as positive control (GM-CSF). Total RNA of monocytes was subjected to real-time PCR to measure the relative expression of CD11c, CD206, IL-12a, IL12b, iNOS and PPBP. The fold induction was calculated as compared with vehicle group. **(E)** Bone marrow derived cells were cultured in DMEM supplemented with 20% FBS and 20 ng/ml GM-CSF or 50 ng/ml M-CSF for 7 days, followed by treatment of ox-LDL and FFA (16:0; Palmitate, 5μM) as indicated. Total RNA was subjected to real-time PCR to measure the expression of IL-12a, IL-12b, iNOS and PPBP. The fold induction was calculated as compared with the cells primed by M-CSF at time 0. **(F)** BMDMs of WT male mice primed by either M-CSF or GM-CSF were plated in the bottom wells of Boyden chambers, with or without 3T3 adipocytes in the inserts at a ratio of 5:1 (adipocytes: BMDMs cell numbers). mRNA expression levels of IL12a, IL12b, IRF5 and iNOS in the BMDMs were analyzed. The fold induction was calculated as compared with the cells primed by M-CSF and cultured alone. mRNA expression was normalized to β-actin expression. **(C-F)** Data represent the mean ± S.E.M. of triplicate samples from a single experiments, and all results are representative of three independent experiments. (*P<0.05, **P < 0.01).

D. Discussion

The study presented here aimed to address how TLR signaling in different cellular compartments contributes to the initiation and pathogenesis of obesity-associated inflammatory diseases through the specific deletion of MyD88 in endothelial cells or myeloid cells. MyD88 deficiency in myeloid cells ameliorated diet-induced systemic inflammation and global insulin resistance, preserving insulin sensitivity in all the tested tissues including muscle, liver and adipose tissue. On the other hand, endothelial-specific deficiency of MyD88 improved diet-induced insulin resistance at early phase with moderate effect on systemic inflammation, selectively restoring insulin sensitivity in adipose tissue. While both myeloid- and endothelial-derived MyD88 were equally critical for the initiation of atherosclerosis in chow fed ApoE-deficient mice, myeloid MyD88 clearly plays a more critical role than endothelial MyD88 in HFD-induced atherosclerosis. Taken together, these results for the first time demonstrate the non-redundant role of MyD88-dependent signaling in myeloid and endothelial cells for the development and progression of atherosclerosis and metabolic inflammatory diseases.

The participation of macrophages and endothelium in atherosclerosis has been extensively studied. In this study, we found that MyD88 deficiency in endothelial or myeloid cells inhibited vascular lesion formation in chow fed ApoE-deficient mice, with similar reduction in atherosclerotic area (60-70%). It is interesting to note that MyD88-dependent pathology in chow fed ApoE-deficient mice is restricted to the aorta, since under chow diet ApoE deficiency does not influence myeloid or endothelial MyD88-dependent WAT macrophage abundance, polarization or inflammatory cytokine production. These results clearly indicate the critical role of the MyD88-dependent pathway in the interplay

between the endothelium and macrophages in the aortic tissue during the initiation of atherosclerosis. The key initiating event in atherosclerosis is retention and oxidation of LDL in the vascular wall [267]. Our study suggests that endothelial cell activation by ox-LDL through the TLR-MyD88-dependent pathway probably plays an important role in the initiation of atherosclerosis. While ox-LDL strongly induces the expression of GM-CSF in a MyD88-dependent manner in endothelial cells, the expression of GM-CSF was greatly reduced in the arterial tissue of the chow fed $MyD88^{EC\text{-}KO}ApoE^{-/-}$ mice compared to that in the control mice. GM-CSF was indeed detected in endothelial cells of atherosclerotic lesions, which was abolished in the $MyD88^{EC\text{-}KO}ApoE^{-/-}$ mice. Furthermore, ox-LDL-induced expression of M1-associated genes was more robust in GM-CSF-primed macrophages than that in M-CSF-primed macrophages. Therefore, MyD88-dependent GM-CSF production from endothelial cells might serve as an important link between endothelial cells and macrophages by promoting M1-like inflammatory macrophages. In support of this, GM-CSF has been shown to be important in plaque development. Using the hypercholesterolaemic $ApoE^{-/-}$ mouse, it was found that GM-CSF treatment resulted in increased atherosclerotic lesion extent [268, 269] . LDLR-null mice have been employed in a study which combined 5-bromo-2'-deoxyuridine pulse labeling with en face immunoconfocal microscopy to demonstrate that systemic injection of GM-CSF markedly increased intimal cell proliferation (including dendritic cells), whilst functional GM-CSF blockade inhibited proliferation[270]. Therefore, in addition to macrophage polarization, the impact of GM-CSF on dendritic cell proliferation may also contribute to the reduced lesions in our endothelial cell-MyD88 deficient mice. Future studies using cell-type

specific GM-CSF receptor knockout mice will be required to clarify the pathogenic role of GM-CSF in atherosclerosis.

Interestingly, when the mice were fed the HFD, there was a dramatic reduction (70%) in atherosclerotic area in MyD88^{MC-KO} ApoE$^{-/-}$ mice, but a more moderate reduction (40%) in MyD88^{EC-KO} ApoE$^{-/-}$ mice. The question is why myeloid MyD88 plays a more critical role than endothelial MyD88 in HFD-induced atherosclerosis. It is important to note that myeloid MyD88 deficiency led to greater improvement in HFD-induced systemic inflammation (circulating TNFα, IL-6 and IL-1) and global insulin resistance than that by endothelial-specific MyD88 deficiency. Under HFD-induced systemic inflammation, in addition to ox-LDL, the endothelium can also be activated by a variety of circulating inflammatory stimuli [222], including TNFα and IL-6. As a result, the activation of endothelium, the interface between vascular structures and blood, becomes less dependent on the MyD88-dependent pathway over the course of HFD. Consistently, endothelial MyD88 deficiency improved global insulin resistance more dramatic at early phase (6 weeks after HFD) than that after 3 months of HFD**.**

One important question is how systemic inflammation is initiated in a HFD setting. Previous studies have suggested that metabolic-triggered inflammation in white adipose tissue plays a key role in the initiation of metabolic syndrome [223, 225-227]. ATMs are exposed to high local concentrations of FFAs released from adipocytes in obesity, and these serve as important activating ligands for TLR4 and TLR2 signaling in macrophages [231, 237, 241, 271-273]. The results from our co-culture model suggest that MyD88 participates in the cross-talk between adipocytes and macrophages and FFA released by adipocytes might be one of the initial ligands for TLR-MyD88 in this cross-talk. The

cytokines (e.g. IL-1 and IL-6) may feedback on adipocytes to further promote this cross-talk [274-278]. Consistently, compared to controls, $MyD88^{MC-KO}$ mice showed markedly reduced infiltration of macrophages and decreased adipose expression of inflammatory genes. Furthermore, the elimination of MyD88 in myeloid cells increased the number of M2-like macrophages (CD11c-CD206+) with decreased M1-like macrophages (CD11c+CD206-) in the adipose tissue, confirming the critical role of MyD88-dependent signaling in HFD-induced ATM switching from M2- to M1-like macrophages. Myeloid-specific MyD88-dependent switch of ATMs from M2-like to M1-like might play a key role in the initiation of obesity-associated inflammatory diseases. However, it is important to note that in addition to adipose tissue, myeloid-specific MyD88 deficiency also preserved insulin sensitivity in liver and muscle, which probably contribute to the improvement of HFD-induced global insulin resistance and systemic inflammation. Since CD11bCre mediates deletion of floxed sequences in myeloid cells, we have now crossed $MyD88^{fl/fl}$ mice with LysMCre mice to delete MyD88 in macrophages. Preliminary data from $LysMCreMyD88^{fl/fl}$ mice showed similar results with that in $MyD88^{MC-KO}$ mice as compared to the littermate controls.

Interestingly, $MyD88^{EC-KO}$ mice also showed moderate reduction in macrophage infiltration, M2-like to M1-like switching and adipose expression of those pro-inflammatory cytokine and chemokine genes. While FFAs released from adipocytes might directly act on endothelial cells, IL-1 released from FFA-induced M1-like macrophages could also activate endothelium through a paracrine manner. While IL-1 strongly induced the expression of GM-CSF, the GM-CSF levels were substantially reduced in adipose tissue of HFD fed $MyD88^{EC-KO}$ mice. IL-1-induced GM-CSF in endothelial cells was able

to promote M1-like inflammatory macrophages. Furthermore, the expression of M1-associated gene expression was more robustly enhanced in the adipocyte-macrophage ex vivo co-culture system when using GM-CSF-primed macrophages as compared to that of M-CSF-primed macrophages. Thus, endothelial MyD88 might impact on switching of ATMs from M2-like to M1-like through the production of GM-CSF, which may account for the selective rescue of insulin sensitivity in adipose tissue of HFD fed MyD88$^{EC\text{-}KO}$ mice. In support of this, endothelial deletion of MyD88 also moderately reduced M1-like macrophages in the aortas with substantial reduction of GM-CSF expression, which correlated with improved insulin sensitivity of aortic tissues from HFD-fed MyD88$^{EC\text{-}KO}$ mice. It is important to mention that the GM-CSF levels were not significantly reduced in liver and muscle of HFD-fed MyD88$^{EC\text{-}KO}$ mice (unpublished data, Yu and Li), which might explain why these two tissues remain insulin insensitive in HFD-fed MyD88$^{EC\text{-}KO}$ mice.

It is important to note that in addition to MyD88, TLR4 also utilizes TRIF to mediate NFκB activation to upregulate inflammatory gene expression. TRIF deficiency [279] or *TRIF*^{LPS2} lack-of-function mutation were shown to be atheroprotective in hyperlipidemic LDL receptor knockout (LDLr$^{-/-}$) mice [280]. Both studies supported a critical role of TRIF-dependent pathway in the pathogenesis of atherosclerosis. However, it is important to point out that TLR4 specifically utilizes TRIF to mediate the activation of transcription factor IRF3 to upregulate Type 1 IFN production which in turn impacts on IL-10 production [166]. Furthermore, it was reported that TRIF is not required for TLR4 signaling in endothelial cells [281], which was confirmed by our own studies in primary aortic vascular endothelial cells (Yu and Li, unpublished data). Therefore, mice with cell-

type specific TRIF deletion will be critical reagents for future studies to compare the molecular and cellular mechanisms by which MyD88- versus TRIF-dependent pathway contributes to the development and pathogenesis obesity-associated inflammatory diseases.

In summary, this study has demonstrated that MyD88-dependent signaling in both myeloid and endothelial cells contributed to the initiation/progression of atherosclerosis and as well as the development and pathogenesis of HFD-induced inflammatory diseases. Both myeloid- and endothelial-derived MyD88 are critical for the initiation of atherosclerosis in chow fed mice. One possible mechanism is that ox-LDL activates endothelial cells to produce GM-CSF, which in turn primes the monocytes in the arterial tissues and synergizes with ox-LDL to promote M1 inflammatory macrophages. On the other hand, MyD88-dependent signaling in myeloid cells makes a greater contribution to the development of HFD-induced systemic inflammation and consequent exacerbation on atherosclerosis. FFAs released from adipocytes act on ATMs to promote HFD-induced switching of ATMs from M2-like to M1-like, resulting in systemic inflammation and aggravating atherosclerotic lesions. Nevertheless, endothelial-derived MyD88 still has a noticeable contribution to the diet-induced inflammatory diseases, possibly also through the production of GM-CSF to feedback on macrophages. Future studies are required to elucidate how the cell-type specific MyD88-mediated signaling events contribute to the cross-talks among adipocytes, macrophages, and endothelial cells to establish the diet-induced inflammatory state, leading to inflammatory diseases associated with metabolic syndrome.

E. Materials and Methods

Animals. CD11bCre transgenic mice were provided by G. Kollias (Biomedical Sciences Research Centre ‘‘Alexander Fleming’’) [205]. Tie2eCre transgenic mice were a gift of X.-Y. Fu (National University of Singapore) [203]. MyD88 flox mice were provided by A. DeFranco (University of California, San Francisco) [282]. All these transgenic mice used backcrossed 10 times to C57/ BL 6 background. $ApoE^{-/-}$ mice in the C57/BL6 background were purchased from Jackson laboratory. Mice were housed in a specific pathogen-free facility (12-h light/dark cycle) and were fed either standard rodent chow or a high fat, Western style diet (HFD, Harlan Teklad 88137) [283-286]. Animals were fasted overnight and blood samples were taken for assessment of insulin (Crystal Chem), FFA(Cayman), cholesterol (Sigma), triglycerides (Sigma) and IL-1β, IL-6, TNF-α, CXCL1 (R&D systems) levels according to manufacturer’s instructions. All experimental procedures were carried out with the approval of the Institutional Animal Care and Use Committee of Cleveland Clinic (Cleveland, OH).

Primary cell isolation. Bone marrow derived macrophages (BMDMs) were differentiated from bone marrow flushed from the tibia and femur of mice using Dulbecco’s Modified Eagle’s Media (DMEM). The cells were cultured in DMEM supplemented with 20% FBS and 30% L929 supernatant for 5 days. Aortic endothelial cells (MAVECs, ECs) were harvested from mouse aorta under sterile conditions as previously described [287]. The aorta was excised; all periadventitial fat was removed, and the aortic pieces were placed onto Matrigel in DMEM plus 15% heat-inactivated FBS following the methods outlined by Shi et al [288]. After 3 days, the aortic explants were removed, and the endothelial cells were allowed to grow in DMEM plus 15% heat-

inactivated FBS supplemented with 180 μg/ml heparin and 20 μg/ml endothelial cell growth supplement. At confluence, the cells were passaged using dispase and then cultured for 2 days in DMEM plus 15% heat-inactivated FBS containing d-valine to eliminate possible fibroblast contamination. After 2 days, the EC were returned to growth medium without d-valine and allowed to grow to confluence. Mouse endothelial cell cultures were used in experiments from passages 2–4. Spleens were minced and digested with Liberase Blendzyme 2 for 15 min in PBS at 21 ℃, passed through a 40-mm cell strainer, treated with ACK Buffer (Lonza) to remove red cells, and resuspended in PBE (PBS with 0.5% BSA, endotoxin free; 1mM EDTA). splenocytes were subsequently sorted on a Dako MoFlo. Postsort analysis confirmed purity of 96% and viability of 95%.

Biological reagents and cell culture. Human low density lipoprotein (LDL, 1.019<density<1.063) was isolated from plasma of normolipidemic donors by sequential ultracentrifugation. Native and modified LDL preparations were tested for possible endotoxin contamination using a Limulus amebocyte lysate kit (Cambrex, Walkersville, MD). Oxidized LDL (ox-LDL) was prepared by incubating LDL (0.2 mg protein/ml) at 37 ℃ in 50 mM sodium phosphate (pH 7), 100 mM DTPA (diethylene-triamine-pentaacetic acid) in the presence of 30 nM myeloperoxidase, 100 mg/ml glucose, 20 ng/ml glucose oxidase (grade II; Boehringer Mannheim Biochemicals, Indianapolis, IN), and 0.5 mM $NaNO_2$ for 8 hours unless otherwise specified. Preliminary studies demonstrated that under these conditions, a constant flux of H_2O_2 (0.18 mM/min) is generated by the glucose oxidase system. Unless otherwise stated, oxidation reactions were terminated by addition of 40 mM butylated hydroxytoluene (from a 100 mM ethanolic stock) and 300 nM catalase to the reaction mixture[289]. FFA solutions were prepared as described previously [290].

Briefly, 100mM palmitate (Sigma No. P-0500) stocks were prepared in 0.1M NaOH at 70 ℃ and filtered. Five percent (wt/vol) FFA-free BSA (Sigma No. A-6003) solution was prepared in double-distilled H_2O and filtered. A 5mM FFA/5% BSA solution was prepared by complexing an appropriate amount of FFA to 5% BSA in a 60 ℃ water bath. The above solution was then cooled to room temperature and diluted 1:5 in RPMI 1640 without FBS to a final concentration of 1 mM FFA/1% BSA. Antibodies against MyD88, β-actin and phosphotyrosine (PY20) were purchased from Santa Cruz Biotechnology. Antibodies against p85-PI3K, GM-CSF, M-CSF and AKT were purchase from Abcam. Anti-Insulin receptor substrate 1 (IRS1) antibody was purchased from Upstate Biotechnology. Anti-Phospho-Akt (Ser473) Antibody, anti-arginase1 and anti-iNOS was purchased from Cell Signaling. Anti-F4/80 was purchase from Ab serotec. 3T3 L1 pre-adipocytes were cultured in DMEM, 10% FBS and 1% penicillin/streptomycin, and differentiated using the Adipogenesis Kit at 37 ℃ and 5% CO_2 (Cayman Chemical). Differentiation was initiated 1 day after 100% confluence was reached. Confluent 3T3-L1 cells preadipocytes were treated with 50ml initiation medium containing 500μM IBMX, 10μM Dexamethasone, 10μg/ml insulin in DMEM/10% FBS for 2 days. Afterwards, medium was changed to 40ml progression medium consisting of DMEM/10% FBS supplemented with 10μg/ml insulin. The 3T3-L1 cells were incubated with progression medium for 2 days. Subsequently, medium was changed at day 6 into 50ml fresh DMEM/10% FBS followed by another 2 day incubation at 37 ℃. Eight days after the initiation of differentiation, 3T3-L1 cells were ready for co-culture experiments. Preadipocytes were only differentiated and used prior to passage 12 greater than 95% of cells displayed the fully differentiated phenotype. For the co-culture system, differentiated 3T3-L1 adipocytes were co-cultured with differentiated

BMDMs in DMEM/10% FBS for a maximum of 24 hours using 6-well plates containing transwell inserts with a 0.4m ² porous membrane. $1*10^4$ BMDMs were seeded on the bottom of the well, while $1*10^4$ or $5*10^4$ 3T3-L1 adipocytes were seeded with into the insert. BMDMs cultured in the well without adipocytes seeded were set as control culture. After 24 hours of incubation, supernatants were collected, centrifuged for 10 minutes at 10,000g and 4°C; samples were stored at −20°C for cytokines measurement. mRNA was collected from BMDMs for further gene expression analysis.

Glucose tolerance test (GTT)/Insulin tolerance test (ITT). GTTs were performed by intraperitoneal injection (IP) of 2g/kg body weight of dextrose (Abbott Laboratories) after overnight fast. For ITTs, mice were injected with insulin (1mU/g BW, Sigma) IP after 3 hour fasting. Blood samples were obtained at 0, 15, 30, 60, 90, and 120 minute time points and glucose levels were measured with an ultra-one glucometer.

Insulin signaling analysis. Epididymal fat, liver and quadriceps muscle were collected from mice in the basal state or 5 minutes after an IP injection of insulin (25 mU/kg), and quickly frozen in liquid nitrogen. Frozen tissues were homogenized on ice in a Triton-containing lysis buffer (0.5% Triton X-100, 20 mM HEPES (pH 7.4), 150 mM NaCl, 12.5 mM β-glycerophosphate, 1.5 mM $MgCl_2$, 10 mM NaF, 2 mM dithiothreitol (DTT), 1 mM sodium orthovanadate, 2 mM EGTA, 1 mM phenylmethylsulfonyl fluoride and complete protease inhibitor cocktail from Roche), then ground and rocked for 1 hour in the cold room. Cellular debris was removed by centrifugation at 10,000 x g for 5 minutes. Immunoprecipitations were performed with the indicated amount of lysates. Supernatants were incubated with 5 μg of polyclonal antibody overnight and then incubated with protein A beads for another 1 hour at 4℃. Samples were washed extensively with lysis buffer

before solubilization in sodium dodecyl sulfate (SDS) sample buffer.Bound proteins and whole lysates (40 μg) were resolved by 4-12% or 4-20% SDS-polyacrylamide gel electrophoresis and transferred to nitrocellulose membranes (BioRad). Individual proteins were detected with the specific antibodies and visualized on film using horseradish peroxidase-conjugated secondary antibodies (BioRad) and Western Lightning Enhanced Chemiluminescence (Perkin Elmer Life Sciences). The levels of IRS1, p85-PI3K, activated AKT (pSer473, pAKT), and total AKT, were determined by immunoblotting of the whole lysates. Protein extracts were immunoprecipitated with anti-IRS-1, followed by western analyses with antibodies specific for phosphotyrosine (PY20, pY) or p85-PI3K.

Atherosclerosis lesion measurements. Atherosclerotic lesions were quantified by 2 independent and blinded assessments [291]. Mice were sacrificed by pentobarbital overdose, perfused with phosphate buffered saline (PBS) and 10% formalin (Formaldefresh, Fisher), and the entire aortic tree, including the heart, dissected free of fat and other tissue. Aortae were stained with oil red O, and digitally scanned. En face lesion area was assessed using Adobe Photoshop software, analyzed by Mann-Whitney U test. Data are expressed as percent of total aortic area ± S.E.M.

Immunohistochemistry. Freshly isolated adipose tissues were fixed with phosphate-buffered formalin overnight, then paraffin wax embedded and subsequently deparaffinized. Sections of 5 μm were incubated overnight with monoclonal anti-F4/80 antibody (AbD Serotec). After washing in PBS, slides were stained and developed using ABC staining system (Santa Cruz Biotechnology) and counterstained with hematoxylin (Sigma-Aldrich). The total number of cells and crown-like structure were counted in 10 different high-power fields from each section. Frozen aortic root sections were blocked

with 2% bovine serum albumin (diluted in PBS) containing 0.1% sodium azide for 1 hour followed by overnight incubation with the primary antibody (1:50 dilution for anti-GM-CSF, and 1:100 for anti-CD31; or 1：50 for anti-F4/80, 1:100 for anti-Arginase1 and 1:100 for anti-iNOS) at 4^{o}C. After washing in PBS, slides were incubated with the fluorochrome-conjugated secondary antibody (Alexa fluor-488 labeled donkey-anti-rat IgG and Alexa fluor-594 labeled mouse-anti-rabbit IgG, or Alexa fluor-488 labeled mouse-anti-rabbit IgG and Alexa fluor-594 labeled donkey-anti-rat IgG 1:200 diluted in blocking buffer) for 2 hr in the dark at room temperature, washed again in PBS and mounted with VECTASHIELD containing anti-fade reagent (Vector Laboratories, Inc., Burlingame, CA). Fluorescent images were acquired using a LEICA confocal microscope. No specific immunostaining was seen in sections incubated with PBS rather than the primary antibody.

Flow cytometry. The visceral adipose tissue (epididymal fat pad) and aorta were digested as described previously [229, 292]. SVF cells from adipose depots and aortic single cells were stained with anti-F4/80, CD11b, CD206, and CD11c (eBiosciences) to identify macrophage subsets. FACS analysis was conducted using FACS Calibur (BD Pharmingen) and the FACS data was analyzed by post collection compensation using FlowJo (Treestar Inc) software.

Quantitative real-time PCR. Total RNA was prepared from endothelial cells or BMDMs of mice with TRIzol reagent (Invitrogen). Tissues were preserved in RNAlater solution (Ambion), and subsequently homogenized in TRIzol reagent. Three micrograms of total RNA were then used for the reverse transcription reaction using SuperScript reverse transcriptase (Invitrogen). Quantitative PCR was performed using an AB 7300 Real-Time PCR System, and gene expression was examined by SYBR GREEN PCR Master Mix

(Applied Biosystems). PCR amplification was performed in triplicate, and water was used to replace cDNA in each run as a negative control. The reaction protocol included preincubation at 95 ℃ to activate FastStart DNA polymerase for 10 min, 40 cycles of amplification beginning with 15 seconds of denaturation at 95 ℃, followed by annealing/extension for 60 seconds at 60 ℃. The results were normalized to the housekeeping gene mouse β-actin. Primer sequences were designed using online tools from GeneScript. The primer sequences used will be distributed upon request.

Statistical analysis. Data are expressed as mean ± S.E.M. Differences were analyzed by Student *t*-test and one-way ANOVA. $P \leq 0.05$ was considered significant.